

**Against the Flow: Coil Arrangement and Design
Modulate Hemodynamics and Clotting in Model
Saccular Bifurcation Intracranial Aneurysm In
Vitro**

A Dissertation

Presented to

the faculty of the School of Engineering and Applied Science

University of Virginia

in partial fulfillment
of the requirements for the degree

Doctor of Philosophy

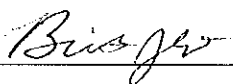
by

Brittany Earnest

May 2018

APPROVAL SHEET

This Dissertation
is submitted in partial fulfillment of the requirements
for the degree of
Doctor of Philosophy

Author Signature: 

This Dissertation has been read and approved by the examining committee:

Advisor: Brian P. Helmke, Ph.D.

Committee Member: William Guilford, Ph.D.

Committee Member: Avery Evans, M.D.

Committee Member: Michael Lawrence, Ph.D.

Committee Member: Shayn Peirce-Cottler, Ph.D.

Committee Member: _____

Accepted for the School of Engineering and Applied Science:



Craig H. Benson, School of Engineering and Applied Science

May 2018

ACKNOWLEDGEMENTS

I would like to thank my adviser, Dr. Brian Helmke, for his support throughout my time at UVa. Thank you for allowing me to build a project from the very foundation, and allowing me to pursue almost every crazy idea in the process, even if it was only once. Thank you for your fantastic mentorship and guidance.

Thank you to each member of my committee, Dr. William Guilford, Dr. Shayn Peirce-Cottler, Dr. Michael Lawrence and Dr. Avery Evans, for being understanding, thoughtful, supportive, and genuinely interested in my work. I cannot thank you enough for your dedication to developing my dissertation and to supporting me as a person.

Many people made this work possible. Thank you to Emily Nagel for her work in the permeability study and on the coil arrangement paper, and for teaching me about mentorship. Thank you to the American Heart Association, the Cardiovascular Research Center Training Grant and the UVa-Coulter Translational Research Partnership for their support of this work. A huge thank you goes to the healthy volunteers who donated blood for these experiments. This work would not have been possible without you. Thank you to Marty Beech and Marlin Tool, Inc. for helping to design and build the flow chambers and for generously donating materials and machining time. Thank you to the Peirce-Cottler and Isaakson labs and to Dr. Ammasi Periasamy and the WM Keck Center for the use of their confocal microscopes.

Thank you to my colleagues—undergraduate, graduate and faculty—at UVa and beyond who supported me and were my rock throughout the last several years through collaboration, feedback, teaching, and encouragement in work and life and friendship.

I especially want to thank my parents, Joe and Diane Earnest, and to my family for raising me in a world where I believed I could do anything with my life. Thank you for endlessly supporting and encouraging my personal and career decisions, even when it means being away from home.

TABLE OF CONTENTS

Abstract	v
List of Figures and Tables.....	vi
List of Abbreviations	xiii
Chapter 1: Background and significance	1
1.1 A brief history of IA treatment.....	1
1.1.1 Clipping.....	2
1.1.2 Coiling.....	2
1.1.3 Modified coils in clinical trials	3
1.1.4 Endoluminal devices	4
1.1.5 Intra-aneurysmal flow diversion devices	5
1.2 IA healing paradigm and its shortcomings.....	5
1.3 IA healing models: a history	7
1.4 IA healing models: the emergence of <i>in vitro</i> models	8
1.4.1 Device thrombogenicity studies	8
1.4.2 Cellularization studies.....	9
1.4.3 Flow dynamics studies	10
1.5 <i>In vitro</i> models of thrombosis under flow	13
1.6 Objectives and approach of the study	14
1.7 Significance of the study	14
Chapter 2: Flow and stasis clotting models	15
2.1 Rationale.....	15
2.2 Methods.....	16
2.2.1 Coil preparation	16
2.2.2 Clot formation without flow	16
2.2.3 Flow chamber and coil preparation.....	17
2.2.4 Recirculating flow experiments	17
2.2.5 Scanning electron microscopy (SEM) preparation	17
2.2.6 Image analysis.....	18
2.2.7 Statistical analysis.....	18

2.3 Results	18
2.3.1 Coil design and coil packing did not modify clot structure in the absence of flow	18
2.3.2 IA-like hemodynamics were required to reproduce physiological clot structure	19
2.4 Discussion	20
2.5 Conclusions	22
Chapter 3: Coil arrangement modulates hemodynamics and clotting	23
3.1 Rationale.....	23
3.2 Methods.....	23
3.2.1 Flow chamber and coil preparation.....	23
3.2.2 Recirculating flow experiments	24
3.2.3 Single-pass flow experiments	24
3.2.4 Scanning electron microscopy (SEM) preparation	25
3.2.5 Image analysis.....	25
3.2.6 Clot permeability experiments	25
3.2.7 Statistical methods	25
3.3 Results	26
3.3.1 Increased coil wire packing reduced clot permeability.....	26
3.3.2 Hemodynamics were dependent on coil configuration in IA sac flow chamber.....	27
3.3.3 Rate and location of clot formation were dependent on coil configuration in sac model.....	28
3.4 Discussion	32
3.5 Conclusions	34
Chapter 4: Coil design modulates hemodynamics and clotting.....	35
4.1 Rationale.....	35
4.2 Methods.....	36
4.2.1 Flow chamber and coil preparation.....	36
4.2.2 Recirculating flow experiments	36
4.2.3 Single-pass flow experiments	36
4.2.4 Scanning electron microscopy (SEM) preparation	36
4.2.5 Image analysis.....	36
4.3.6 Statistical methods	37
4.4 Results	37
4.4.1 Coil design modulates hemodynamics in IA neck model.....	37

4.4.2 Braided coil did not promote more clot accumulation than clinical coil in neck model.....	38
4.4.3 Coil design facilitated clot structure in IA neck model.....	39
4.4.4 Braided coils were associated with faster flow than clinical coils in IA sac model.....	41
4.4.5 Coil design facilitated clot structure in IA sac model	42
4.4.6 Coiled coils slowed flow more than braided coils in framing and filling coil positions.....	44
4.4.7 Braided coils promoted less clot accumulation than coiled coils in sac model	45
4.4.8 Framing coil type impacted clot structure in hybrid coil arrangements in sac model.....	46
4.5 Discussion	47
4.5.1 Neck model insights.....	47
4.5.2 Sac model insights	49
4.5.3 Overall insights	50
4.6 Conclusions	52
Chapter 5: Limitations and Achievements.....	53
5.1 Overall conclusions	53
5.2 Limitations of models.....	56
5.3 Achievements and contributions to the field.....	57
Chapter 6: Future Work	59
6.1 Alternatives in coil packing and coil design	59
6.2 Model of clotting and cellularization under flow.....	61
Works Cited	64
Appendix.....	73
Chamber cover schematic	73
Neck model chamber base schematic.....	74
Sac model chamber base schematic	75
Island contouring diagram.....	76

ABSTRACT

Intracranial aneurysm (IA) healing after endovascular coiling has been studied extensively *in silico* and *in vivo*; however, it is still unclear what causes IAs to recur. *In vitro* models of IA thrombosis contribute to an understanding of why IAs recur by providing a way to interrogate acute healing mechanisms and to screen treatments. In this work, novel models of saccular bifurcation IA thrombosis were developed and used to explore how coil properties drive hemodynamics and clot formation. Two parallel plate flow chambers were designed: one to model thrombosis at the neck of a bifurcation IA and another to analyze thrombosis within a coiled “sac”. Clots were formed in the presence of coils during fluorescence imaging of fibrin polymerization and flow tracers. Clots were analyzed post-fixation using scanning electron microscopy. Comparisons with clotted coils in the absence of flow indicate that arterial shear rates were required to produce clot structure similar to that observed *in vivo* and differences in clotting on coils with different packing densities and designs. In order to determine whether coil arrangement and local packing density affect thrombosis, a coil arrangement was analyzed in which filler coiled coils were arranged parallel to one another to create areas of high local packing density. Slower flow with nondivergent streamlines and larger clots were observed around these coils compared to coils arranged circumferentially. Clot distribution over time was also affected by coiled coil arrangement. To determine whether coil secondary shape facilitates thrombosis, rectangular wires were braided together to create a novel braided coil design that was compared to the coiled coil design. In the neck model, braided coils produced more circular flow patterns and denser platelet-fibrin clot structure than coiled coils, but clot accumulation was not dependent on coil design. In the sac model, coiled coils reduced flow velocity and correlated with fibrous mesh clot when located at the neck. Braided coils promoted flow disturbances and faster velocities that correlated with less clot formation and dense platelet-fibrin clot structures. These results suggest that slow flow with nondivergent streamlines around coils may be optimal for the formation of large fibrous clots, and that framing coil design may have a stronger influence on coil structure within the sac than filling coil design. These results indicate that coil arrangement and design influence hemodynamics and thrombosis in coiled IAs. Extracellular matrix structure modulates cell behavior; therefore, coil arrangement and design likely impact cellularization and subsequent healing in IAs. Further studies are necessary to elucidate the effects of coil-mediated IA hemodynamics and clot structure on cellularization.

LIST OF FIGURES AND TABLES

Figure 1: A: Representative image of a single coil that is used clinically. B: Coil placement inside an IA. A microcatheter containing the coil (tan) is placed at the neck of the IA. The coil (gray) is deployed directly into the IA. Once the IA is packed with coils, the coils are detached and the microcatheter is retracted.

Figure 2: Schematic of idealized IA healing. Once coils are placed inside the IA (A), clot (green) begins to form around the coils (B). The clot is infiltrated by cells (purple and orange), including macrophages and fibroblasts, as endothelial cells begin to cover coil at the neck (C). After approximately six months, a monolayer of endothelial cells has covered the IA neck and the clot has been reorganized into vascularized tissue (D).

Figure 3: The three core healing aspects are isolated and modeled *in vitro*. These aspects can be combined to generate models of interactions between the key components. The models developed in this manuscript fall under the “Blood Flow Model”. All three components can ultimately be incorporated into a novel “Cellularized Blood Flow Model”. It is important to note that many different models of cellularization under flow are possible, yet the models depicted in the figure assume that adherent cells are located along the inner dome wall in models exposed to flow and are located throughout the aneurysm in the absence of flow.

Figure 4: Preliminary acoustic radiation force microscopy study of clotting on a coil. Relative PRP clot stiffness increases faster close to coils than away from coils. Inset shows relative measurement locations.

Figure 5: Representative SEM images of coil and wire types used in the study. Inset shows the surface roughness of wire used in each coil type. “Clinical coils”, which are used clinically, consist of a smooth wire with a round cross-section that is coiled. “Ribbon coils” consist of a smooth wire with a rectangular cross-section that is coiled. “Braided coils” consist of rough wires with a rectangular cross-section that are braided. Inset scale bar, 5 μ m.

Figure 6: A: Representative fluorescent confocal images and segmented fibers for each condition. Clots were formed in the presence of clinical coils, ribbon coils and braided coils, and in the absence of coils. Clots were formed in the presence of either a single coil or multiple coils balled together to increase coil packing. Scale bar, 100 μ m. B: Fiber density of the clot was insensitive to sample type (one-way ANOVA, $p=0.18$).

Figure 7: A: Representative fluorescent confocal images and segmented fibers for each single wire sample condition. Clots were also formed in the presence of a single wire of each type. Scale bar, 100 μm . B: Fiber density was insensitive to sample type for each donor (two-way ANOVA, $p=0.94$). There was significant variability between donors (two-way ANOVA, $p<0.05$).

Figure 8: Representative SEM images of clots formed in each coil condition. There were no differences in structure between sample types. Scale bar, 10 μm .

Figure 9: A: Schematic of neck IA model flow chamber. Coils (red) are placed against the island and PRP is perfused through the chamber. Scale bar, 1 cm. B: Flow shear rate modulates clot morphology in flow chamber. Clot (green) is more heterogeneous, smaller and isolated to the coil (red outline) under flow (left), compared to clots formed without flow (right). A green arrow indicates the direction of PRP flow. Both clots were formed in the neck model. Scale bar, 100 μm .

Figure 10: Schematic of sac IA model flow chamber. Coils (red) were placed inside a hole in the island and PRP was perfused through the chamber. Scale bar, 1 cm.

Table 1: PRP flow conditions in Chapter 3

Figure 11: A: Diagram of permeability assay setup. B: Darcy constant as a function of coil packing density. As the packing density of clots increased, the permeability decreased. * $p<0.005$, $n=28$.

Figure 12: Representative images of coil arrangements in sacs (“Coil arrangement”), clot accumulation, and velocity profiles of flow tracers tracked at the neck and back of the dome for each coil condition. Particles moved slower around coils in a linear arrangement than in a circumferential arrangement. Flow velocity was slowed from neck to back of dome. Flow was faster without coils than with coils. In all images, neck opening is to the left and back dome is to the right (see inset diagram). Flow moved left to right. Aneurysm diameter, 5 mm. Velocity profile scale bar, 500 μm .

Figure 13: Velocity profiles were translated into heat maps with lower maxima to identify differences in the slowest flow velocities at the neck and back of the dome for each condition. Heat maps with a maximum of 500 $\mu\text{m}/\text{sec}$ show that particles moved slower around coils in a linear arrangement than in a circumferential arrangement at the neck. Heat maps with a maximum of 125 $\mu\text{m}/\text{sec}$ show that flow velocity was slowed from neck to back in both arrangements, and that flow velocity was slower around a linear arrangement than a circumferential arrangement. Aneurysm diameter, 5 mm. Scale bar, 500 μm .

Figure 14: Quantitative analysis of clot sizes. Clot sizes are shown after 17 minutes of PRP flow, 4 minutes of PRP flow for all perfusions, 4 minutes of PRP flow and 15-second perfusions and 4 minutes of PRP flow and 10-minute perfusions for each condition (* $p < 0.05$). Note differences in y-axis scale magnitude. Dotted outline represents a condition where two or fewer replicates were examined.

Figure 15: A: Locations of clot accumulation for coils arranged linearly and circumferentially. Color scale indicates percent of total experiments that were clotted at each pixel in the sac. Red indicates locations of accumulation in all trials. Neck opening is on the left of each image (see inset diagram). Aneurysm diameter, 5 mm. B: Proportion of red pixels located in the front half and back half of the sac for each condition. Measurements were calculated after 17 minutes of recirculating flow, 4 minutes of single-pass flow with all perfusion times and 4 minutes of single-pass flow with 15 seconds of perfusion.

Figure 16: A: Locations of clot accumulation for clot accumulation around coils arranged linearly and circumferentially after 4 minutes of single-pass flow with 10 minutes of perfusion. Color scale indicates percent of total experiments that were clotted at each pixel in the sac. Red indicates locations of accumulation in all trials. Neck opening is on the left of each image (see inset diagram). Aneurysm diameter, 5 mm. B: Proportion of red pixels located in the front half and back half of the sac. Two and three replicates were measured in the circumferential and linear arrangements, respectively. Additional replicates are necessary to draw accurate comparisons to the circumferential arrangement condition.

Figure 17: Representative SEM images of clots. Above: Images of clots after 4 minutes of PRP flow in the single-pass model show wavy, short fibers, in both linear (left) and circumferential (right) arrangements. Below: Images of clots after 17 minutes of PRP flow in the recirculating model show more straight, longer fibers, in both linear (left) and circumferential (right) arrangements. Insets show a representative magnified section of each image, where fibers have been outlined to illustrate differences in fiber structure. Scale bar, 5 μm .

Table 2: PRP flow conditions in Chapter 4

Figure 18: Hemodynamics around clinical coils in the neck model. A: Representative image of a clinical coil placed in the neck model before PRP flow. A schematic of the island indicates the direction of flow. Neck width, 1 cm. B: Velocity profiles of flow around clinical coils (gray) in different replicates. Each column represents the profile in a single replicate. These profiles demonstrate how the coil placement and orientation affected hemodynamics. C: The velocity profiles were translated to heat maps to demonstrate differences in the slowest velocities. Flow tends to be slowest immediately leading up to and behind the coil. Velocity profile scale bar, 500 μm .

Figure 19: Hemodynamics around braided coils in the neck model. A: Representative image of a braided coil placed in the neck model before PRP flow. A schematic of the island indicates the direction of flow. Neck width, 1 cm. B: Velocity profiles of flow around braided coils (gray) in different replicates. Each column represents the profile in a single replicate. These profiles demonstrate how the coil placement and orientation affected hemodynamics. C: The velocity profiles were translated to heat maps to demonstrate differences in the slowest velocities. Flow tended to be slowest behind the coil and in eddies surrounding the coil. Velocity profile scale bar, 500 μm .

Figure 20: Images of clot accumulation (green) in each coil (gray) replicate tested in the neck model after 20 minutes of PRP flow. Each column represents a different experiment where PRP from the same blood draw was recirculated around a clinical coil and a braided coil in different chambers simultaneously. The location of the neck wall is represented as a black line. Flow moved left to right. Coil length, 1 cm.

Figure 21: Average clot accumulation for all coil samples tested in the neck model after 20 minutes of PRP flow. There was no significant difference between conditions ($p=0.26$).

Figure 22: Quantitative analysis showed no correlation between wall-coil distance and clot accumulation. The distance between the coil periphery and the wall was plotted against the corresponding clot accumulation after 20 minutes of PRP flow in each sample for both clinical (blue) and braided (red) coils. Linear regression indicated no trend between wall-coil distance and clot accumulation for both clinical and braided coils (dotted lines). Open marker indicates PRP was recirculated at an average flow rate 1.3 mL/min faster than in the case of closed markers.

Figure 23: Clot morphologies observed on clinical coils in SEM after 4 minutes of single-pass flow (above) and 20 minutes of recirculating flow (below) in the neck model. After 4 minutes of flow, platelets were observed adhered to the coil surface and often spread out (black arrows). After 20 minutes of flow, more aggregates of spread and adhered platelets were observed (black arrows). Dense regions of platelets and fibrin and fibrin meshes interspersed with platelet aggregates were observed in experiments were large regions of clot accumulated (*). Scale bar, 10 μm .

Figure 24: Clot morphologies observed on braided coils in SEM after 4 minutes of single-pass flow (above) and 20 minutes of recirculating flow (below). Dense regions of platelets and fibrin (white arrowheads) were observed on the coil surface and in “pockets” in the coil. Adhered and spread platelets were also present on the coil surface (black arrows). In some locations, “fuzzy” clot structures were observed that might indicate underdeveloped clot (white arrow). In the

sample where a large amount of clot accumulated, fibrin mesh was observed (*). Scale bar, 10 μ m.

Figure 25: Representative images of sacs filled with braided and SS coil types before clotting (“Coil design”), clot accumulation, and velocity profiles of flow tracers tracked at the back of the dome for each coil condition (“Velocity Profile”). Clot accumulation was greater and particles moved slower around SS coils in a linear arrangement than braided coils. In all images, neck opening is to the left and back dome is to the right (see inset diagram). Flow moved left to right. Aneurysm diameter, 5 mm. Velocity profile scale bar, 500 μ m.

Figure 26: Dome mixing analysis. A: Sample image analysis of a model that was coiled linearly. A field of view was not considered mixed until a uniform intensity was observed around the coil (t=10 sec). “t” indicates time after flow initiation. The sample was devoid of PRP at t=0 sec and was fully mixed at t=10 sec. Scale bar, 100 μ m. B: Average time until a well-mixed field of view was observed at the back of the dome. (*p<0.05).

Figure 27: Representative SEM images of clots on braided and SS coils. Above: Images of clots after 4 minutes of PRP flow in the single-pass model showed wavy, short fibers, on both braided coils (left) and SS coils in a linear arrangement (right). Below: Images of clots after 17 minutes of PRP flow in the recirculating model showed wavy, short fibers on braided coils (left) but straighter, longer fibers on SS coils (right). Braided coils presented clots with dense fiber and platelet aggregates (white arrowhead). Some areas on SS coils presented “fluffy” clot structures that might have indicated underdeveloped fibrin (white arrow). Insets show a representative magnified section of each image, where fibers have been outlined to illustrate differences in fiber structure. Scale bar, 5 μ m.

Figure 28: Representative images of sacs filled with braided and coiled coil (CC) types and in different arrangements (“Coil design”), clot accumulation, and velocity profiles of flow tracers tracked at the neck and back of the dome for each coil condition. Particles moved slower around coiled coils than around braided coils. Clot accumulation was not dependent on these conditions. Flow velocity was slowed from neck to back of dome in a sac with filling coiled coils, but not in a sac with filling braided coils. Flow was slower inside a sac with a framing coiled coil than a sac with a framing braided coil. In all images, neck opening is to the left and back dome is to the right (see inset diagram). Flow moved left to right. Aneurysm diameter, 5 mm. Velocity profile scale bar, 500 μ m.

Figure 29: Velocity profiles were translated into heat maps with lower maxima to identify differences in the slowest flow velocities at the neck and back of the dome for each condition. These heat maps emphasize the trend that flow velocity was slowed across and around coiled

coils (CC) in the framing and filling positions, respectively, but not across or around braided coils. Aneurysm diameter, 5 mm. Velocity profile scale bar, 500 μm .

Figure 30: Quantitative analysis of clot sizes after 17 minutes of recirculating flow. Clinical coil arrangements are included for comparison. Dotted outline represents a condition where two or fewer replicates were examined. Significant differences shown in Figure 14 are not displayed.

Figure 31: Quantitative analysis of clot sizes after 4 minutes of single-pass flow. Clinical coil arrangements are included for comparison. Dotted outline represents a condition where two or fewer replicates were examined. Significant differences shown in Figure 14 are not displayed.

Figure 32: Representative SEM images of clots on hybrid coil designs. Since these designs consist of two different coil types, clot structure trends on the coiled coil (CC) surfaces (above) and braided coil surfaces (below) were outlined separately. In images of sacs filled with braided framing coil and CC filling coils (A-C), adhered platelets (black arrow) and dense clots of platelets and fibrin (white arrowheads) were observed on both CC (A-B) and braided coil (C) surfaces. In images of sacs filled with CC framing coil and braided filling coils (D-G), adhered platelets and dense clots of platelets and fibrin (white arrowheads) were observed on both CC (D) and braided coil (F) surfaces. Additionally, large areas of fibrin mesh were observed on both CC (E) and braided coil (G) surfaces, which were interspersed with small platelet and fibrin aggregates (white arrowheads). Scale bar, 10 μm .

Table 3: Trends in hemodynamics and clotting observed in sac flow model.

Figure 33: Summary table of conditions tested and the models used to test them in each chapter. Chapter 2 utilized the stasis clot model and neck flow model to test the hypotheses that clot structure is insensitive to coil design and packing in the absence of flow (on clinical, ribbon and braided coils), and that flow is necessary to recapitulate clot structure seen in *ex vivo* human IAs (comparing clots formed in the absence of flow to clots formed under 200s^{-1} shear flow. Chapter 3 used the sac flow model to test the hypothesis that coil arrangements with high local packing densities promote space-filling clot formation under flow (comparing the linear arrangement, the circumferential arrangement and a sac without coils). Chapter 4 used the neck flow model and sac flow model to test the hypothesis that coil designs that create disturbed flow patterns promote space-filling clot formation under flow (comparing clinical coils and braided coils in the neck flow model, and comparing braided coils, stainless steel (SS) coils in a linear arrangement and hybrid designs in the sac model).

Figure 34: A: Coiled coil arrangement modulated flow velocity (green arrows), initial distribution (dotted outline) and accumulation of fibrin mesh (dark green hatch) clot. B: Coil design modulated flow velocity and pattern (green arrows). The presence of braided coils

correlated with small areas of dense platelet-fibrin clot accumulation (light green), and a coiled coil in the framing coil position correlated with small areas of fibrin mesh accumulation (dark green hatch).

Figure 35: Clots were formed on coverslips using PRP treatments discussed in the methods. Left: PRP was anticoagulated with buffered sodium citrate to 3.2% and activated with 20 mM CaCl_2 . Middle: PRP was diluted to 51% in saline and anticoagulated with buffered sodium citrate, then activated with CaCl_2 . PRP used in the single-pass model was treated using the same protocol. Right: PRP was diluted to 24% in saline. This increases coagulation time so that coagulation around coils could be observed in the recirculating model. Fiber density is independent of dilution. High intensity locations show platelet-mediated fiber bundling. Scale bar, 100 μm .

Figure 36: SEM image of three round wires braided together. Scale bar, 100 μm .

Figure 37: Representative images of a sac filled with braided framing coil and coiled coil (CC) filling coils in a circumferential arrangement before clotting (“Coil design”) and after 17 minutes of clot accumulation. In all images, neck opening is to the left and back dome is to the right (see inset diagram). Flow moved left to right. Aneurysm diameter, 5 mm.

Figure 38: EC attachment is higher on clotted coils than bare coils but is not dependent on coil design. A: Representative SEM images of ECs cultured on a bare clinical coil (left), a clotted clinical coil (middle) and a clotted ribbon coil (right). Scale bar, 50 μm . B: Quantitative analysis of SEM images shows that the number of ECs per field of view is higher on bare tissue culture polystyrene dishes and clotted coils than bare metal coils. EC attachment was not dependent on coil design across three different experiments ($p=0.35$, $p=0.97$, $p=0.83$).

Figure 39: Feedback exists between cell behavior and clot structure. Left: Clots (green) on edged coils (*) formed net structures (above, arrow) that produced EC (cyan) monolayer nets (below, arrow) at low fibrinogen concentration. Scale bar, 100 μm . Right: On glass surfaces, ECs also reorganized clot structure (green) around them. Scale bar, 20 μm .

Figure 40: Preliminary studies show that the sac model can be lined with ECs. A: Phase contrast image of an EC monolayer on the bottom surface of the sac flow chamber. Scale bar, 100 μm . B: Nucleus staining shows that the EC monolayer extends up the dome wall (arrow). C: Endothelialized sac was coiled and clotted. ECs (green dots) were observed on clot (green line) that formed between the coils and the wall (red outlines). Inset shows magnified view. Scale bar, 100 μm . Schematic indicates the field of view for A and B (orange) and C (green) within the sac.

LIST OF ABBREVIATIONS

bovine serum albumin	BSA
coiled coil	CC
endothelial cell	EC
extra-cellular matrix	ECM
red blood cells labeled with DiI	DiI-RBCs
hexadimethylsilazane	HMDS
modified HEPES-Tyrodes' buffer	HT buffer
intracranial aneurysm	IA
phosphate-buffered saline (without magnesium or calcium ions)	PBS
platelet-rich plasma	PRP
red blood cell	RBC
scanning electron microscopy	SEM
stainless steel coiled coils	SS

CHAPTER 1: BACKGROUND AND SIGNIFICANCE

Water coils anyways?

Intracranial aneurysms (IAs) are a serious and prevalent condition with innumerable phenotypes that present a complex challenge to those who treat them. Unruptured IAs are present in 1 in 50 Americans, and when one ruptures, it is 40% likely to result in fatality. Furthermore, IAs account for 3-5% of new stroke cases each year.¹ Therefore, it is necessary that IAs are treated effectively and before rupture. Many treatment options have emerged for unruptured IAs, but the most commonly and widely used is endovascular coiling (Figure 1).² Resected human IAs and animal models have revealed a general mechanism of optimal healing after treatment.³⁻⁶ However, in approximately 30% of IAs treated with coils, blood flow re-enters the aneurysm, causing it to recur and increasing the risk of rupture,⁷ but it is still unclear why this occurs in specific aneurysms. Although *in vivo* animal models of IA healing allow for evaluation of tissue pathology post mortem, these models cannot give insight into time-dependent mechanisms. *In vitro* models enable the isolation and control of clinically relevant factors such as aneurysm geometry^{8,9} and coil placement^{10,11} to determine their impact on IA healing processes. Coil designs that better promote aneurysm healing would reduce the rate of recurrence.

1.1 A BRIEF HISTORY OF IA TREATMENT

An aneurysm occurs when the blood vessel wall weakens due to loss of internal elastic lamina and extra-cellular matrix (ECM). The wall expands, creating a predominantly fusiform or saccular shape.^{12,13} Since most IAs are saccular (Figure 1B, left),¹² treatment of saccular IAs will be discussed in this work. Saccular aneurysms are composed of the sac (also called a dome), which is the part of the vessel that expanded, and the neck, which is the opening into the aneurysm sac. They are predominantly categorized as sidewall, where the aneurysm sac is located on the side of a vessel (depicted in Figure 1B), or bifurcation, where the aneurysm sac is located at a fork or bifurcation in the vessel. IA size is typically characterized by the sac-to-neck ratio, which is the ratio of the maximum diameter of the sac to the maximum diameter of the neck. Daughter aneurysms can sometimes form, which are secondary aneurysms that form from the aneurysm wall. When the wall continues to weaken to the point of breakage, rupture occurs. IA diagnosis is often difficult: patients who have an unruptured or ruptured IA typically present with symptoms ranging from a persistent headache to coma or neurologic compromise. Cranial computed tomography (CT) imaging is typically used to identify and diagnose an IA.⁷ In some circumstances, such as if the IA is very small or if treatment poses a very high risk to the patient, the clinician may choose not to immediately treat the aneurysm but to continue to monitor it instead. However, often surgical or endovascular treatment is required, after or in addition to observation, to prevent rupture and subarachnoid hemorrhage in the brain.

1.1.1 Clipping

Prior to endovascular coiling, unruptured IAs that required intervention and ruptured IAs were primarily treated with small metal clips that are positioned around the neck of the aneurysm, eliminating blood flow at the neck and excluding the IA from the parent vessel.⁷ This treatment is invasive, since it requires a craniotomy with clip placement. Clipping has been observed to correlate with more complications during surgery, longer hospital stay and higher treatment costs than coiling. The risks of clipping compared to coiling can be more serious depending on the depth of the IA into the brain and the patient's history.¹⁴ However, recurrence rates tend to be lower in clipped IAs than in coiled IAs, and some IAs cannot be coiled due to high tortuosity of the vessel or incompatible aneurysm geometry; consequently, clipping is still used in certain circumstances.

1.1.2 Coiling

In the coiling process, small coils (approximately 300-1000 μm secondary diameter, Figure 1A), typically platinum and sometimes with a hydrogel coating,¹⁵ are inserted and packed into the aneurysm until it is as full as possible, then the coils are detached via electrolysis (Figure 1B).¹⁶ The aneurysm is "occluded" when little to no blood flow is observed. The coils are radiopaque, allowing them to be visualized in fluoroscopy during positioning. IA rupture during coil placement is the most serious complication during coiling. The coils reduce blood flow into the aneurysm, allow a clot to form and help initiate a wound healing response that results in tissue formation that fills the aneurysm, preventing rupture. IA recurrence after coiling is approximately 25% higher than that after clipping, and coiled IAs that recur are often clipped.

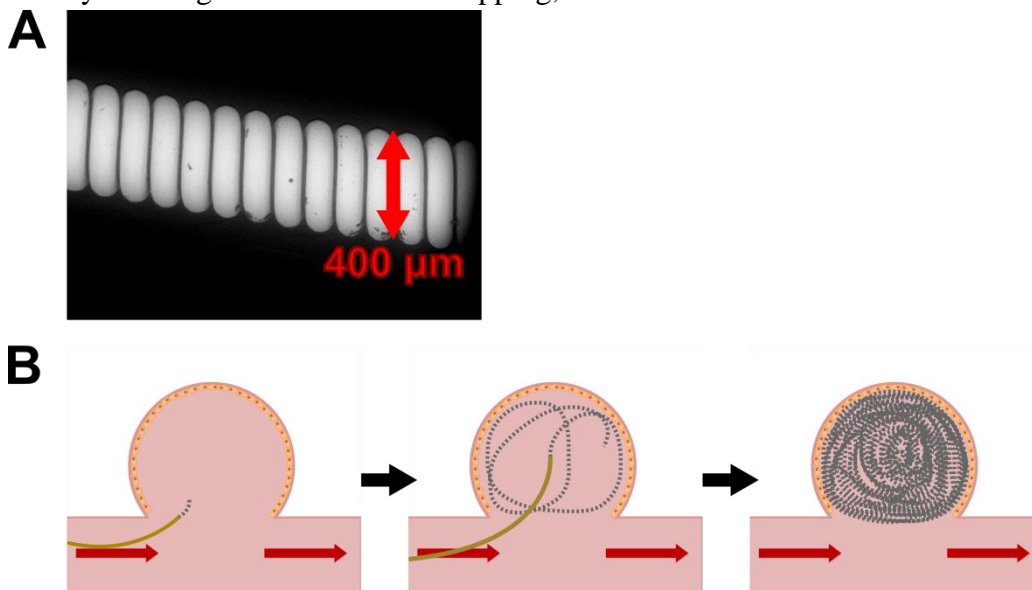


Figure 1: A: Representative image of a single coil that is used clinically. B: Coil placement inside an IA. A microcatheter containing the coil (tan) is placed at the neck of the IA. The coil (gray) is deployed directly into the IA. Once the IA is packed with coils, the coils are detached and the microcatheter is retracted.

Coiling effectiveness is dependent on myriad factors, including aneurysm geometry, vessel tortuosity, neck width, patient history and operator expertise.^{7,17}

Coil design can be modified on multiple levels. The “primary shape” describes the shape of the coil wire. Conventional clinically available coils consist of smooth wires that have a circular cross-section, but a variety of cross-section wire shapes and degrees of surface roughness can be utilized in coil design. The “secondary shape” of the coil is the orientation of the wire. For example, conventional coils are made up of wires that are wrapped around a cylinder to create a spring-like shape, but multiple wires can be braided to create a different secondary shape. Many commercially available coils are coated with a biodegradable material, modifying the secondary shape. The “tertiary shape” of the coil is described by how coils interact with each other. Many conventional coils are designed to fold into a ball, but some have been designed to fold into a helix or other complex shapes.^{18,19} This tertiary arrangement of coils can modulate intra-aneurysmal hemodynamics, which likely modulates initial clot formation.

1.1.3 Modified coils in clinical trials

Novel coil designs have been developed and tested in clinical trials, yet they perform as well as, or in some cases worse than, bare platinum coils. Since 2007, a handful of studies using randomized, controlled trials have investigated the effect of “bioactive” coil coatings, such as Matrix, hydrogel, polyglycolic acid, and polylactic acid, on initial occlusion and long-term procedural outcomes. These coatings are designed to fill more space in the sac and promote cell adhesion and proliferation in order to increase the likelihood of occlusion and prevent the aneurysm from recurring. However, there was little to no consistent improvement in patient outcome. In one study, aneurysms treated with hydrogel-coated coils called HydroCoils were 9% less likely to recur and had higher coil packing densities than those treated with bare metal coils,²⁰ but the morbidity and mortality rates were higher with the use of HydroCoils, and there was no difference in retreatment rate despite a difference in recurrence rate.²¹ Four additional randomized controlled trials published between 2011 and 2014 tested coils that were coated with polyglycolic/polylactic acid copolymer, polyglycolic acid, or hydrogel, and each of the studies individually concluded there was no improvement in outcome after bioactive coiling compared to bare metal coiling.²² Specifically, there were no differences in rates of aneurysm recurrence, aneurysm rupture, additional intervention or stroke. Additionally, in an attempt to improve occlusion rates by modifying the mechanical stiffness of the coil, the use of “very soft” platinum coils increased packing density but did not improve short or long term patient outcome.²³ The lack of consistent improvement in patient improvement and recurrence rates in these studies indicates that an improved coil design may not yet be identified. Endovascular coils are used in many types of IAs, often in conjunction with other devices such as stents, so improvements to coil design would increase treatment efficacy in the widest range of IAs.² An understanding of the conditions that drive the variability in individual IA healing is necessary to determine how coil treatments fail and to design better coil designs.

1.1.4 Endoluminal devices

IAs with wide necks (those with a sac-to-neck ratio of less than approximately 1.5)¹⁷ pose a challenge to coiling since parts of the coil called “coil remnants” that are not contained within the IA sac are more likely to occur in the parent vessel. This led to the invention of devices placed in the lumen of the parent vessel that assist or replace coiling. Balloon-assisted remodeling is one method used to improve the effectiveness of coiling in wide-neck IAs, where a balloon is inflated across the aneurysm neck during each coil placement to prevent protrusion into the parent vessel. This technique is commonly used in sidewall IAs, but balloons made of compliant materials have been used in bifurcation IAs to assist coiling and to reshape the neck and daughter vessels that make up the bifurcation.²⁴

Stents are another category of devices that are utilized in tortuous or wide-necked IAs and in other circumstances where coils alone are likely to fail. These devices are deployed in the parent vessel over the IA neck and are classified according to porosity as low coverage of the parent vessel wall (5-10%), intermediate coverage (approximately 15%) or high coverage (approximately 30%).²⁵ Stents can help reduce recurrence rates; however, currently all stents require extended dual anti-platelet therapy, which can increase the risk of complications particularly in patients with intracranial hemorrhage. Low coverage stents, including the Neuroform and Enterprise stents, are constructed from nitinol tubes and are used in stent-assisted coiling to prevent coil protrusion into the vessel. Recurrence rates of stent-assisted coiling tend to be lower than coiling alone, but the complication rates of early stent designs were higher than coiling alone. Further studies are necessary to determine the safety and effectiveness of newer designs, such as the next generations of Neuroform and Enterprise stents and the Liberty and Solitaire stents. Intermediate coverage stents are composed of woven or braided nitinol fibers and can provide more support to the coils and lumen than low coverage stents. Nevertheless, these stents tend to have higher complication rates, allow less coil access through the stent struts to the IA and in the United States are only used in clinical trials.

Flow diverters are high coverage stents that are most often used as an alternative to coiling and clipping, especially for IAs with wide necks. Flow diverters rely on the mechanism where the majority of blood flow is redirected from the aneurysm through the parent vessel, slowing flow into the aneurysm and allowing it to thrombose and often regress in size.¹⁷ Recurrence rates of the pipeline embolization device (PED), made of platinum-tungsten and cobalt-chromium-nickel microfilaments, and the silk flow diverter (SFD), made of nitinol and platinum microfilaments and recommended for use with coils, are approximately 10% lower than that of coiling alone.²⁵ Flow diverters are also more effective in treatment of IAs with wide necks. However, drawbacks include delayed occlusion of the IA, which may cause the expansion of the sac and/or increase the risk of rupture, and elimination of blood flow into perforating branches of the cerebral arteries, which can cause stroke. The SFD is not yet available in the United States, and the

Surpass flow diverter and flow redirection endoluminal device (FRED), which demonstrate approximately 1% and 20% lower recurrence rates than that of the PED, respectively,²⁵ are not yet available outside of clinical trials.

Flow diverters have been shown to be successful in treating wide-neck aneurysms, but are not yet recommended to be used in bifurcation aneurysms² and have more restricted availability than endovascular coils. It is possible that another factor contributing to the more widespread use of coils over flow diverters is the operator's experience with the device, which affects treatment selection and patient outcome.^{17,25} Flow diverters have more recently become present in clinical use than coils, and so fewer interventional neuroradiologists, neurosurgeons and neurologists may be comfortable using them in patients. As more clinicians become accustomed to flow diverters, the prevalence, success and applications of their use are likely to increase.

1.1.5 Intra-aneurysmal flow diversion devices

A more recent category of devices has emerged that are placed directly within the IA sac. These devices are potentially beneficial in that they can slow blood flow in the IA but may not require dual anti-platelet therapy or induce parent vessel occlusion.²⁵ However, only a handful of these devices are currently being used in clinical trials. The woven endo-bridge (WEB) device, for instance, is optimal for bifurcation aneurysm treatment, but has demonstrated variable occlusion rates (7-56%) and recurrence rates (14-35%) in trials to date.^{26,27} The pCONus device is a stent-like device designed for coil-assistive intra-aneurysmal and endoluminal placement in bifurcation IAs. One end is deployed into the neck of the IA, which opens up into leaflets that anchor the device in the sac and prevent coil protrusion, which are attached to a low coverage stent that is placed in the parent vessel lumen. This process of placing a stent partially inside the IA sac is called the "waffle cone technique".²⁸ While the pCONus device alone is not effective in slowing flow into the IA, the pCANvas device, in which a membrane covers the leaflets, has been shown to reduce flow rate into the sac without coils. The pCONus device is not yet available in the United States.

New IA treatment devices outside of endovascular coil design have been developed and tested, but coils continue to be the most versatile and accessible in IA treatments.² Therefore, alternatives to coiling will not be covered in the scope of this work from this point forward. In order to develop more effective coil designs, however, the mechanism by which IAs heal such that they are prevented from rupture needs to be understood.

1.2 IA HEALING PARADIGM AND ITS SHORTCOMINGS

The generally accepted mechanism of coiled human IA healing has been deduced from many studies involving animal models and resected human IAs.³ Briefly, blood flow in the aneurysm is slowed and clotting is initiated by the presence of coils in the dome (Figure 2B). Unorganized thrombus forms within the aneurysm sac and around the coils, and immune cells begin to enter

the sac. In the next week, the fibrin clot thickens, immune cell and myofibroblast infiltration increase and endothelial cells (ECs) begin migrating across the neck. Throughout the two to four weeks after treatment, more cells infiltrate the sac and remodel the clot into “organized thrombus” (Figure 2C). In the second and third months, apoptosis begins and the number of macrophages and myofibroblasts in the sac decreases, while endothelialization of the neck progresses and thrombus is further remodeled into tissue. Through three to twelve months, the dome becomes mostly acellular with some multinucleated giant cells due to a lingering foreign body reaction and is filled with vascularized connective tissue and sometimes collagen. A complete layer of fibrous tissue and ECs is formed across the aneurysm neck (Figure 2D). By this time, the aneurysm sac is effectively isolated from the parent vessel.

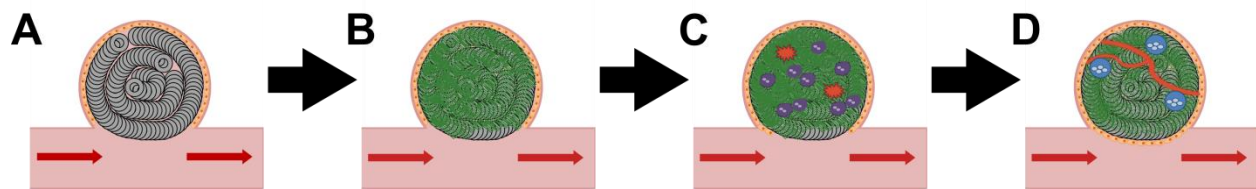


Figure 2: Schematic of idealized IA healing. Once coils are placed inside the IA (A), clot (green) begins to form around the coils (B). The clot is infiltrated by cells (purple and orange), including macrophages and fibroblasts, as endothelial cells begin to cover coil at the neck (C). After approximately six months, a monolayer of endothelial cells has covered the IA neck and the clot has been reorganized into vascularized tissue with few multinucleated giant cells (D).

Although this mechanism is accepted as the ideal progression of a well-healed aneurysm, many aspects of this process are not well defined in the literature. In contrast with the aforementioned mechanism of a homogeneous, organized thrombus in healed IAs, some studies of stable, healed human IAs show tissue heterogeneity. In one study, organized, vascularized tissue was present with EC coverage in some areas of a healed IA, but unorganized thrombus and a lack of endothelialization were found in other areas of the same IA.^{4,29} In other cases, organized thrombus was not accompanied by endothelialization,³⁰ or endothelialization was accompanied by unorganized thrombus at early healing stages,³¹ indicating that organized thrombus may not be necessary for endothelialization. Endothelialization of IA thrombus and cell phenotypes associated with rupture are variable between patients, and their relationships to recurrence are unclear.^{12,30,31} This variability may be partly due to the absence of an objective distinction between organized and unorganized thrombi. Moreover, the prevalence and role of cell-derived matrix proteins in human IA healing are not well understood. Collagen content is variable between healed IAs, ranging from virtually absent⁴ to dense regions.^{32,33} In some cases, cartilage or bone forms in the IA dome, the source of which is currently unknown.³ Additionally, matrix metalloproteases and pro-apoptotic genes have been cited as indicators of both normal IA healing³ and rupture.³⁴

In the same vein, multiple theories have been proposed regarding the cause of IA rupture. Both low and high wall shear stresses have been associated with IA rupture,^{35–37} indicating that the

relationships between IA hemodynamics, cell behavior and ECM are complex. A binary theory to explore this complexity^{12,38} states that low wall shear stress and oscillatory flow patterns cause “inflammatory-cell-mediated” destructive remodeling, where large, thick-walled atherosclerotic aneurysms form. In contrast, high wall shear stress and a positive wall shear stress gradient cause “mural-cell-mediated” destructive remodeling, where small, thin-walled aneurysms form. In these circumstances and in IAs that contain both types of remodeling, the aneurysm is at risk for rupture. This hypothesis begins to shed light on the variability in shape, cell phenotype and hemodynamics in human IAs and shows how these characteristics of the IA can cause different intra-aneurysmal conditions and therefore different IA physiologies and outcomes. These theories are a step towards understanding the spectrum in IA healing in order to develop more effective treatments for individual patients.

1.3 IA HEALING MODELS: A HISTORY

Animal and computational models have been the most common tools used to better understand how and why coiling fails in saccular IAs. The two most widely used IA animal models are the venous pouch model and the enzymatic model. The venous pouch model consists of removing a section of a vein, typically the external jugular vein, and grafting it to the common carotid artery to produce an aneurysm.³⁹ This model is often performed in swine, where the IA is coiled immediately after aneurysm formation since spontaneous thrombosis tends to occur in the venous pouch.⁴ Unlike human IAs, the venous pouch aneurysms tend to be resistant to rupture and the venous areas have different physiology than arterial aneurysms. The healed aneurysm is typically characterized by more collagen and fibrosis than most human healed IAs.⁴ In the enzymatic model, typically performed in swine, rabbits, rats and mice, a section of the left or right common carotid artery is incubated with elastase or papain for about 20 minutes. An aneurysm is formed after approximately two weeks and is coiled.⁴⁰ Leakage of elastase out of the region of interest can be lethal to the animal.³⁹ The phenotype of the healed aneurysm is more similar to human healed IAs but is typically characterized by slightly less collagen and unorganized thrombus formation than in most human IAs.⁴ Computational models generally model hemodynamics in various aneurysm sizes and shapes and often correlate these parameters with rupture and daughter aneurysm incidence.^{8,36,41,42} Many computational studies analyze the relationships between intra-aneurysmal hemodynamics and coil packing density or placement.^{11,18,43,44} However, a few of these models analyze thrombosis in the IA and are described below.⁴⁵⁻⁴⁷ *Ex vivo* aneurysms that were resected from patients provide some insight into IA healing in humans but are often limited to IAs that recurred, a challenge to understanding the histology of an IA that is protected from recurrence.

The aforementioned general healing mechanism is based on information from these animal and computational models and does not explain why bioactive coils and other treatments fail in certain patients, indicating that this paradigm is incomplete. *In vitro* models provide an important supplement to *in vivo* animal models and *ex vivo* human samples and make up an underexplored

niche in the field of IA healing. They provide new insight into human-specific IA healing mechanisms by using human-derived materials, allowing analysis of the system at early time points and providing control over each variable in the system. Validation of computational models via *in vitro* studies is beneficial in that it ensures accuracy of the models and allows computational studies to move forward to more complex models and informative outputs. *In vitro* models shed light on mechanisms in IAs *in vivo* and allow faster and cheaper screening of treatments that can supplement animal studies, computational models and clinical trials.

1.4 IA HEALING MODELS: THE EMERGENCE OF *IN VITRO* MODELS

In vitro models that are designed to determine the mechanisms of healing and efficacy of coil designs in IAs begin to interrogate some of these mechanisms by focusing on one of the three overall components of IA healing: thrombosis, cellularization, and hemodynamics within the IA. Visualizations of *in vitro* models that focus on one or more of these components are depicted in Figure 3.

1.4.1 Device thrombogenicity studies

Intra-aneurysmal thrombus formation is the first stage of healing and sets the scaffold for cell migration and tissue formation into the aneurysm. Formation occurs within the first few days of treatment,³ making it difficult to observe in animal studies *in vivo*. Yet, it is not completely understood what is the role of thrombus in healing, including how thrombosis is influenced by IA dimensions, location and other characteristics, and how thrombus structure, formation rate and size affect long term patient outcome. *In vitro* thrombosis models (Figure 3, “Thrombosis”) provide an analysis of short-term endpoints in thrombus formation that are costly and difficult to observe *in vivo* and examine the dependency of clot formation on factors that cannot be easily controlled *in vivo* but can differ between patients, such as IA shape, hemodynamics and coil organization.

In vitro studies that aim to compare coil thrombogenicities typically examine the rate and extent of clotting on coils and coil surface materials. The majority of these experiments involve the use of blood without flow or an aneurysm sac geometry. These stagnant thrombogenicity studies are fast and relatively inexpensive methods for screening different metal coatings and materials, and often agree with clinical trial literature. For example, multiple *in vitro* studies concluded that coils with nylon fibers promoted faster clot formation and higher thrombin generation in stagnant human blood than bare metal coils.^{48,49} A retrospective analysis of results in 474 patient aneurysms treated with nylon fibered coils, bare metal coils or both demonstrated a higher occlusion rate in aneurysms treated with fibered coils than in those treated with only bare metal coils.⁵⁰ These results suggest that the nylon fibers promoted more clot formation that prevented blood flow from entering IAs. Stagnant clotting models examine thrombin generation, platelet adhesion, clotting time, RBC attachment and other phenomena in real time that are challenging

or currently infeasible to analyze *in vivo*. This information provides an understanding of clot dynamics in response to coil surface material, which is an important property of treated IAs.

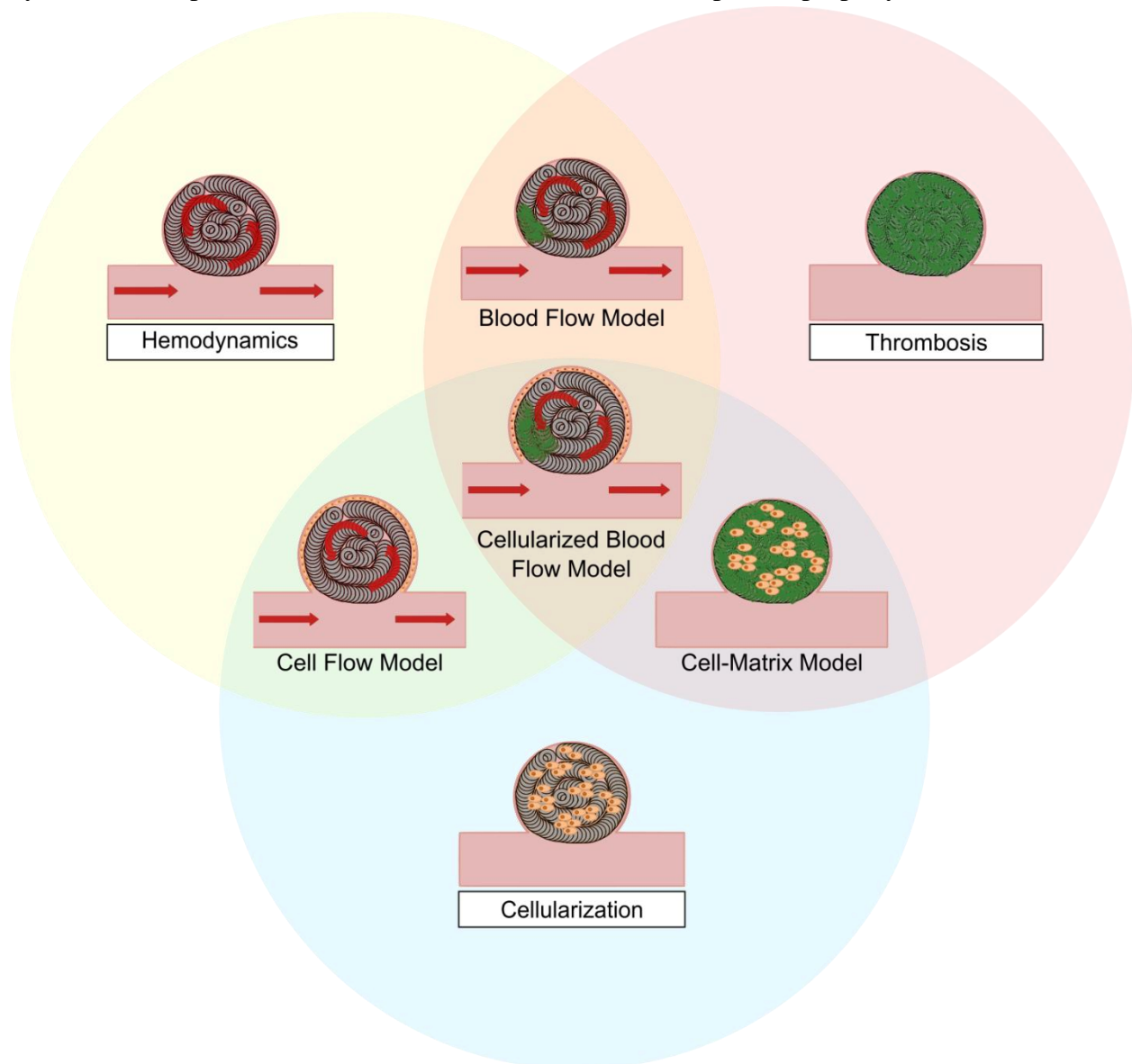


Figure 3: The three core healing aspects are isolated and modeled *in vitro*. These aspects can be combined to generate models of interactions between the key components. The models developed in this manuscript fall under the “Blood Flow Model”. All three components can ultimately be incorporated into a novel “Cellularized Blood Flow Model”. It is important to note that many different models of cellularization under flow are possible, yet the models depicted in the figure assume that adherent cells are located along the inner dome wall in models exposed to flow and are located throughout the aneurysm in the absence of flow.

1.4.2 Cellularization studies

The next phase of healing during and after initial clot formation is cellularization of the clot and coils within the IA, which is vital to stable healing and recurrence prevention. While cellularization of the aneurysm occurs throughout the entire healing process and is observable with long-term endpoints in animal studies, cellular gene and protein expression and motility of

individual cells are difficult to analyze in animal models *in vivo*. *In vitro* models are better suited than *in vivo* models for tracking individual cells. They also have the capability to isolate and analyze cell types and introduce them in co-culture models to obtain both individual cell behaviors and cell-cell interactions within and between cell types.

In vitro studies of cellularization (Figure 3, “Cellularization”) in the literature incorporate cell types including vascular smooth muscle cells (VSMCs), endothelial cells (ECs), fibroblasts, endothelial progenitor cells, and neointimal cells. These studies typically examine cell adhesion and viability in stagnant medium on coated coils, but most do not incorporate hemodynamics or interactions with fibrin clot. These studies suggest fibroblasts are most proliferative on coils coated with basic fibroblast growth factor,⁵¹ type I collagen or fibronectin,⁵² ECs are most proliferative on Cerecyte coils,⁵³ which contain polyglycolic acid fibers,⁵⁴ or on coils coated with type I collagen,⁵⁵ and VSMC coverage occurs the fastest on coils impregnated with type I collagen fibers⁵⁶ or on coils coated with ion-implanted type I collagen.⁵⁷ Some studies measure aspects of cellularization on geometries other than coils. For instance, cell density on coated platinum surfaces after high flow shear stress has been measured *in vitro* as an indicator of cell adherence.⁵⁷ Other studies assessed biomaterials as potential coil coatings by measuring cell migration towards solutions of monocyte chemotactic protein-1⁵⁸ or towards nitrogen-rich plasma-polymerized biomaterial.⁵⁹ Using short-term endpoints and live imaging, *in vitro* models of cellularization provide new information about the dynamics of cell behavior on coils that cannot be examined *in vivo*.

Analyses of how coil presence, coating, packing density and other characteristics affect cell behavior provide invaluable insight into the IA healing process and the factors that promote or inhibit IA healing. Continued expansion of these models would provide more information on individual aspects of IA healing. However, these cellularization studies, like thrombogenicity studies, are limited in that they do not account for intra-aneurysmal hemodynamics.

1.4.3 Flow dynamics studies

Thrombosis and cell biology literature show that clotting^{60,61} and VSMC,⁶² fibroblast^{62,63} and EC^{64,65} behaviors are sensitive to flow shear and pattern. During acute thrombosis, ECs and VSMCs are exposed to flow, which determines whether they promote inflammation and coagulation in the IA. EC phenotype in terms of procoagulant and proinflammatory state and SMC phenotype in terms of growth and ECM secretion also affect one another,^{66,67} and EC phenotype modulates platelet-driven clotting in the IA.⁶⁸ Additionally, ECs at the neck are exposed to flow throughout endothelialization: flow shear rate and pattern affect EC proliferation, apoptosis and monolayer barrier function that dictate the stability and progression of endothelialization across the neck. Therefore, hemodynamics plays an important role in multiple stages of the IA healing process. However, without a controlled environment where hemodynamics can be manipulated, the relationships between hemodynamics and IA recurrence

cannot be directly evaluated. Since hemodynamics fluctuates between different patient aneurysms, the study of intra-aneurysmal flow dynamics is vital to understand variability in mechanism in IA healing. Blood flow rate and IA geometry cannot be modified *in vivo* to reveal relationships between aneurysm geometry, coiling and flow pattern and velocity, so tunable *in vitro* models of coiled IAs that examine different flow rates and geometries are necessary to analyze these relationships.

Due to the importance of IA hemodynamics to recurrence, it is not surprising that the largest category of *in vitro* IA models in the literature is those that characterize flow patterns within saccular aneurysms (Figure 3, “Hemodynamics”). Most of these studies measure the wall shear stress and velocity distributions throughout IAs with different geometries and sizes,^{8,9,36,69} parent vessel characteristics,^{69–71} coil arrangements and coil packing densities.^{10,11,72} These studies are often conducted using particle image velocimetry within a polymer aneurysm model or computational methods to simulate blood flow; some studies use both to determine the accuracy of the computational model. They provide relationships between hemodynamics and IA characteristics that combined with information about how similar flow patterns dictate fibrin polymerization, platelet phenotype and vascular cell behavior, prove useful in predicting how the course of IA healing will be affected. In cases where patient information is used to calculate the aneurysm dimensions, shear stress distributions are correlated to incidence of rupture^{9,36,69} or recanalization⁷³ in order to better understand how flow dynamics affect patient outcome. With this information, optimal treatment strategies can be identified that are specific to IA geometry. For example, given an IA with a specific location, dimension and parent vessel size, a physician may better evaluate whether the IA should be coiled and with what coil configuration, and if the patient is at high risk for recurrence. A few hemodynamics models have stepped further to include thrombus formation or cell behavior to more directly evaluate how flow patterns affect aspects of IA healing.

Few *in vitro* studies evaluate the relationship between intra-aneurysmal flow dynamics and thrombosis (Figure 3, “Blood Flow Model”) or EC behavior (Figure 3, “Cell Flow Model”). Hemodynamics and subsequent thrombus formation were investigated in a computational model of thrombosis in a saccular IA that was treated with a flow diverter.⁴⁵ Using a series of biochemical reactions to model the different stages of fibrin polymerization under flow, the study revealed a theoretical progression of three-dimensional clot development in a variety of IA sac morphologies, with and without coils. Although the study does not explore coiling, it provides a controlled system that predicts thrombosis rate and occlusion and begins to elucidate relationships between IA dimensions (i.e. size and aspect ratio), hemodynamics and thrombosis. Another computational model provides information regarding platelet and red blood cell accumulation in an IA with a given geometry and flow rate, which indicates the location and structure of IA thrombus formation.⁴⁶ A platelet-rich clot is degraded more slowly than a more fibrin-rich clot,⁷⁴ so IA clot structure predicted by the model provides information about the

potential rate of clot fibrinolysis and cell-mediated thrombus reorganization into tissue. Both of these models predict properties of thrombus formation in response to IA characteristics and hemodynamics that provide insight into cellularization and tissue formation. However, these computational models are predictions of how clot would form in an IA; a model with complete blood biochemistry *in vitro* is necessary to fully elucidate the relationships between hemodynamics and clotting in patient IAs.

Thrombosis under flow *in vitro* was analyzed in a silicone model sidewall aneurysm that was treated with a flow diverter and perfused with recirculating whole blood.⁷⁵ Although this study did not examine coiling, it is the only *in vitro* model of thrombosis in an IA under flow. A glycerol-water blood substitute was used to define the velocity profiles within aneurysms that were treated with diverters of different porosities, while whole blood clots were formed and dissected for clot structure in a parallel experiment. Velocity magnitude and clot red blood cell content were decreased with increased flow diverter porosity. This study provides insight into the relationship between velocity profile and structure of acute clot formation in aneurysms treated with flow diverters. These initial clotting time points would be more costly to observe in animal models and are not widely examined in the literature to date. While computational models of thrombosis and hemodynamics can quickly and relatively inexpensively predict clotting mechanism based on hemodynamics, *in vitro* models are necessary to confirm these predictions. With a better understanding of clotting mechanism in IAs, optimal personalized treatments can be prescribed that are dependent on IA geometry, location, and other characteristics.

EC morphology and its correlation to location and wall shear stress in a saccular bifurcation IA were evaluated in an endothelialized aneurysm model *in vitro*.⁷⁶ A compliant aneurysm was modeled based on patient image data, constructed, lined with ECs and perfused with cell medium. ECs in the sac had the same morphology as those cultured in the absence of flow, while ECs in the parent vessel had an elongated morphology. This indicates that EC intracellular signaling in the IA dome wall was responsive to slow circulating intra-aneurysmal flow, producing new information about relationships between cell behavior and flow dynamics that are specific to IA geometry and intra-aneurysmal flow patterns. The addition of coils to this model would also provide valuable information regarding how coil-mediated hemodynamics impacts EC phenotype and coil endothelialization. *In vitro* models that incorporate the effects of IA flow dynamics on processes in IA healing can elucidate the sensitivity of these processes to variables such as flow pattern that are specific to IAs.

In vitro models of IA flow dynamics provide information about how aneurysm characteristics and treatments dictate intra-aneurysmal hemodynamics and in some models, how these relationships affect clot formation or cell behavior. This information would be more difficult and expensive to obtain *in vivo* and can help guide optimal treatment of specific aneurysms. Although the aforementioned models reveal direct relationships between IA hemodynamics and

clotting or EC behavior, they are a minority in the field of *in vitro* IA models, and none of the hemodynamics models in the literature to date investigate the thrombogenicity or cell compatibility of coil design or material. Hemodynamics models, like coil thrombogenicity and cellularization models in the literature, are limited. Combining these models with technologies available in related fields would produce *in vitro* systems that better recapitulate *in vivo* human IA conditions, and allow a better understanding of treatment effectiveness and optimal design. IA *in vitro* models are incomplete in that they do not identify the relationships between hemodynamics, thrombosis and cell behavior, which are vital to IA healing.

The extension and continued development of these *in vitro* models would produce information important to the field of IA healing. However, existing models can be improved in order to better understand complex IA healing phenomena, namely how IA hemodynamics drives thrombosis and cellularization, and the relationships between them. A larger variety of *in vitro* models that recapitulate aspects of human IA healing are necessary to supplement animal models, *ex vivo* samples and computational models in order to elucidate mechanisms that drive complete IA healing and the variability in individual IA healing, to determine how coil treatments fail and to screen new coil designs.

1.5 IN VITRO MODELS OF THROMBOSIS UNDER FLOW

Acute clot accumulation and structure are important to cellularization during IA healing since the clot provides an initial scaffold for cellularization and tissue formation.³ Additionally, fibrous matrix structure influences EC behavior,⁷⁷ EC phenotype affects clotting,⁶⁸ and fibrinogen concentration influences fibroblast behavior,⁷⁸ indicating that acute clot structure also influences vascular cell infiltration and coverage, and vice versa, in IA healing. Nevertheless, it is unclear why thrombus frequently does not reorganize into tissue in patient IAs,^{4,29} underlining the need for models that perturb IA thrombosis in order to elucidate the factors that drive it.

In vitro models of thrombosis under flow in fields outside of IA healing provide insight into the factors that likely facilitate clot structure and accumulation in IAs. Low wall shear stress allows the formation of more fibrin fibers than high wall shear stress, which promotes platelet-rich clots.⁶¹ Fibrin fiber morphology under flow is also modulated by wall shear stress.⁷⁹ Zones of recirculating flow patterns promote clot accumulation.⁸⁰ These findings point to a relationship between flow pattern and thrombosis in saccular IAs. Therefore, since blood flow rate and flow pattern in IAs are influenced by coil placement¹¹ and increased packing density,¹⁰ coil-mediated regulation of blood flow into the aneurysm likely modulates clot formation and structure.

A better understanding of the relationship between intra-aneurysmal hemodynamics and clotting in coiled saccular IAs would provide information about acute IA healing *in vivo*. In addition, an understanding of the clot structure on coils would provide insight into long-term clot and coil

compression, clot degradation and clot suitability for cell infiltration and remodeling. *In vitro* models of IA thrombosis under flow are necessary to elucidate these phenomena in IA healing.

1.6 OBJECTIVES AND APPROACH OF THE STUDY

In this work, three types of *in vitro* models were developed. Models of clotting on coils without (Figure 3, “Thrombosis”) and with (Figure 3, “Blood Flow Model”) arterial flow were developed in order to evaluate if flow shear is required to reproduce aspects of clot structure *in vivo*. A model of clotting on coils was developed that captures some of the hemodynamics at the neck of a coiled bifurcation IA. This model was designed to focus on clotting at the neck, since the neck is an area likely to recanalize in IA recurrence. This model assumes that the sac of the IA is fully packed with coils. Another model was developed in which clot formation occurs around coils in a sac similar to that of a bifurcation IA. This model allows the analysis of complex hemodynamics present within the IA dome and evaluates the effect of local packing densities and irregular coil designs on hemodynamics and subsequent clotting.

Using these models, three hypotheses were evaluated in this work:

- 1) Flow is necessary to recapitulate clot structure seen in *ex vivo* human IAs and to identify differences in performance of different coil arrangements and designs.
- 2) Coil arrangements with high local packing densities promote space-filling clot formation.
- 3) Coil designs that create disturbed flow patterns promote space-filling clot formation.

The investigation of these hypotheses will be described in Chapters 2, 3 and 4, respectively.

1.7 SIGNIFICANCE OF THE STUDY

These models are the first to examine the dynamics of acute thrombosis in a coiled saccular bifurcation IA. They provide novel methods that were utilized to better understand the relationships between intra-aneurysmal hemodynamics and clot rate, structure and spatiotemporal dynamics in coiled saccular IAs. They also provide new methods to rapidly screen new coil treatments before use in animal studies. This work is the first to examine the effectiveness of a novel coil design in impinging the flow field and promoting thrombosis, and the first *in vitro* study of the effect of coil arrangement on hemodynamics and thrombosis.

This work contributes new information to the field of IA healing that will contribute to existing perceptions of coil design development, coil placement during surgery, and the importance and contribution of *in vitro* models to understanding IA recurrence. With the combined use of tools including *in vitro* models, animal models, computational models, clinical experiences and *ex vivo* samples, we can understand what causes specific IAs to recur and work to prevent it.

CHAPTER 2: FLOW AND STASIS CLOTTING MODELS

Clotting flow models aren't mainstream enough: Shear flow is required to simulate physiological clotting and observe differences in thrombogenicity of coil designs

2.1 RATIONALE

Coil design has not changed significantly since its introduction in 1991.¹⁶ Small modifications, including hydrogel coating²⁰ and metal softening,²³ have been introduced with the goal of increasing coil packing in order to slow the inflow of blood, thereby promoting stable clots that lay the foundation for cellularized tissue. Stent modifications have been introduced that perform the opposite function: reducing clot formation within the diseased lumen. These developments in the stent literature can be applied to endovascular coils. Specifically, stent struts with micron-level surface irregularities increased platelet accumulation, clot formation, and intimal hyperplasia in atherosclerotic arteries.^{81,82} Additionally, endothelial cells were sensitive to stent strut edge angle under flow,⁸³ indicating that platelets may also be responsive to edge geometry. Acoustic radiation force microscopy techniques⁸⁴ were used in a preliminary study that suggests faster clotting occurs near the coil than away from it (Figure 4). These studies together suggest that modifications to coil wire shape and surface roughness may promote clot formation in a coiled IA.

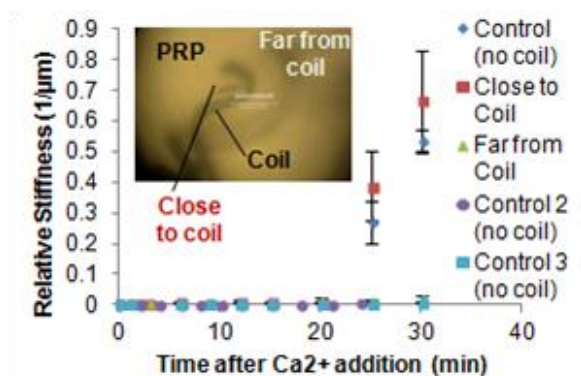


Figure 4: Preliminary acoustic radiation force microscopy study of clotting on a coil. Relative PRP clot stiffness increases faster close to coils than away from coils. Inset shows relative measurement locations.

Many *in vivo* and computational studies have demonstrated the importance of high packing density to IA healing. Higher packing densities slow blood flow in the IA¹⁰ and reduce recurrence in humans⁸⁵ and animal models.⁸⁶ Also, thrombosis is known to depend on flow rate and pattern,^{60,61} however, most coil thrombosis studies *in vitro* are conducted in the absence of flow.^{48,49} Therefore, since the literature suggests that edged wire, surface irregularities and increased packing density promote thrombosis, an *in vitro* stasis clot model was used to test the thrombogenicity of packed coils and novel coil designs.

In order to test the effect of flow on coil thrombogenicity, a flow chamber was developed and constructed that imitates some aspects of hemodynamics at the neck of a coiled saccular bifurcation IA. A bifurcation model was selected due to the oscillating flow patterns and higher recurrence rates in bifurcation IAs compared to sidewall IAs.^{87,88} The neck was chosen because EC coverage of the neck is one of the markers of an IA that is protected from recurrence.³ Clot coverage and structure at the neck is likely to affect cellularization^{77,89-91} and subsequent IA healing and is therefore important to examine in this study.

The study in this chapter tests the hypotheses that (1) edged and braided wire promote platelet adhesion and increased space-filling fibrin formation compared to clinical coils, and (2) flow shear is necessary to recapitulate clot structure *in vivo*. The results of this study may drive the future design of coils and coil thrombogenicity models *in vitro*.

2.2 METHODS

2.2.1 Coil preparation

Ribbon coils and rectangular wires (Figure 5) were obtained from MicroDyne Technologies (Plainsville, CT). Ribbon coils (Figure 5, “Ribbon”) were constructed from two layers of wires with a 25 μm by 75 μm rectangular cross-section and smooth surfaces that were coiled to generate an outer diameter of approximately 400 μm . To create braided coils (Figure 5, “Braided”), wires with a 23 μm by 230 μm rectangular cross-section were supercoiled such that an indentation was made in the metal approximately every centimeter. These wires had micron-sized surface irregularities that produced rough surfaces (Figure 5, “Braided” inset). Three supercoiled rectangular wires of equal length were braided. Commercially available aneurysm coils were used for the “clinical coil” condition (Figure 5, “Clinical”). All coils were soaked in 70% ethanol for 1 hr and dried overnight in a biosafety cabinet before each experiment. Coils were adhered to a 12 mm round glass coverslips (Ted Pella Inc., Redding CA) for SEM imaging, 24 mm² No. 1.5 glass coverslips (Corning) or a 4-well Lab-Tek chambered glass slide (ThermoFisher Scientific) with one or two 2-5 μL drops of clear nail polish per sample. Samples were allowed to dry overnight in a biosafety cabinet.

Wire cross section:



Coil shape:

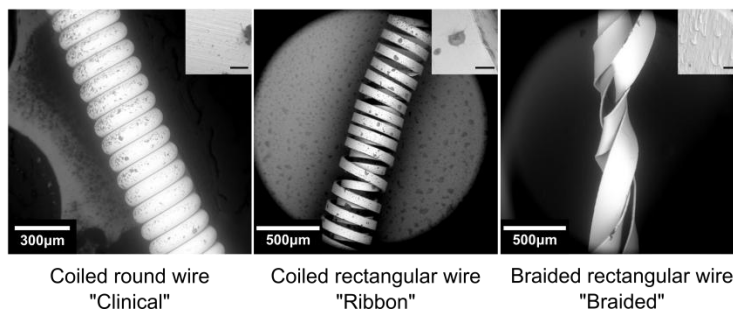


Figure 5: Representative SEM images of coil and wire types used in the study. Inset shows the surface roughness of wire used in each coil type. “Clinical coils”, which are used clinically, consist of a smooth wire with a round cross-section that is coiled. “Ribbon coils” consist of a smooth wire with a rectangular cross-section that is coiled. “Braided coils” consist of rough wires with a rectangular cross-section that are braided. Inset scale bar, 5 μm .

2.2.2 Clot formation without flow

The UVa Institutional Review Board approved all protocols for blood donations (IRB-HSR Protocol No. 17524). Whole blood from healthy volunteers was drawn into 1.8 mL 0.109 M

buffered sodium citrate vacuum-sealed tubes (BD) and immediately centrifuged at 100×g for 20 min. The top layer of platelet-rich plasma (PRP) was collected from each tube and mixed by slight stirring with a pipette tip. Oregon green-tagged fibrinogen (Molecular Probes) and CaCl₂ were added to PRP to 0.010 mg/mL and 20 mM final concentrations, respectively. 10 μL of PRP solution was immediately added to each sample in 100% relative humidity. 75 μL of PRP solution was added to each coil ball sample. Clots formed for 2 hr at room temperature and then were imaged using confocal microscopy. After imaging, samples were fixed in 4% paraformaldehyde (PFA) for 20 minutes and rinsed in phosphate-buffered saline without calcium or magnesium ions (PBS) before preparation for SEM imaging.

2.2.3 Flow chamber and coil preparation

Polycarbonate chambers (Marlin Tool Inc., Cuyahoga Falls, OH) and tubing were rinsed in de-ionized water, dried, and coated by circulation of 2.5% (w/v) bovine serum albumin (BSA) in modified HEPES-Tyrode's buffer without phosphate or calcium ions (HT buffer)^{74,92} at 5 mL/min for 6 hr. Chambers and tubing were rinsed in 20 mL PBS at 7.5 mL/min. Chambers and tubing were dried overnight. Immediately before each experiment, chambers and tubing were coated by circulation of 30 U/mL heparin in HT buffer at 5 mL/min for 2 hr and then rinsed with 20 mL PBS at 12 mL/min. A 1 cm long coil was placed against the island support, and the systems were primed with PBS.

2.2.4 Recirculating flow experiments

Whole blood from healthy volunteers was drawn directly into 30-cc syringes pre-loaded with 12 mL PBS and simultaneously mixed to dilute the whole blood to 50%. To slow clotting to an observable rate, this mixture was further diluted to 25% in PBS and immediately centrifuged at 100×g for 20 min. The top layer of diluted PRP was collected from each tube and mixed by inversion. Oregon green-tagged fibrinogen (Molecular Probes) was added to PRP to 0.005 mg/mL final concentration. PRP was immediately transferred to flow chambers via syringe at 7.5 mL/min, and flow and confocal imaging were initiated (in stasis experiments within the chamber, flow was not initiated). After 17 minutes of recirculating flow, chambers were perfused with PBS for 10 minutes at 12 mL/min to remove excess fibrinogen, fixed in 5 mL 4% PFA for 20 minutes, rinsed in 10 mL PBS at 12 mL/min, and imaged using confocal microscopy. PRP was used to imitate whole blood, as previously described,⁹³ because it is less opaque and more suitable for optical measurements.

2.2.5 Scanning electron microscopy (SEM) preparation

After confocal imaging, 12 mm coverslips with adhered clotted coils were rinsed in solutions of increasing ethanol concentration in water (25% to 100%) and dried in a critical point dryer (Advanced Microscopy Facility, UVA). Samples were immediately imaged using SEM.

2.2.6 Image analysis

Confocal images were analyzed using ImageJ.⁹⁴ Fibers were segmented from background and overlaid with the original image to ensure consistent and accurate fiber coverage using the following steps. Visible pixels were adjusted to that the minimum intensity value was just larger than the first peak in the histogram. The maximum intensity value was set to half of the difference between the maximum intensity in the histogram and the second peak in the histogram. The image was set to 8 bit type. An Unsharp Mask Filter was applied with a radius of 4 pixels and mask weight of 0.6. A Bandpass Filter was applied that filtered large structures down to 100 pixels and small structures up to 1 pixel, with no stripe suppression, 5% tolerance of direction, autoscaling and image saturation. The image was then thresholded via the Percentage algorithm with dark background. The mask was created by using the Analyze Particles macro, sizes 0 to infinity and circularity 0 to 0.4, showing masks. The mask was then overlaid with the original image to ensure that 5 to 10 fiber segments of the original image were not present in the mask. If not, the thresholded level was adjusted by 6 to 12 intensity levels. In this way, all of the masks were equally accurate to their originals, while preventing false positives, i.e. the creation of masks that were denser than their originals. Fiber density was calculated as a percent of the total area. Only areas outside of the metal surfaces were measured in order to eliminate light reflections off of the metal. Average fiber density was calculated from at least three images from different randomly selected locations in the sample. The OrientationJ plugin⁹⁵ was also used to compare fiber orientation between images.

2.2.7 Statistical analysis

At least three replicates were analyzed for each condition in the stasis model. Two-way ANOVAs, one-way ANOVAs and student's t-tests were used to evaluate variability within and between groups.

2.3 RESULTS

2.3.1 Coil design and coil packing did not modify clot structure in the absence of flow

Edged, smooth wires that have rectangular cross-sections were coiled to create a "ribbon coil" design similar to clinically available coils that are made up of coiled round smooth wires that have a circular cross-section (Figure 5). Rectangular wires with surface irregularities that produced rough surfaces were braided to create an irregular secondary coil structure with pockets where platelets and fibrin may accumulate.

Fluorescent images of clot mesh that had formed around each sample were segmented, converted into binary masks, and used to calculate fiber density (Figure 6A). Fiber density was found to be similar across all conditions (Figure 6B, $p=0.18$). In order to determine if this trend in clot structure is the same for all blood donors, fiber density was calculated in clots formed around all coil and wire types (Figure 7A) for four different donors. Fiber density across all conditions was similar for each donor ($p=0.94$); however, there was a significant difference between donors

($p < 0.05$, Figure 7B). SEM images of clots indicate no difference in fiber structure between the conditions (Figure 8).

2.3.2 IA-like hemodynamics were required to reproduce physiological clot structure

In order to evaluate the importance of flow in clot formation in coiled aneurysms, a parallel plate flow chamber was designed to expose coils to flow patterns mimicking those at the neck of a bifurcation saccular aneurysm (Figure 9A). An island in the middle of the chamber divided flow to create a bifurcation and supported the coil during flow. Flow leading up to the supported coil was laminar and fully developed. Inlet flow velocity was 1.6 cm/s.

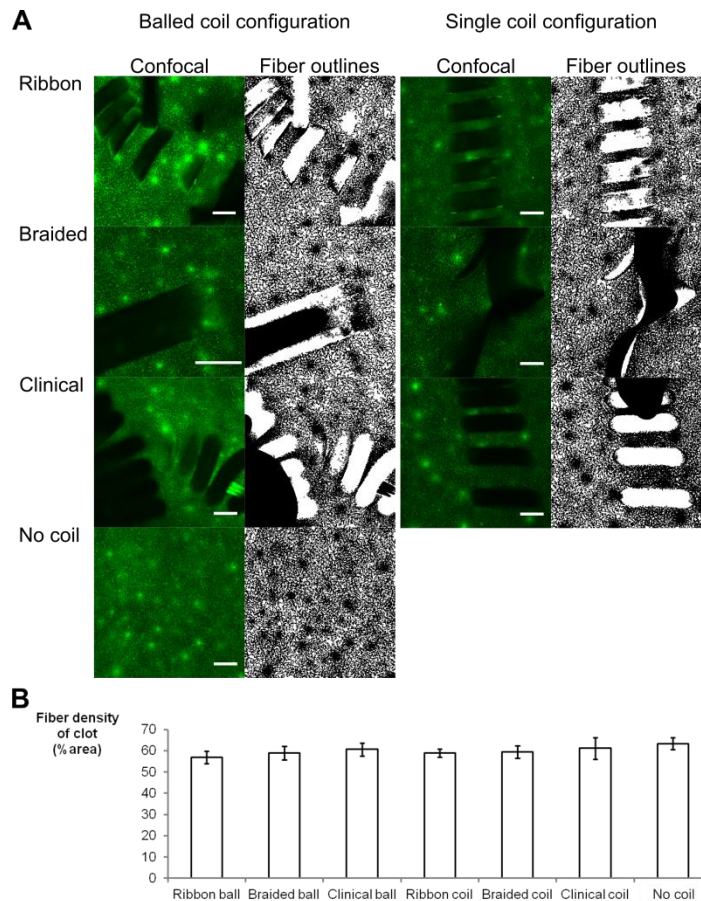


Figure 6: A: Representative fluorescent confocal images and segmented fibers for each condition. Clots were formed in the presence of clinical coils, ribbon coils and braided coils, and in the absence of coils. Clots were formed in the presence of either a single coil or multiple coils balled together to increase coil packing. Scale bar, 100 μm . B: Fiber density of the clot was insensitive to sample type (one-way ANOVA, $p=0.18$).

Clot formation in the flow chamber was compared in the presence and absence of flow. Clots that formed on 1 cm long clinical coils after 20 minutes of PRP flow at 200 s^{-1} shear rate were heterogeneous, clustered, and confined to the coil periphery (Figure 9B, “ 200 s^{-1} shear rate”). PRP clots that formed in the absence of flow were more uniform in fiber density and covered a large area around the coil (Figure 9B, “No flow”). Clots formed during fluid flow more closely

resembled thrombus formed around coils *in vivo*⁹⁶ than the more uniform clots formed in stasis, so subsequent coil clotting experiments were performed under flow.

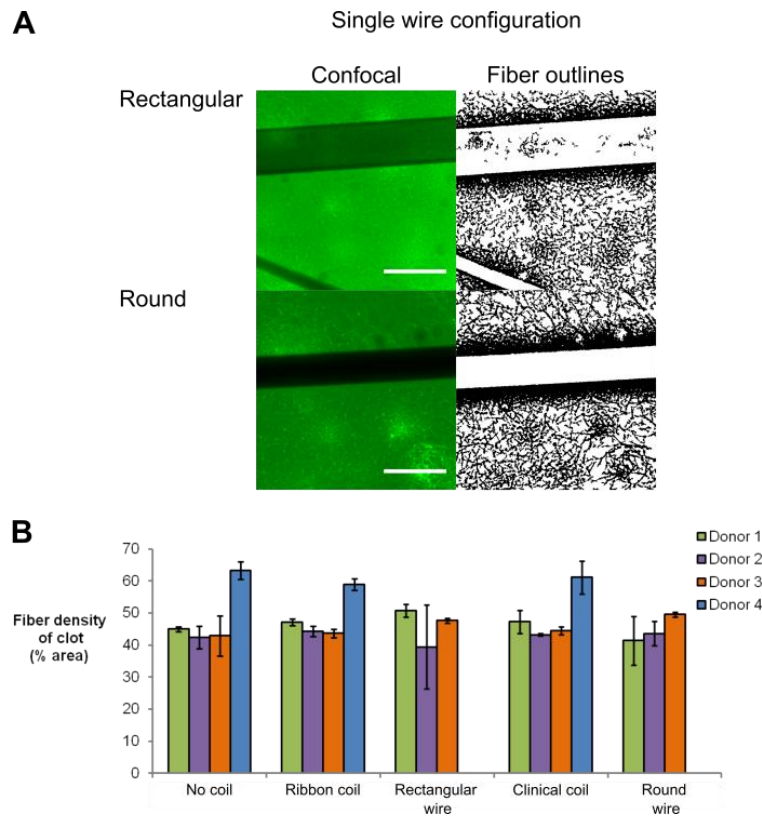


Figure 7: A: Representative fluorescent confocal images and segmented fibers for each single wire sample condition. Clots were also formed in the presence of a single wire of each type. Scale bar, 100 μm . B: Fiber density was insensitive to sample type for each donor (two-way ANOVA, $p=0.94$). There was significant variability between donors (two-way ANOVA, $p<0.05$).

2.4 DISCUSSION

This study demonstrates that novel models of endovascular coil clotting under flow are necessary to recapitulate clot structure observed in coiled IAs. This is consistent with *in vitro* thrombosis studies showing that clot structure is dependent on shear stress and flow velocity.⁶¹ Clots that formed in the absence of flow were characterized by similar fiber densities regardless of coil presence, shape, packing, secondary shape and wire shape. Yet coil packing and presence impact recurrence rate^{85,86} and flow velocity¹⁰ within IAs. Therefore, since coil packing impacts clot structure, but clot structure was similar for different packing densities, the stasis clot model may be insufficient to reveal differences in clot structure that form around coils with different packing densities in aneurysm models *in vivo*. In this study, fibrin formation was also insensitive to surface roughness and wire shape in the absence of flow. However, studies that demonstrated platelet dependence on surface roughness^{81,82} and endothelial cell dependence on strut angle⁸³ were conducted under flow, indicating that clot formation in the flow chamber (but not the stasis

model) may be sensitive to surface roughness and wire shape. These results guided the development of subsequent studies that are detailed in Chapters 3 and 4.

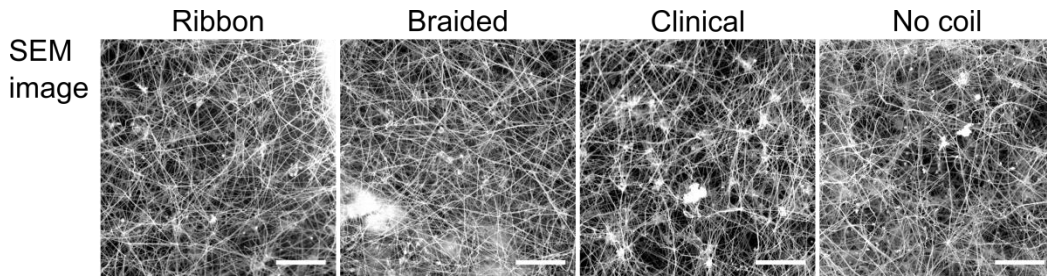


Figure 8: Representative SEM images of clots formed in each coil condition. There were no differences in structure between sample types. Scale bar, 10 μm .

The preliminary acoustic radiation force microscopy study described in Figure 4 indicated that clot located close to the coil formed and became stiff faster than clot located away from the coil. Results from the study detailed in this chapter indicate that clot structure was insensitive to coil presence in the absence of flow, but the timing of clot formation was not observed or measured. These results suggest that the rate of clot formation, but not clot structure, may be dependent on coil presence in the absence of flow. It is also possible that the ultrasound pulses used in the

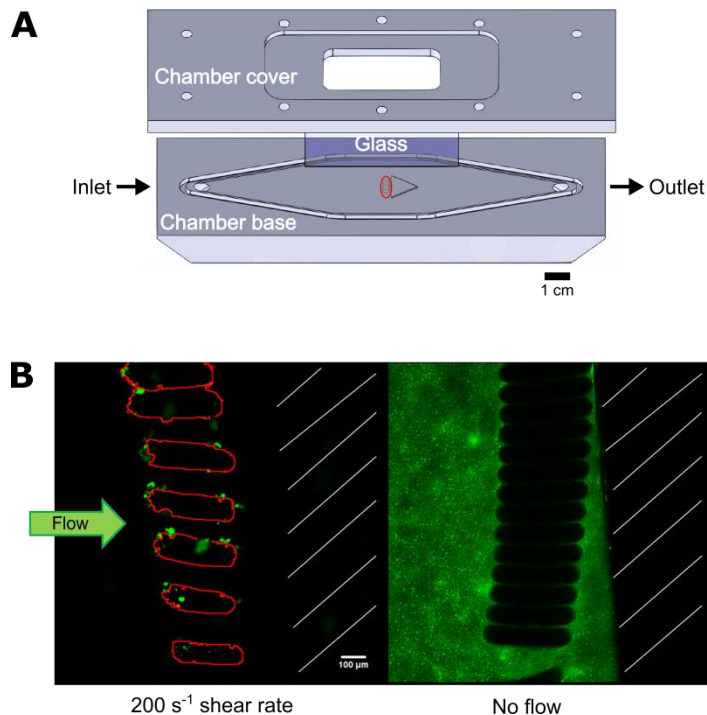


Figure 9: A: Schematic of neck IA model flow chamber. Coils (red) are placed against the island and PRP is perfused through the chamber. Scale bar, 1 cm. B: Flow shear rate modulates clot morphology in flow chamber. Clot (green) is more heterogeneous, smaller and isolated to the coil (red outline) under flow (left), compared to clots formed without flow (right). A green arrow indicates the direction of PRP flow. Both clots were formed in the neck model. Scale bar, 100 μm .

acoustic radiation force microscopy study may have been sufficient to perturb the clot closest to the coil surface, causing shear forces that affected clot rate.

The results from this study suggest that flow is necessary to reproduce clots similar to those observed *in vivo*. However, this study has limitations. The shortcomings of the flow chamber model itself will be addressed in Section 5.2, but there are additional limitations specific to this study. First, in the stasis model, nail polish was used to anchor the coils and prevent clot structure disruption caused by coil movement during handling but contains volatile compounds that are not typically used in thrombosis models. The nail polish was allowed to dry overnight to reduce these volatile compounds. Moreover, the same amount of nail polish was used for all conditions in each of the ball, single coil and single wire studies, and no nail polish was used in the absence of coils. Since fiber density was similar with and without coils, and consequently with and without nail polish, the dried nail polish likely had minimal effect on clot structure. In the flow chamber model, clot that formed on the coil under flow was more similar, but not identical, to clot that formed *in vivo*. This result may be at least partly due to the differences in blood chemistry and geometry between the model and IAs *in vivo*. Nevertheless, the model demonstrates the importance of flow in understanding coil performance and thrombogenicity. While it is not an identical representation of clotting in bifurcation IAs *in vivo*, the flow chamber model is sufficient to reveal differences in clotting under different shear conditions, which contributes new information to the field about coil thrombosis.

The neck flow chamber model and stasis clot model provide new information about the impact of flow shear on clotting around coils. The flow chamber model developed in this study measures the spatial and temporal clot development around coils and its dependency on flow shear rate, which cannot be observed in animal or computational models. The model provides new information that supplements resected *ex vivo* human IAs and animal and computational models and in order to better understand the relationships between IA hemodynamics and clot formation, which will help guide the development of better coil designs.

2.5 CONCLUSIONS

The study indicates that shear flow is necessary to reproduce physiological clot structure in models of coiled saccular bifurcation IAs. Clot structure in the absence of flow was insensitive to coil presence, packing, secondary shape, or wire shape. This result is in contrast with studies *in vivo* indicating that coil presence indicating that coil packing affects initial IA occlusion⁹⁷ and late recurrence,⁸⁵ suggesting that flow models are necessary to reveal trends in coil performance in IAs.

CHAPTER 3: COIL ARRANGEMENT MODULATES HEMODYNAMICS AND CLOTTING

Coil arrangement can turn the tides: Coil arrangements with local high packing density promote clotting in a coiled IA model *in vitro*

3.1 RATIONALE

Coil placement¹¹ and increased packing density¹⁰ influence blood flow rate and pattern in IAs, and flow rate and pattern modulate clot progression and structure.^{61,79} Therefore, coil regulation of blood flow within the aneurysm likely modulates clot formation. Clots formed during PRP flow in Chapter 2 more closely resembled thrombus formed around coils *in vivo*⁹⁶ than the more uniform clots formed in stasis, indicating that flow is required to produce physiological clot structure. However, the relationship between coil-dependent hemodynamics and intra-aneurysmal thrombosis has not been directly evaluated.

In this study, an *in vitro* bifurcation IA model was used to examine the sensitivity of thrombosis to clinical coil placement at the neck and in the dome. We hypothesized that clinical coil arrangements that create high local packing density promote faster, space-filling clot formation. The analyses in this study provide new information about coil impingement on the flow in a saccular bifurcation IA and its relationship to acute thrombosis. This information is a step towards understanding acute healing and coil treatment efficacy, which will help drive future coiling techniques.

3.2 METHODS

3.2.1 Flow chamber and coil preparation

See Section 2.2.3: *Flow chamber and coil preparation*. Commercially available platinum aneurysm coils (“clinical coils”) were used. A total of 33 mm of coil length, including a 12 mm framing coil, was used in each coiled sample. Linearly arranged filling coils were cut into 6 to 8 sections that were 2 to 4 mm long. Circumferentially arranged filling coils were cut into 3 to 4 sections that were crimped by hand using forceps to assume curved shapes. Instead of ethanol cleaning, all coils were washed for 20 minutes in piranha wash (1 part 30% H₂O₂, 3 parts H₂SO₄) and rinsed in three tap water washes for 5 minutes each, then three deionized water washes for 5 minutes each, 24 hours prior to each experiment. For single-pass flow experiments, chambers (Figure 10) and tubing were rinsed and primed with modified

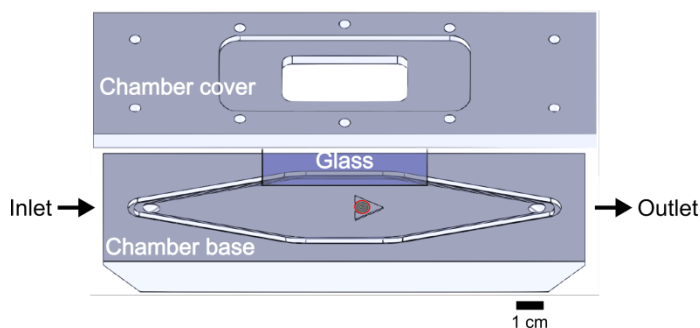


Figure 10: Schematic of sac IA model flow chamber. Coils (red) were placed inside a hole in the island and PRP was perfused through the chamber. Scale bar, 1 cm.

HEPES Tyrodes' buffer (HT buffer) instead of phosphate-buffered saline without magnesium or calcium ions (PBS) to prevent calcium phosphate precipitation during clotting, and a reservoir was also coated with bovine serum albumin (BSA) and heparin in the same way as the chambers and tubing.

3.2.2 Recirculating flow experiments

See Section 2.2.4: *Recirculating flow experiments*. Table 1 describes PRP flow conditions tested in this study. Red blood cells (RBCs) labeled with DiI (Sigma) were added to platelet-rich plasma (PRP) before flow at 500 cells/ μL final concentration. DiI-RBCs acted as flow tracers in image analysis. Coils were placed by inserting the framing coil first, then inserting filling coils.

Table 1: PRP flow conditions in Chapter 3

Model type	Sac model	
Flow type	Single-pass flow	Recirculating flow
PRP flow time	4 minutes	17 minutes
Buffer perfusion time	15 seconds or 10 minutes	10 minutes

3.2.3 Single-pass flow experiments

Whole blood from healthy volunteers was drawn directly into 60-cc syringes pre-loaded with 5.5 mL buffered sodium citrate and simultaneously mixed to 0.0109 M final sodium citrate concentration. Blood was immediately centrifuged at $100\times g$ for 20 min. The top layer of PRP was collected from each tube and diluted to whole blood concentration in HT buffer. Oregon green-tagged fibrinogen (Molecular Probes) was added to PRP to 0.005 mg/mL final concentration. Red blood cells labeled with DiI were added to PRP at 500 cells/ μL final concentration. CaCl_2 in water was added to PRP at 20 mM final concentration,⁹⁸ PRP was mixed by inversion and immediately transferred to the chamber reservoir, and flow and confocal imaging were initiated. Once PRP in the reservoir was depleted, chambers were perfused with PBS for 10 minutes or 15 seconds at 12 mL/min, fixed in 5 mL 4% (w/v) PFA, rinsed in 10 mL PBS at 12 mL/min and imaged. Table 1 describes PRP flow conditions tested in this study.

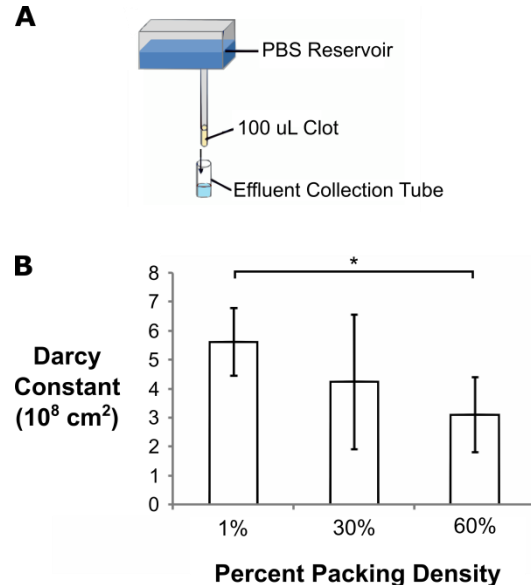


Figure 11: A: Diagram of permeability assay setup. B: Darcy constant as a function of coil packing density. As the packing density of clots increased, the permeability decreased. $*p < 0.005$, $n = 28$.

3.2.4 Scanning electron microscopy (SEM) preparation

Coils were removed from chambers post-imaging and rinsed in solutions of increasing ethanol concentration in water (25% to 100%), then in 50% hexamethyldisilazane (HMDS) in ethanol and finally in 100% HMDS.⁹⁹ Coils were dried overnight and imaged using SEM.

3.2.5 Image analysis

Confocal images were analyzed using ImageJ.⁹⁴ Clot area was calculated by selecting the pixels with grayscale intensity higher than the 97.5th percentile of the background intensity distribution (background regions were manually selected in ImageJ). Total aneurysm area was identified by isolating the aneurysm sac boundary and manually eliminating artifacts caused by laser reflections from the metal. Clot size was calculated as the percentage of total aneurysm area (in pixels) that was composed of clot (in pixels). DiI-RBCs were manually tracked using the Manual Tracking plugin.¹⁰⁰ Velocities, heat maps, and vector plots were calculated in MATLAB. Modified quiverc¹⁰¹ functions were used to generate color-coded vector plots.

3.2.6 Clot permeability experiments

For permeability experiments, 316 stainless steel wire was used to mimic coils. Three levels of packing were tested: 1, 30, and 60% of 100 μ L total clot volume. The mass of wire was calculated based on metal density (8 g/cm³). Wire was inserted into open-ended tubes. Whole blood from healthy volunteers was drawn into sodium citrate vacutainer tubes and centrifuged for 20 minutes at 100 \times g. PRP was collected and incubated with CaCl₂ at 10 mM final concentration then transferred to the packed open-ended tubes and allowed to clot for 2 hr in a humidified chamber. The tubes were connected to a reservoir containing PBS, which was positioned so that gravitational flow through the clot occurred at a pressure drop of 980 Pa (Figure 11A). The volume of effluent that passed through the column in 20 minutes was used to calculate the Darcy constant (K_s) using the following equation:¹⁰²

$$K_s = \frac{Q \cdot L \cdot \eta}{t \cdot A \cdot \Delta P}$$

where Q is the total volume of effluent collected, L is the total length of the clot (1.5 cm), η is the viscosity of PBS (1.05 x 10⁻² poise), A is the cross-sectional area of the clot (0.0225 cm²), and ΔP is the pressure drop across the clot (980 Pa). The Darcy constant measures the effective surface area of the clot that allows fluid to flow through the fibrin network, which corresponds to a measure of clot permeability.

3.2.7 Statistical methods

Preliminary power analyses based on clot size require a minimum of six replicates per coiled sac condition, allowing 5% and 20% probabilities of Type I and Type II errors, respectively. At least six replicates were analyzed for each coiled condition and at least three replicates were analyzed for the no-coil condition in both models. Two-way ANOVA and student's t-tests were used to evaluate variability within and between groups, respectively.

3.3 RESULTS

3.3.1 Increased coil wire packing reduced clot permeability

To measure the ability of increased coil packing density in clots to impede blood flow, Darcy permeability was measured in clots formed around different packing densities of coil wire (1, 30, and 60%). The data show that increasing the wire packing density in PRP clots resulted in lower permeability values (Figure 11B): permeability of the 60% density clots was 44.6% less than that of the 1% density clots ($p < 0.005$, $n = 28$).

These data suggest that areas of high packing density in the aneurysm sac facilitated the formation of clots that were less permeable to blood flow. These results guided the development of coil arrangements in subsequent experiments.

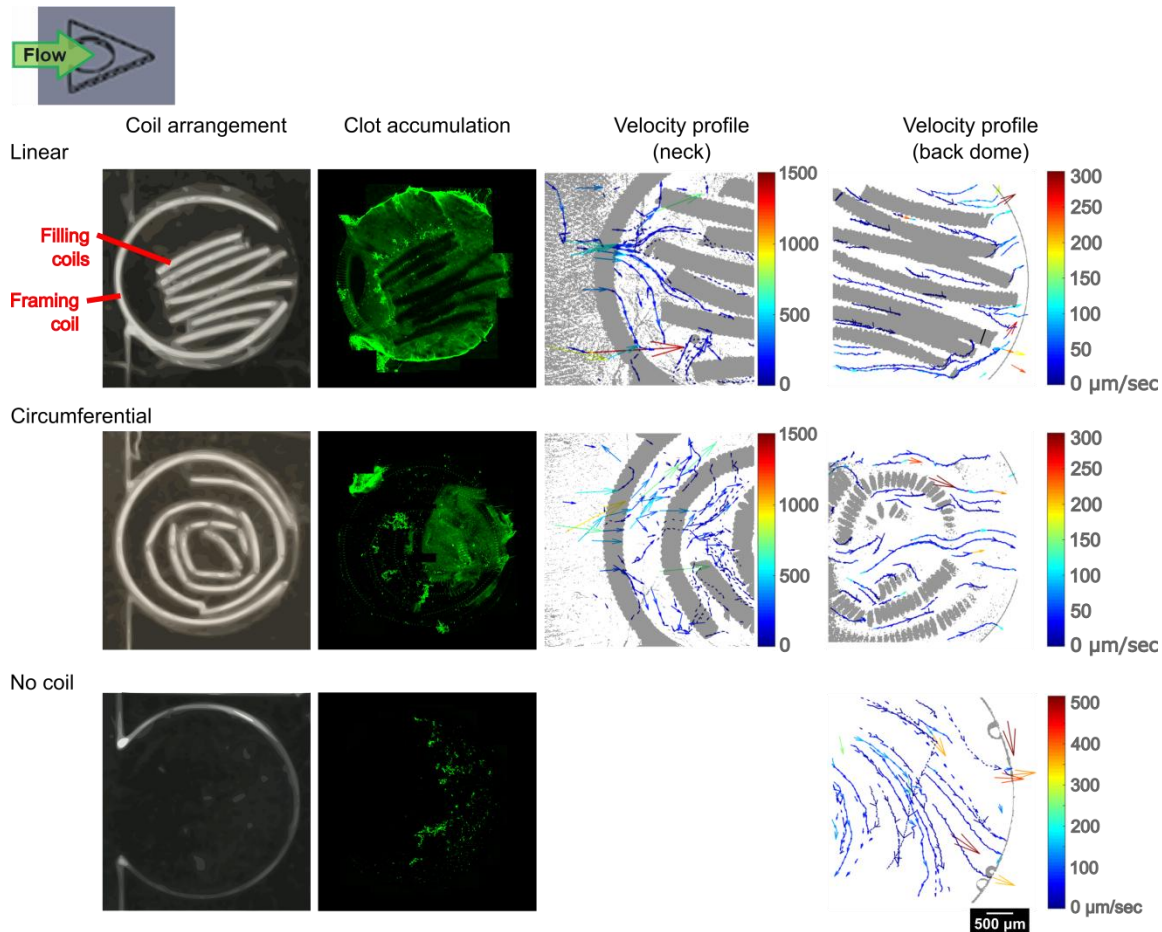


Figure 12: Representative images of coil arrangements in sacs (“Coil arrangement”), clot accumulation, and velocity profiles of flow tracers tracked at the neck and back of the dome for each coil condition. Particles moved slower around coils in a linear arrangement than in a circumferential arrangement. Flow velocity was slowed from neck to back of dome. Flow was faster without coils than with coils. In all images, neck opening is to the left and back dome is to the right (see inset diagram). Flow moved left to right. Aneurysm diameter, 5 mm. Velocity profile scale bar, 500 μm .

3.3.2 Hemodynamics were dependent on coil configuration in IA sac flow chamber

Since the island in the neck model (Chapter 2) does not support coils in arrangements with different packing densities, a saccular model was developed with a hole drilled into the island to create the sac (Figure 10). The sac had a 5 mm internal diameter and 3 mm neck opening, representing the average size of a small human aneurysm.⁵ Coiling consisted of a framing coil and filling coils (Figure 12, “Coil arrangement”). Coils were placed in either a linear arrangement, where filling coils were parallel to one another in order to reduce space and increase packing density between the coils, or a circumferential arrangement, where filling coils were placed in a spiral to imitate a 2-D arrangement of coil placement in patients. Sacs were coiled to 14% (v/v) metal packing density.¹⁰³

Images of fluorescent fibrin after 17 minutes suggested higher clot accumulation in sacs with a linear arrangement compared to sacs with a circumferential arrangement (Figure 12, “Clot accumulation”). Fibrin mesh formation was observed in both coil arrangements. Very little clot accumulated in sacs with no coils. Representative flow streamlines and velocities at the neck and back of the dome are depicted in Figure 12. In general, streamlines tended to follow coils. The linear arrangement demonstrated slower velocities along straight streamlines between filling coils, and the circumferential arrangement demonstrated slightly faster velocities and more curved streamlines with locations of streamline divergence and mixing (Figure 12). A large

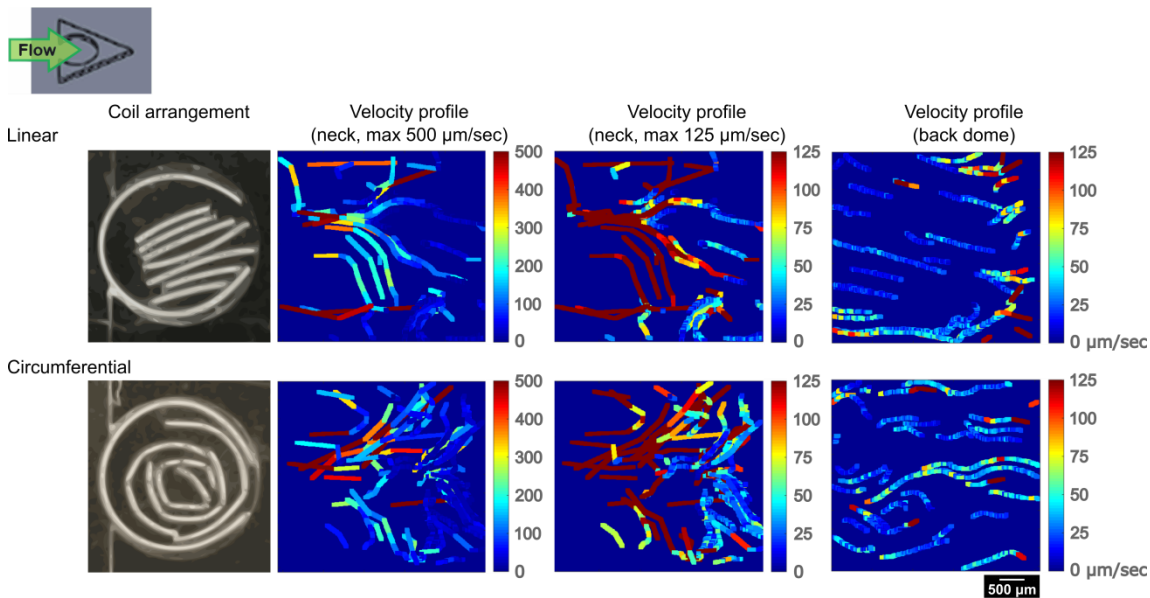


Figure 13: Velocity profiles were translated into heat maps with lower maxima to identify differences in the slowest flow velocities at the neck and back of the dome for each condition. Heat maps with a maximum of 500 $\mu\text{m}/\text{sec}$ show that particles moved slower around coils in a linear arrangement than in a circumferential arrangement at the neck. Heat maps with a maximum of 125 $\mu\text{m}/\text{sec}$ show that flow velocity was slowed from neck to back in both arrangements, and that flow velocity was slower around a linear arrangement than a circumferential arrangement. Aneurysm diameter, 5 mm. Scale bar, 500 μm .

region of streamline divergence was observed immediately inside the framing coil at the neck in both arrangements. In the circumferential arrangement, a second region of streamline divergence with slower velocities located farther towards the sac middle was observed. In the absence of coils, the hemodynamic profile was similar to that in spherical *in vitro* IA models that used a blood substitute fluid.¹⁰ This similarity indicates that the sac flow chamber model captures a cross-section of the flow pattern observed in a spherical saccular bifurcation IA.

Velocity profiles were translated into heat maps with lower maxima in order to more clearly show differences in the slowest flow velocities at the neck and back of the dome for each condition (Figure 13). In these heat maps, the flow speed at a particular point in the vectorized profile shown in Figure 12 corresponds to the color at that point in the heat map. All points where the speed is greater than the scale maximum are colored red. Velocity profiles at the neck with a maximum of 500 $\mu\text{m}/\text{sec}$ show that particles moved slower around a linear than a circumferential arrangement at the neck. Velocity profiles at the neck and back with a maximum of 125 $\mu\text{m}/\text{sec}$ show that flow speed was reduced from neck to back in both arrangements. These heat maps also demonstrate that flow velocity was slower around a linear arrangement than a circumferential arrangement at the back of the dome. These data suggest that areas of local high packing density in the linear arrangement were more effective in slowing flow and reducing mixing than in the circumferential arrangement. Hemodynamics through the saccular aneurysm model were modulated by coil arrangement.

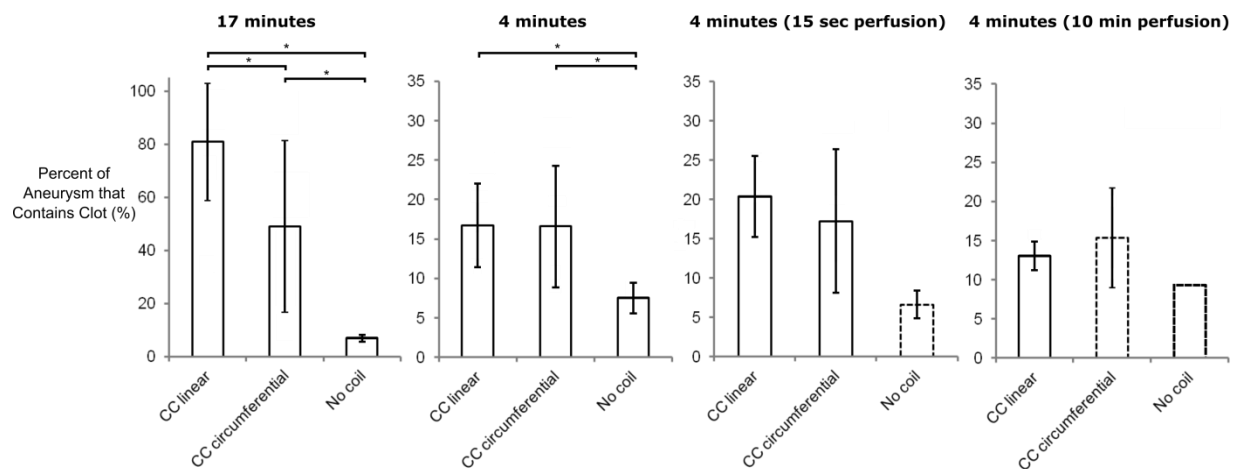


Figure 14: Quantitative analysis of clot sizes. Clot sizes are shown after 17 minutes of PRP flow, 4 minutes of PRP flow for all perfusions, 4 minutes of PRP flow and 15-second perfusions and 4 minutes of PRP flow and 10-minute perfusions for each condition ($*p < 0.05$). Note differences in y-axis scale magnitude. Dotted outline represents a condition where two or fewer replicates were examined.

3.3.3 Rate and location of clot formation were dependent on coil configuration in sac model

Clots were imaged using confocal microscopy in both the single-pass and recirculating flow models after 4 and 17 minutes, respectively, which demonstrated early and late time points of

clot formation. Table 1 describes the PRP flow conditions tested in this study. Clot size was calculated in ImageJ as a percent of the total aneurysm area.

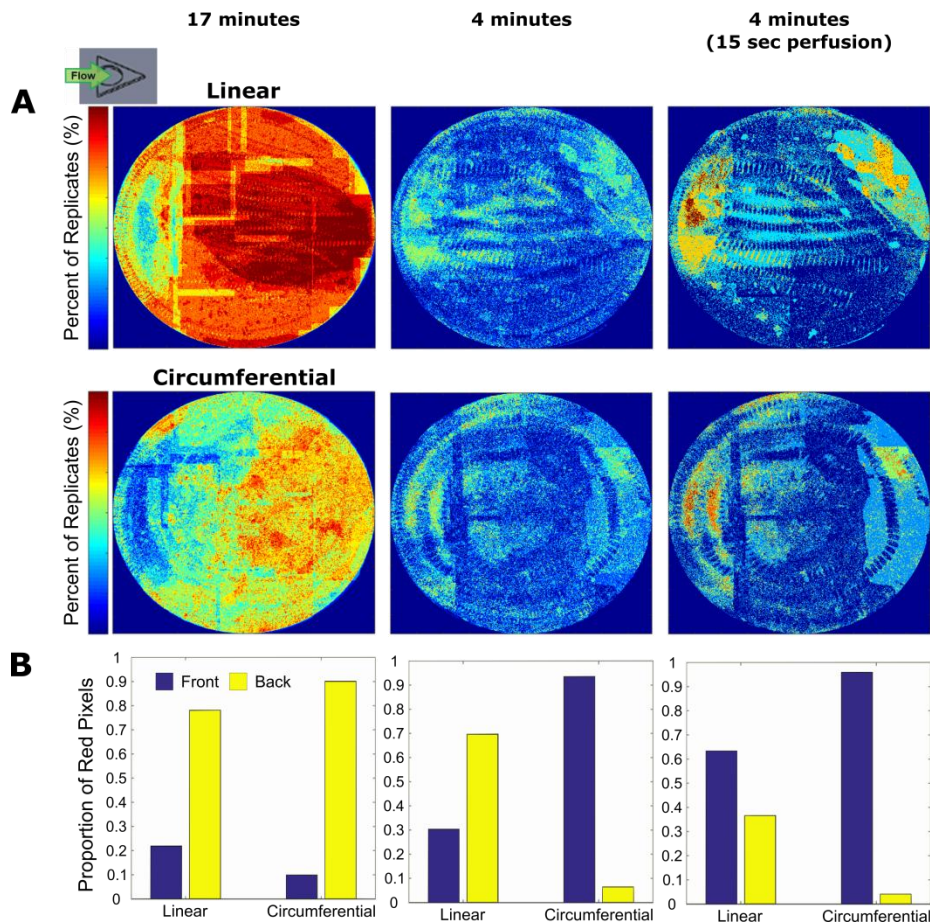


Figure 15: A: Locations of clot accumulation for coils arranged linearly and circumferentially. Color scale indicates percent of total experiments that were clotted at each pixel in the sac. Red indicates locations of accumulation in all trials. Neck opening is on the left of each image (see inset diagram). Aneurysm diameter, 5 mm. B: Proportion of red pixels located in the front half and back half of the sac for each condition. Measurements were calculated after 17 minutes of recirculating flow, 4 minutes of single-pass flow with all perfusion times and 4 minutes of single-pass flow with 15 seconds of perfusion.

Clot size was quantified from images of clot accumulation (Figure 14). Clot size after 17 minutes in sacs filled with linearly arranged coils was significantly higher than those filled with circumferentially arranged coils (80.8% vs 49.0%, $p < 0.05$). Clot size in sacs with coils was significantly higher than that without coils (6.81%, $p < 0.05$). After 4 minutes of flow, clot size was not significantly different between the two arrangements (16.6% vs 16.7%, $p = 0.98$). Clot size increased between 4 and 17 minutes for both the linear (16.7% vs 80.8%, $p < 0.05$) and circumferential (16.6% vs 49.0%, $p < 0.05$) arrangements but not in sacs without coils (7.49% vs 6.81%, $p = 0.64$). After 4 minutes of PRP flow, sacs were perfused with PBS to remove unpolymerized fibrinogen before fixation. In optimizing this process, chambers were perfused for either 15 seconds or 10 minutes. The subsets of 15-second perfusion experiments and 10-minute perfusion experiments were selected from the set for comparison. Clot size after 15

second perfusions was approximately the same as that after 10 minute perfusions (20.4% vs 13.0% linear, $p=0.12$; 17.3% vs 15.3% circumferential, $p=0.78$).

In order to identify trends in clot accumulation relative to the direction of flow, clot images from all experiments were overlaid for each arrangement, clotting time, and perfusion time. A color scale was generated in which “warmer” colors (orange-red) indicate locations where clots occurred frequently and “cooler” colors (blue-green) indicate locations where clots occurred infrequently (Figure 15A). Red pixels show positions where clotting occurred in all replicates. At 17 minutes (Figure 15A, left column), clot occurred more frequently (orange-red) in a linear coil arrangement (22% of the sac contained red pixels) than in a circumferential arrangement (0.20% of the sac) and occurred infrequently near the neck (blue) in both arrangements. At 4 min with all perfusions (Figure 15A, middle column), regions of clotting occurred at the neck and back of the sac (green) of both arrangements and were more frequent after 15 seconds of buffer perfusion (orange-red) (Figure 15A, right column). Similar to the trend after 17 minutes, more red pixels occurred around the linear arrangement (1.5% of the sac) than the circumferential arrangement (0.36% of the sac). Preliminary results from two replicates of the circumferential arrangement indicate that frequent clotting occurred uniformly throughout the sac after 10 minutes of buffer perfusion in both arrangements (Figure 16A).

Proportions of red pixels located in the front half (near the neck) and back half (near the dome wall) of the sac were plotted to evaluate the spatial distribution of clotting (Figure 15B and Figure 16B). Clotting around both linear and circumferential arrangements at 17 minutes occurred most frequently at the back of the dome. At 4 minutes for all perfusions, more red pixels occurred at the back (70% of red pixels) than the neck

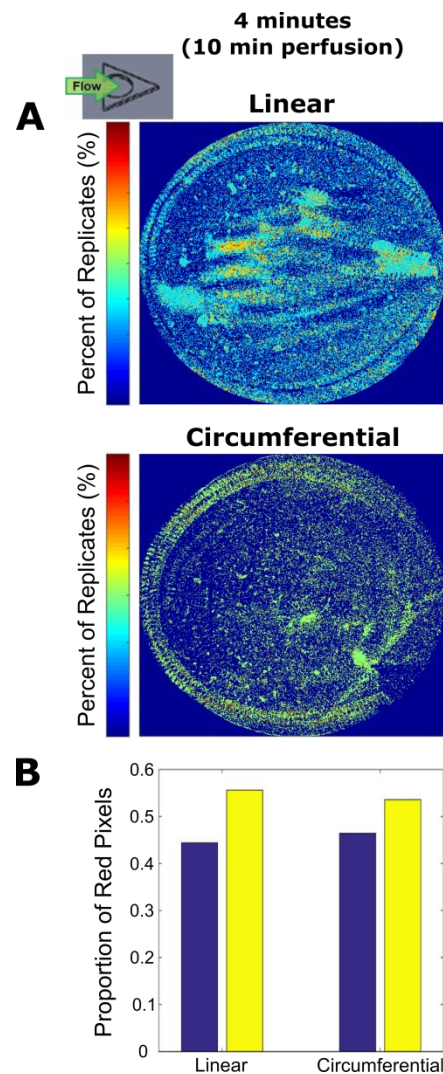


Figure 16: A: Locations of clot accumulation around coils arranged linearly and circumferentially after 4 minutes of single-pass flow with 10 minutes of perfusion. Color scale indicates percent of total experiments that were clotted at each pixel in the sac. Red indicates locations of accumulation in all trials. Neck opening is on the left of each image (see inset diagram). Aneurysm diameter, 5 mm. B: Proportion of red pixels located in the front half and back half of the sac. Two and three replicates were measured in the circumferential and linear arrangements, respectively. Additional replicates are necessary to draw accurate comparisons to the circumferential arrangement condition.

(30%) of the linear coil arrangement; however, more frequent clotting occurred at the neck (94%) than the back (6%) of the circumferential coil arrangement. Conversely, sacs that were perfused with buffer for 15 seconds showed more frequent clotting at the neck (63%) than at the back (37%) of the linear coil arrangement. In addition, the proportion of red pixels at the neck was higher in the circumferential coil arrangement (96%) than the linear arrangement. This suggests that clot initiates more uniformly throughout coils arranged linearly than coils arranged circumferentially, in which clot initiates almost exclusively towards the neck. Preliminary results show that red pixels were distributed uniformly between the neck (44% linear, 46% circumferential) and back (56% linear, 54% circumferential) of both arrangements in sacs that were perfused for 10 minutes (Figure 16B). These results together indicate that spatial clot progression is dependent on both time and coil arrangement.

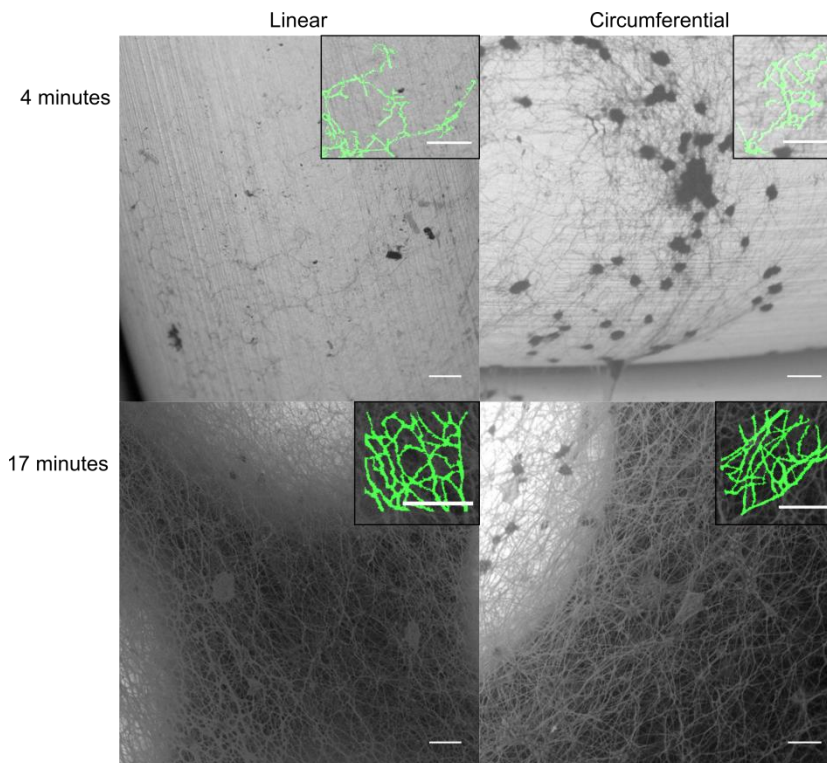


Figure 17: Representative SEM images of clots. Above: Images of clots after 4 minutes of PRP flow in the single-pass model show wavy, short fibers, in both linear (left) and circumferential (right) arrangements. Below: Images of clots after 17 minutes of PRP flow in the recirculating model show more straight, longer fibers, in both linear (left) and circumferential (right) arrangements. Insets show a representative magnified section of each image, where fibers have been outlined to illustrate differences in fiber structure. Scale bar, 5 μ m.

Clot mesh structure was observed in SEM (Figure 17). Fibers that formed after 4 minutes were shorter and more curved than those at 17 minutes for both arrangements. Fibers observed at 4 minutes were located in small quantities on the coil, typically towards the back of the dome. Most of the coils throughout the dome were covered with spread and aggregated platelets.

3.4 DISCUSSION

In this study, clinical coil arrangement modulated hemodynamics and subsequent thrombosis in an *in vitro* saccular bifurcation IA model, which is consistent with computational and *in vivo* results relating clotting to increased coil packing density and reduced flow rate in IAs.^{10,61} Slower flow velocities and more clot formation were observed within the linear coil arrangement than the circumferential arrangement, which agrees with *in vitro* thrombosis studies showing that slow flow initiates more space-filling fibrous clot formation than fast flow.⁶¹ Likewise, in the permeability assay, clots with higher metal packing density exhibited less permeability to flow, indicating that more space-filling clot had formed. In the flow model, coils in both arrangements reduced the flow rate from the neck to the back of the dome, indicating that clinical coils were effective in slowing flow through the sac. Increased coil packing density correlates with reduced IA recurrence rate,⁸⁵ suggesting that a linear coil arrangement may promote more optimal long-term healing than a circumferential arrangement. Moreover, streamlines through the linear coil arrangement were less divergent with less mixing than through the circumferential coil arrangement, which may have contributed to increased clot accumulation around the linear arrangement. Significantly less clot formation occurred in the absence of coils, indicating that not only was slow flow necessary, but a scaffold was also required for clot formation in this aneurysm sac model, just as it is *in vivo*.

Comparison of clotting at 4 minutes with that at 17 minutes provides insight into the time course of coil-dependent clot formation. Clots did not grow significantly in size between these early and late time points in a sac without coils (Figure 14), supporting the hypothesis that a scaffold was required for clot accumulation in the sac. Clot growth over time was greater around the linear arrangement than the circumferential arrangement, indicating that differences in clot size due to coil arrangement took time to appear. SEM imaging (Figure 17) demonstrated short, wavy fibers at 4 minutes and longer, straight fibers at 17 minutes in both coil arrangements. These fiber morphologies correspond to early and late stages of fibrin fiber development under flow,⁷⁹ suggesting that fibrin gel maturation under flow was insensitive to coil arrangement.

Since fibrin gel maturation is associated with clot stabilization, the level and distribution of fibrin gel maturation on coils was examined in sacs with a short buffer wash perfusion after clotting for 4 minutes, and compared to that with a longer buffer wash perfusion. Larger regions of frequent clotting were observed after 15-second perfusions than after 10-minute perfusions, and only small quantities of developing fibrin were observed in SEM for both perfusion times. These observations suggest that underdeveloped fibrin mesh was present after 4 minutes of clotting but was washed out after 10 minutes of buffer perfusion and during the many wash steps of SEM sample preparation. A 15-second perfusion therefore shows all locations of developing fibrin gels, whereas a 10-minute perfusion and SEM imaging show only regions of dense mesh that are well-adhered to the coil surface. Similarly, underdeveloped clot formation in coiled IAs *in vivo* may be washed out by persistent or increased blood flow.

Comparison of clotting locations after 4 and 17 minutes suggests that the spatiotemporal progression of clot distribution was sensitive to coil arrangement. After 4 minutes of PRP flow, clot accumulation was present most frequently in the back of domes containing the linear coil arrangement, but very little was present around the back of domes containing the circumferential coil arrangement. This difference in clot initiation was likely caused by relatively fast flow velocities around the circumferential coil arrangement than around the linear coil arrangement.⁶¹ However, after 17 minutes of PRP flow, clot accumulation was most frequently found at the back of the dome with very few red pixels at the neck for both coil arrangements. Additionally, developing fibrin that was observed in SEM imaging was typically located at the back of the dome, indicating that fibrin was more developed and adherent to coils in the back of the dome than at the neck. These results together suggest that in the linear arrangement, clot that initiated at the back of the dome nucleated clotting in this region and grew to the clot accumulation observed at 17 minutes. On the contrary, in the circumferential arrangement, much less clot initiated at the back of the dome after 4 minutes of PRP flow, so clotting was slower in this region, generating less clot accumulation at 17 minutes. This slower accumulation may have also been caused by the faster flow velocities and divergent flow patterns observed around the circumferential arrangement compared to the linear arrangement.

Moreover, frequent clot accumulation after 4 minutes of blood flow was present at the neck for both coil arrangements, which may have been promoted by large regions of diverging streamlines at the neck immediately behind the framing coil in both arrangements (Figure 12). Slow velocities occurred where these diverging streamlines were redirected by filling coils at the neck (Figure 13). In the circumferential arrangement, slow velocities and few streamlines occurred between the framing and filling coils, indicating that initial clot may have been trapped by the pocket formed between these coils. This phenomenon may have contributed to the larger fraction of initial clot accumulation at the neck in this arrangement. Since less fibrin was observed at the neck in SEM imaging after 4 minutes of PRP flow, clot was likely underdeveloped and not well adhered to coils in this region. After 17 minutes of flow, there was very little clot accumulation at the neck in both arrangements. These findings indicate that initial clot accumulation at the neck was removed in some way. The mechanism of this process is not yet understood, but some hypotheses include local clot dissolution or movement of the clot farther back into the dome in response to fluid pressure at the neck. This phenomenon is similar to that *in vivo*, where blood flow re-entered aneurysms that were initially observed to be occluded.^{5,6} Overall, total packing density remained constant, yet increased local packing density in the linear arrangement caused changes in flow velocity that likely changed the distribution and rate of clot formation. Additionally, these data together suggest that changes in clot distribution appeared gradually and that in studies of coil performance, early initial clot formation may not be sufficient to predict final thrombosis.

This study presents the first measurements of the spatiotemporal distribution of clot formation as a function of coil arrangement; however, this study has its limitations. Limitations of the sac flow model are addressed in Section 5.2. In addition to these limitations, the circumferential arrangements produced highly variable clot sizes, demonstrating that this arrangement was more sensitive to small changes in coil placement. Similarly, coil placement is likely to vary clinically with aneurysm geometry and neurointerventional technique, which may contribute to variability in patient recurrence.

Most endovascular coil thrombogenicity studies *in vitro* are performed in models without flow,^{48,49} which lack a component vital to the model in this study that examined clotting in the coiled IA. The model in this study is the first *in vitro* to analyze clot progression and structure and its dependency on coil arrangement and hemodynamics in a coiled bifurcation IA. An understanding of the dynamic relationship between IA hemodynamics and thrombosis and how this relationship is sensitive to small changes such as coil placement would help shed light on why some aneurysms recur after treatment.

3.5 CONCLUSIONS

This study demonstrates that coil arrangement modulated intra-aneurysmal hemodynamics in a way that affected clot rate and spatial progression. At constant overall packing density, coils in a linear arrangement created areas of high local packing density that slowed flow velocity and directed flow streamlines, which promoted larger clot accumulation than coils in a circumferential arrangement. While clot structure development was similar in both arrangements, coil arrangement modulated the spatial distribution of clotting. This study shows the importance of *in vitro* IA models that examine flow-mediated clot formation and structure.

CHAPTER 4: COIL DESIGN MODULATES HEMODYNAMICS AND CLOTTING

Braided coils make a splash: Braided coil design creates flow disturbances that do not promote fibrous clotting in a saccular bifurcation IA *in vitro*.

4.1 RATIONALE

In Chapter 2, clot structure was found to be independent of coil roughness, wire shape and secondary shape in the absence of flow. However, stent struts with increased surface roughness promote clotting under flow,^{81,82} suggesting that braided coils would promote more clotting in the *in vitro* flow chamber model than clinical coils, since braided coil wire surfaces are rougher than clinical coil wire surfaces. Additionally, small loops in the braided coil secondary shape, caused by bending the wires around each other during braiding, may produce static regions in the flow field around the coil that can promote clotting.¹⁰⁴ Therefore, the neck flow chamber model was used to test the hypothesis that braided coils promote more acute thrombosis at the neck of a packed, coiled bifurcation IA than clinical coils. This neck model can provide new insights into the hemodynamics, thrombosis and potential subsequent endothelialization at the IA neck, the latter of which is one of the most important mechanisms underlying IA recurrence.³

Additionally, since the sac model provides information regarding the spatial distributions of hemodynamics and clot accumulation in a coiled saccular bifurcation IA, this model was used to test the hypothesis that braided coils promote more space-filling fibrin formation throughout the sac than clinical coils. Sacs were also coiled with both braided and clinical coils in different “hybrid” arrangements that elucidate the effect of coil design in different positions in the sac. This study provides information on how different coil designs and their arrangements modulate hemodynamics and subsequent clotting throughout the sac and neck, which would help guide the development of future coil designs.

Table 2: PRP flow conditions in Chapter 4

Model type	Neck model	
	Single-pass flow	Recirculating flow
Flow type	Single-pass flow	Recirculating flow
PRP flow time	4 minutes	20 minutes
Buffer perfusion time	10 minutes	10 minutes
Model type	Sac model	
	Single-pass flow	Recirculating flow
Flow type	Single-pass flow	Recirculating flow
PRP flow time	4 minutes	17 minutes
Buffer perfusion time	10 minutes	10 minutes

4.2 METHODS

4.2.1 Flow chamber and coil preparation

See Section 2.2.3: Flow chamber and coil preparation. Commercially available platinum aneurysm coils (“clinical coils”) and braided coils were used. “Stainless steel coils” or “SS coils” were obtained from MicroDyne Technologies (Plainsville, CT) and consisted of coiled 316 stainless steel wires with a 50- μm diameter cross-section. Coils used in the neck model were cut to 1 cm length. Braided coils were cut to 2 cm length, folded and twisted to 1 cm final length in order to increase metal packing density towards that of the clinical coil. Sacs containing braided coils were filled to 11.5% packing density, those containing braided and coiled coils were filled to 12-12.5% packing density, those containing SS coils were filled to 11% packing density and those containing clinical coils were filled to 14% packing density. Braided coils used in the saccular model were folded and twisted to obtain the reported packing densities. Instead of ethanol cleaning, all coils were washed for 20 minutes in piranha wash (1 part 30% H_2O_2 , 3 parts H_2SO_4) and rinsed in water 24 hours prior to each experiment. For single-pass flow experiments, chambers (Figure 9A and Figure 10) and tubing were rinsed and primed with modified HEPES Tyrodes’ buffer (HT buffer) instead of phosphate-buffered saline without calcium or magnesium (PBS) to prevent calcium phosphate precipitation during clotting, and a reservoir was also coated with bovine serum albumin (BSA) and heparin in the same way as the chambers and tubing.

4.2.2 Recirculating flow experiments

See Section 2.2.4: Recirculating flow experiments. Table 2 describes the PRP flow conditions tested in this study. Red blood cells (RBCs) labeled with DiI (Sigma) were added to platelet-rich plasma (PRP) before flow at 500 cells/ μL final concentration. DiI-RBCs acted as flow tracers in image analysis. Coils were placed by inserting the framing coil first, then inserting filling coils.

4.2.3 Single-pass flow experiments

See Section 3.2.3: Single-pass flow experiments. Table 2 describes the PRP flow conditions tested in this study. Coils were placed by inserting the framing coil first, then inserting filling coils. To obtain mixing data, a 20x objective was focused on the back of the dome of the coiled saccular model prior to PRP transfer to the reservoir. Confocal imaging (488 nm excitation only, 1 second per frame) was initiated at the same time that PRP was added to the reservoir.

4.2.4 Scanning electron microscopy (SEM) preparation

See Section 3.2.4: Scanning electron microscopy (SEM) preparation.

4.2.5 Image analysis

See Section 3.2.5: Image analysis. Clot accumulation in the neck model was measured by calculating the total number of pixels with grayscale intensity higher than the 97.5th percentile of

the background intensity distribution, and converting the number of pixels to square millimeters based on the scale of the image. Average distance between the neck wall and the coil were measured using the “Distance Between Polylines” ImageJ plugin,¹⁰⁵ which measured the shortest distances between the wall and a manually-drawn outline of the coil periphery facing the wall at equidistant points, and averaged these measurements. Mixing time data was generated by calculating the number of frames imaged until uniform Oregon-green fluorescent intensity around the coils was observed in the field of view at the back of the dome. This number was multiplied by the time required to generate each frame.

4.3.6 Statistical methods

Preliminary power analyses based on clot size require a minimum of two replicates per braided coiled sac condition, allowing 5% and 20% probabilities of Type I and Type II errors, respectively. At least four replicates were analyzed for each coiled condition and at least three replicates were analyzed for the no-coil condition in both models. Sample conditions are identified in the figures where two or fewer replicates were analyzed. Linear regression analysis was used to determine correlation between average wall-to-coil distance and clot accumulation. Two-way ANOVA and student’s t-tests were used to evaluate variability within and between groups, respectively.

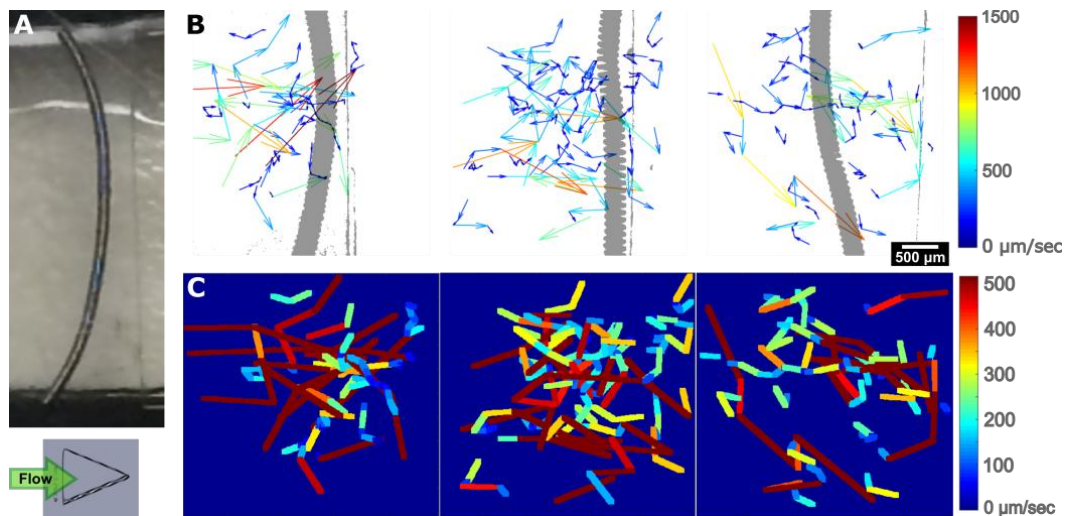


Figure 18: Hemodynamics around clinical coils in the neck model. A: Representative image of a clinical coil placed in the neck model before PRP flow. A schematic of the island indicates the direction of flow. Neck width, 1 cm. B: Velocity profiles of flow around clinical coils (gray) in different replicates. Each column represents the profile in a single replicate. These profiles demonstrate how the coil placement and orientation affected hemodynamics. C: The velocity profiles were translated to heat maps to demonstrate differences in the slowest velocities. Flow tends to be slowest immediately leading up to and behind the coil. Velocity profile scale bar, 500 µm.

4.4 RESULTS

4.4.1 Coil design modulates hemodynamics in IA neck model

To test the hypothesis that braided coils promote more disturbed flow patterns and clotting than clinical coils at a bifurcation IA neck, 1 cm lengths of coil were placed against the island in the

neck flow chamber model. Clinical coils were designed by the manufacturer to fold into 13 mm balls and required slight bending before each experiment in order to straighten the coils to lie as flat as possible against the island. Braided coils had an irregular shape that prevented them from laying flat against the island. These circumstances produced variable coil orientations.

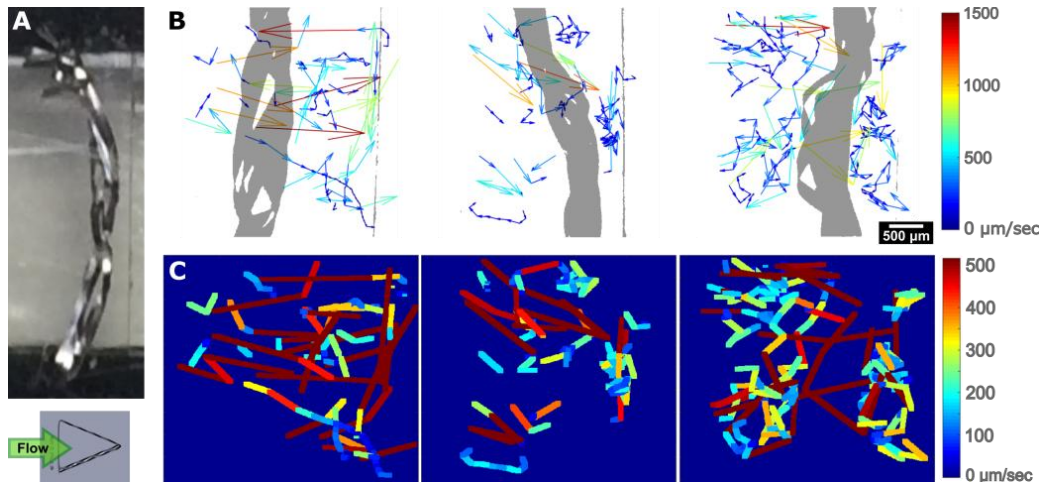


Figure 19: Hemodynamics around braided coils in the neck model. A: Representative image of a braided coil placed in the neck model before PRP flow. A schematic of the island indicates the direction of flow. Neck width, 1 cm. B: Velocity profiles of flow around braided coils (gray) in different replicates. Each column represents the profile in a single replicate. These profiles demonstrate how the coil placement and orientation affected hemodynamics. C: The velocity profiles were translated to heat maps to demonstrate differences in the slowest velocities. Flow tended to be slowest behind the coil and in eddies surrounding the coil. Velocity profile scale bar, 500 µm.

Velocity profiles from three of the replicates from each of the clinical and braided coil conditions are demonstrated in Figure 18B and Figure 19B, respectively. Flow was slowest in the region immediately leading up to clinical coils and in areas where the distance between the coil and wall was small (Figure 18B). Flow speed was high in areas where the distance between the coil and wall was larger than in other replicates. Flow speed around braided coils was similar to that around clinical coils, but more eddies with slow velocities were observed around the braided coil surface (Figure 19B). Slow flow velocities occurred in regions leading up to the braided coil and between the coil and the wall. Heat maps of the velocity profiles were created in order to demonstrate small differences in the slowest velocities present in the velocity profiles (Figure 18C and Figure 19C). Each pixel in the heat map corresponds to the velocity located at that position in the velocity profile. These heat maps emphasize the aforementioned locations of slow flow around the coils. Flow pattern was facilitated by coil type in the neck model.

4.4.2 Braided coil did not promote more clot accumulation than clinical coil in neck model

PRP flow conditions that were used in the study are outlined in Table 2. Clot accumulation around coils after 4 minutes of single-pass flow was negligible. Clot accumulation around braided and clinical coils in the neck model after 20 minutes of recirculating flow was variable, as seen in Figure 20. There appeared to be no trend in accumulation across the experiments. There was no statistically significant difference in average clot size between coil types ($p=0.26$)

due to variability in replicates, although the average clot size around braided coils was higher than that around clinical coils (0.83 mm^2 and 0.58 mm^2 , Figure 21). There was no statistically significant difference between experiments (Two-way ANOVA, $p=0.57$).

Distance between the wall and coil periphery was measured for each sample and plotted against corresponding clot size (Figure 22). Linear regression analysis revealed no correlation between

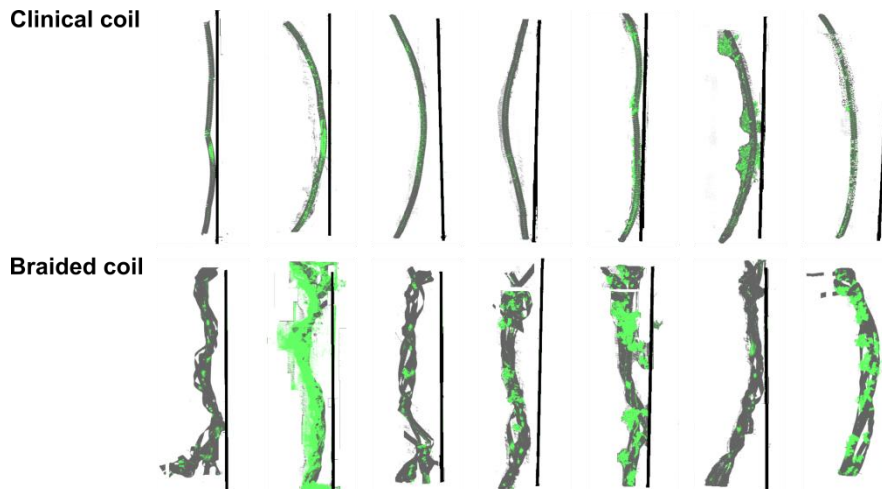


Figure 20: Images of clot accumulation (green) in each coil (gray) replicate tested in the neck model after 20 minutes of PPR flow. Each column represents a different experiment where PRP from the same blood draw was recirculated around a clinical coil and a braided coil in different chambers simultaneously. The location of the neck wall is represented as a black line. Flow moved left to right. Coil length, 1 cm.

average wall-to-coil distance and clot size for either clinical ($R^2=0.001$) or braided ($R^2=0.0167$) coils. In each experiment, two different pumps were used to recirculate PRP in both chambers simultaneously. When the pump flow rates were measured, one pump proved to flow water at a rate 1.3 mL/min faster than the other pump when set to 12 mL/min flow rate. This difference in flow rate corresponds to 20 s^{-1} PRP flow shear, which is a 10% increase in average shear rate in the inlet of the flow chamber. Replicates where the faster pump was used were represented by hollow markers in Figure 22.

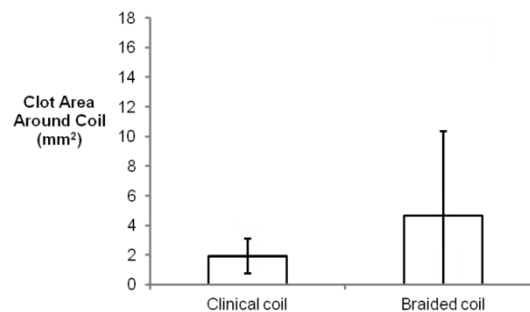


Figure 21: Average clot accumulation for all coil samples tested in the neck model after 20 minutes of PPR flow. There was no significant difference between conditions ($p=0.26$).

4.4.3 Coil design facilitated clot structure in IA neck model

SEM images show that clot morphology

was different between coil types. Clots formed on clinical coils consisted mostly of adhered and spread platelets (Figure 23). These areas were larger after 20 minutes of recirculating flow than after 4 minutes of single-pass flow. In two replicates, large regions of dense platelets and fibrin and large fibrous meshes interspersed with platelet aggregates were observed (*). Clots formed

on most braided coils were denser and contained more fibrin than clots formed on clinical coils that consisted of spread and aggregated platelets.

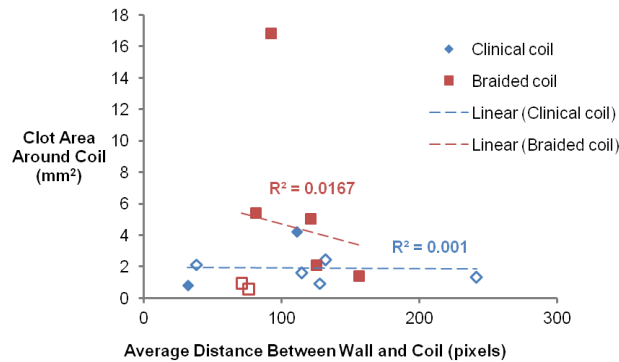


Figure 22: Quantitative analysis showed no correlation between wall-coil distance and clot accumulation. The distance between the coil periphery and the wall was plotted against the corresponding clot accumulation after 20 minutes of PRP flow in each sample for both clinical (blue) and braided (red) coils. Linear regression indicated no trend between wall-coil distance and clot accumulation for both clinical and braided coils (dotted lines). Open marker indicates PRP was recirculated at an average flow rate 1.3 mL/min faster than in the case of closed markers.

Clots formed on braided coils consisted of adhered and spread platelets and dense regions of platelets and fibrin (Figure 24). These dense regions were larger after 20 minutes of recirculating flow than after 4 minutes of single-pass flow. After 4 minutes, some small areas of “fuzzy” clot morphology were observed. In one replicate, clot size was much larger than that of the other replicates, and large meshes of fibrin were observed (*).

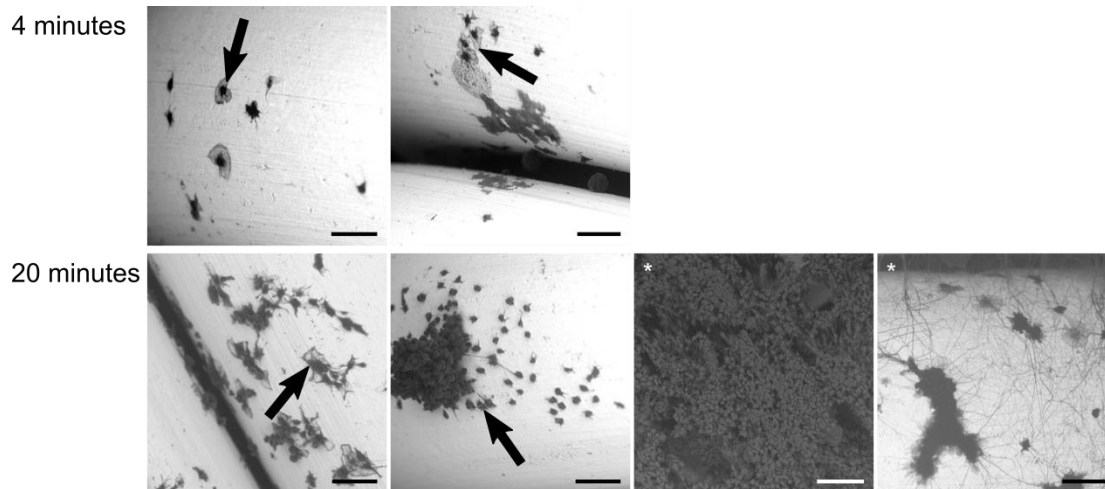


Figure 23: Clot morphologies observed on clinical coils in SEM after 4 minutes of single-pass flow (above) and 20 minutes of recirculating flow (below) in the neck model. After 4 minutes of flow, platelets were observed adhered to the coil surface and often spread out (black arrows). After 20 minutes of flow, more aggregates of spread and adhered platelets were observed (black arrows). Dense regions of platelets and fibrin and fibrin meshes interspersed with platelet aggregates were observed in experiments were large regions of clot accumulated (*). Scale bar, 10 μ m.

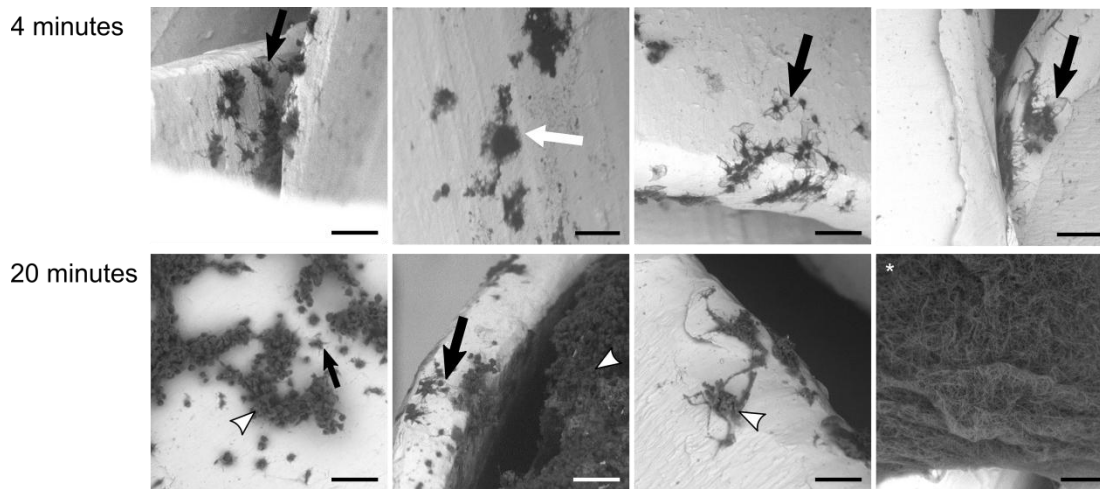


Figure 24: Clot morphologies observed on braided coils in SEM after 4 minutes of single-pass flow (above) and 20 minutes of recirculating flow (below). Dense regions of platelets and fibrin (white arrowheads) were observed on the coil surface and in “pockets” in the coil. Adhered and spread platelets were also present on the coil surface (black arrows). In some locations, “fuzzy” clot structures were observed that might indicate underdeveloped clot (white arrow). In the sample where a large amount of clot accumulated, fibrin mesh was observed (*). Scale bar, 10 μ m.

4.4.4 Braided coils were associated with faster flow than clinical coils in IA sac model

Since the linear arrangement promoted slower flow velocities than the circumferential arrangement in Chapter 3, SS coils were placed in a linear arrangement in the sac. SS coils were tested since they were made of the same metal as braided coils but have the same coiled shape as clinical coils. Braided coils were crimped to create a framing coil with curved filling coils placed in the sac model, but due to their irregular shape were not able to be arranged into distinct linear or circumferential arrangements. Therefore, models coiled with braided filling coils were not distinguished by arrangement.

In general, streamlines tended to follow coiled coils. Flow profiles around braided coils were faster and more erratic compared to SS coils (Figure 25), indicating mixing and high permeability through a sac filled with braided coils. Flow velocity was slowest between coils in both conditions. Flow through a sac with braided coils was faster than a sac without coils (Figure 12). To confirm mixing in models coiled with braided coils, single-pass flow experiments were conducted where PRP was flowed through the sac model from a reservoir, and the time required for complete mixing to occur at the back of the dome was recorded. The field of view at the back of the dome became mixed significantly faster around braided coils compared to a sac without coils or around either arrangement of clinical coils (Figure 26), indicating that the braided coils were more permeable to flow and promoted more disturbed flow patterns than the other conditions. These results together suggest that braided coils were less effective in slowing flow through the sac model than clinical coils, SS coils or even a saccular model without coils. Flow disturbances around the braided coils were characterized by mixing and high flow rates with diverging, erratic streamlines. Conversely, areas of local high packing density in the linear

arrangement of SS (Figure 25) and clinical coils (Figure 12) and in the circumferential arrangement of clinical coils (Figure 12) were more effective in slowing flow and mitigating mixing than braided coils. Overall, hemodynamics through the saccular model was modulated by coil design. Representative images of clot accumulation in Figure 12 and Figure 25 show that clot accumulation in a sac filled with clinical or SS coils was greater than that in a sac filled with braided coils.

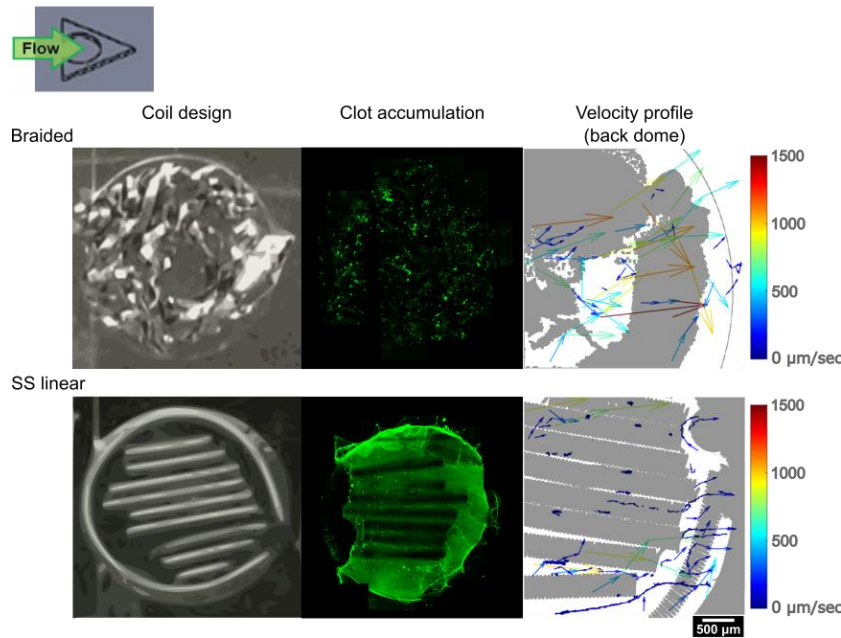


Figure 25: Representative images of sacs filled with braided and SS coil types before clotting (“Coil design”), clot accumulation, and velocity profiles of flow tracers tracked at the back of the dome for each coil condition (“Velocity Profile”). Clot accumulation was greater and particles moved slower around SS coils in a linear arrangement than braided coils. In all images, neck opening is to the left and back dome is to the right (see inset diagram). Flow moved left to right. Aneurysm diameter, 5 mm. Velocity profile scale bar, 500 μm .

4.4.5 Coil design facilitated clot structure in IA sac model

PRP flow conditions utilized in the study are outlined in Table 2. Clot structure was driven by coil design at both early and late time points. Similar to those formed on clinical coils, clots formed on SS coils after 4 minutes of single-pass flow consisted of fibrin meshes made up of short, wavy fibers (Figure 27, “SS linear”). In some areas, “fluffy” clot structures were observed that resembled those seen on braided coils in the neck model after 4 minutes. After 17 minutes of recirculating flow, clots closely resembled those formed on clinical coils and consisted of large fibrin meshes with long, straight fibers. Conversely, clots formed on braided coils at both time points were made up of dense regions of platelets and fibrin, which were larger after 17 minutes than those formed after 4 minutes (Figure 27, “Braided”). Fibrin fibers within these regions were short and wavy.

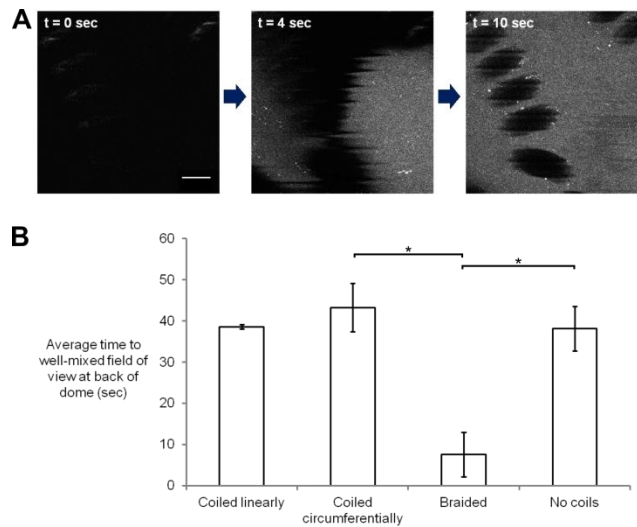


Figure 26: Dome mixing analysis. A: Sample image analysis of a model that was coiled linearly. A field of view was not considered mixed until a uniform intensity was observed around the coil ($t=10$ sec). “t” indicates time after flow initiation. The sample was devoid of PRP at $t=0$ sec and was fully mixed at $t=10$ sec. Scale bar, 100 μ m. B: Average time until a well-mixed field of view was observed at the back of the dome. ($*p<0.05$).

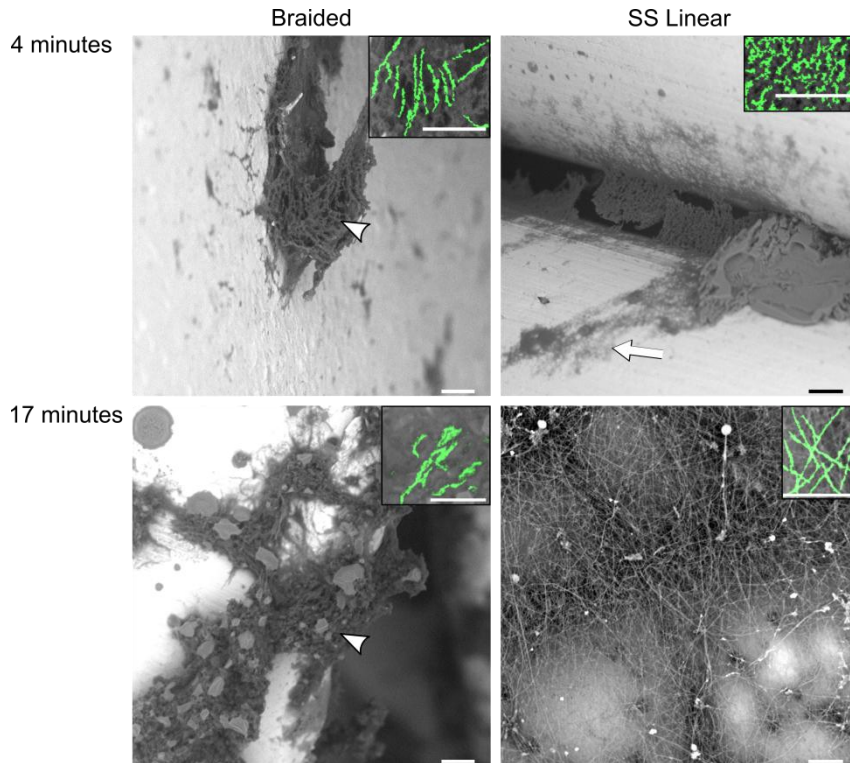


Figure 27: Representative SEM images of clots on braided and SS coils. Above: Images of clots after 4 minutes of PRP flow in the single-pass model showed wavy, short fibers, on both braided coils (left) and SS coils in a linear arrangement (right). Below: Images of clots after 17 minutes of PRP flow in the recirculating model showed wavy, short fibers on braided coils (left) but straighter, longer fibers on SS coils (right). Braided coils presented clots with dense fiber and platelet aggregates (white arrowhead). Some areas on SS coils presented “fluffy” clot structures that might have indicated polymerizing fibrin (white arrow). Insets show a representative magnified section of each image, where fibers have been outlined to illustrate differences in fiber structure. Scale bar, 5 μ m.

4.4.6 Coiled coils slowed flow more than braided coils in framing and filling coil positions

In order to elucidate the roles of filling and framing coils, hybrid coil designs were created where a different coil type was placed in the framing coil position than that in the filling coil position (Figure 28, “Coil design”). SS coils were used as the coiled coil type in these hybrid designs to prevent variable metal types within the sac.

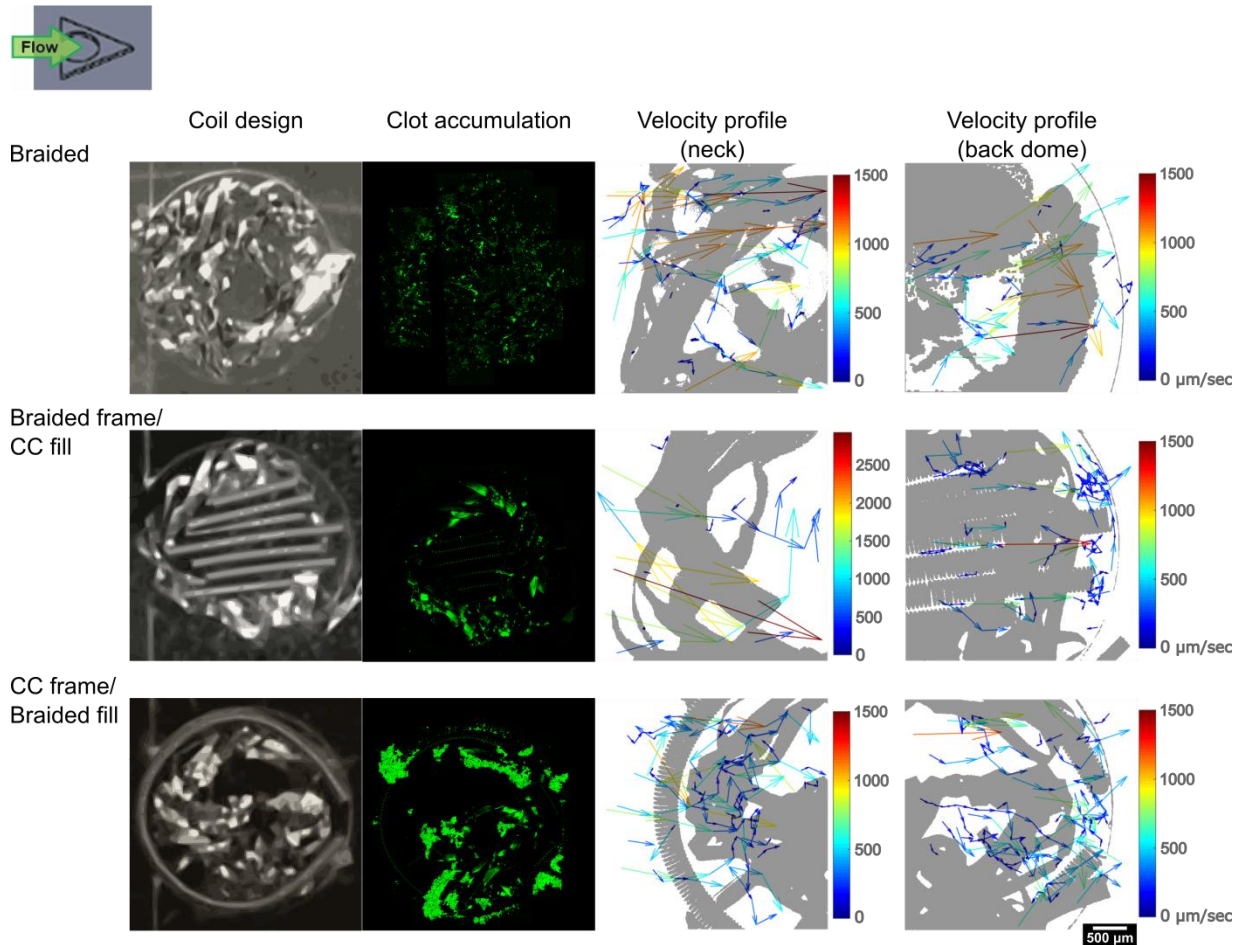


Figure 28: Representative images of sacs filled with braided and coiled coil (CC) types and in different arrangements (“Coil design”), clot accumulation, and velocity profiles of flow tracers tracked at the neck and back of the dome for each coil condition. Particles moved slower around coiled coils than around braided coils. Clot accumulation was not dependent on these conditions. Flow velocity was slowed from neck to back of dome in a sac with filling coiled coils, but not in a sac with filling braided coils. Flow was slower inside a sac with a framing coiled coil than a sac with a framing braided coil. In all images, neck opening is to the left and back dome is to the right (see inset diagram). Flow moved left to right. Aneurysm diameter, 5 mm. Velocity profile scale bar, 500 μm .

In the braided coil condition, flow at the neck and back of the dome was fast with diverging, erratic streamlines (Figure 28, “Velocity profile”). In the braided frame/coiled coil (CC) fill hybrid, the speed of flow entering the sac was high but was reduced around coiled coils in the middle and back of the dome. Flow streamlines in the sac middle followed coiled coils and were nondivergent compared to divergent and erratic streamlines at the neck. On the contrary, in the CC frame/braided fill hybrid, the speed of flow entering the sac was reduced by the framing

coiled coil and remained slow throughout the sac, but flow speed was not reduced between neck and back by filling braided coils. Streamlines were diverging and showed eddies in some locations inside the sac around filling braided coils. These trends in flow velocity are more clearly demonstrated in heat maps produced from velocity profiles (Figure 29, “Velocity profile”). A comparison of heat maps of braided and hybrid coil designs (Figure 29) with those of clinical coils (Figure 13, “Velocity profile”) show that flow velocity in a sac with braided coils in any position was slower than that in a sac with clinical coils in all positions.

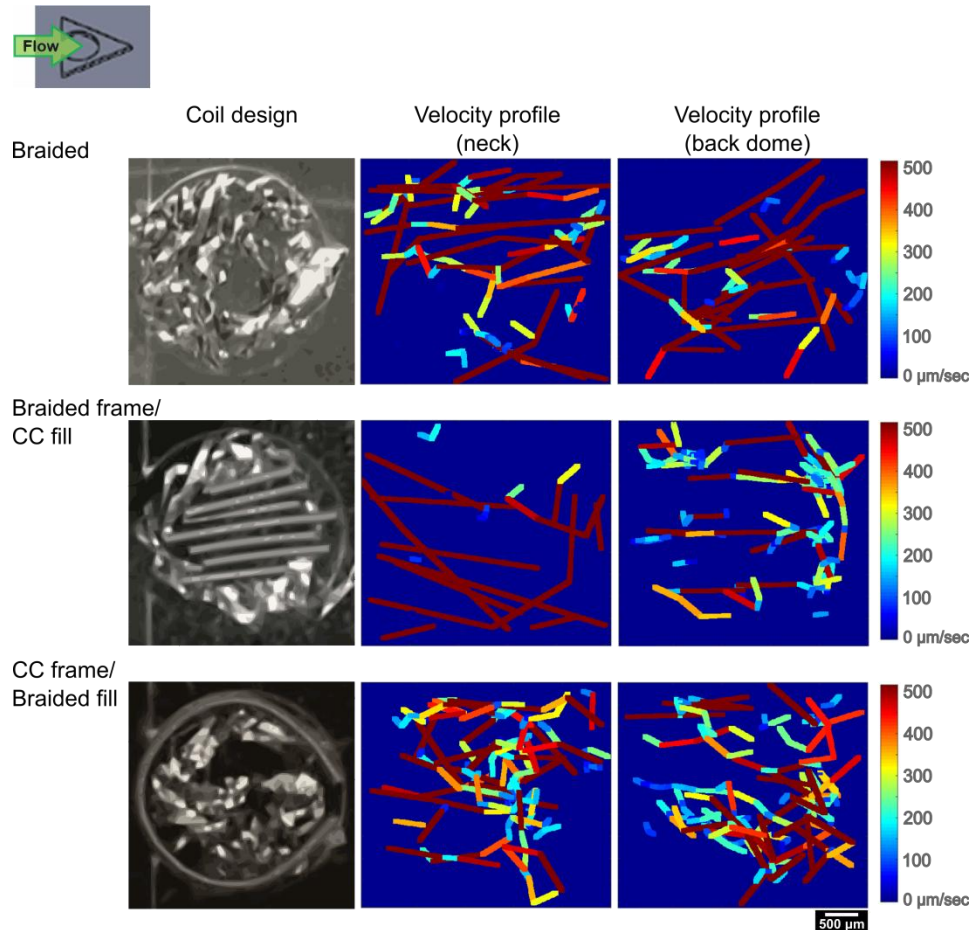


Figure 29: Velocity profiles were translated into heat maps with lower maxima to identify differences in the slowest flow velocities at the neck and back of the dome for each condition. These heat maps emphasize the trend that flow velocity was slowed across and around coiled coils (CC) in the framing and filling positions, respectively, but not across or around braided coils. Aneurysm diameter, 5 mm. Velocity profile scale bar, 500 μm.

4.4.7 Braided coils promoted less clot accumulation than coiled coils in sac model

Clot sizes formed after 17 minutes of PRP flow in each condition are demonstrated in Figure 30. Clot sizes formed in sacs containing clinical coils and in sacs without coils are included for comparison. Clot accumulation around SS coils in a linear arrangement was not different from that around clinical coils in a linear arrangement ($p=0.22$). In preliminary studies, SS coils in a circumferential arrangement and the CC frame/braided fill hybrid design were tested for clot

accumulation, but there were not enough replicates to indicate trends in clot accumulation for these conditions. Clots that formed around both of the clinical coil arrangements and the SS linear arrangement were significantly larger than those that formed around braided coils ($p<0.05$). Clots that formed around SS linear arrangements and braided coils were significantly larger than those that formed in the absence of coils ($p<0.05$). There was no significant difference between clot accumulation around braided frame/CC fill sacs and that around braided coils ($p=0.80$) or that in the absence of coils ($p=0.73$). Coiled coils (SS coils and clinical coils) promoted more clot accumulation than braided coils at 17 minutes.

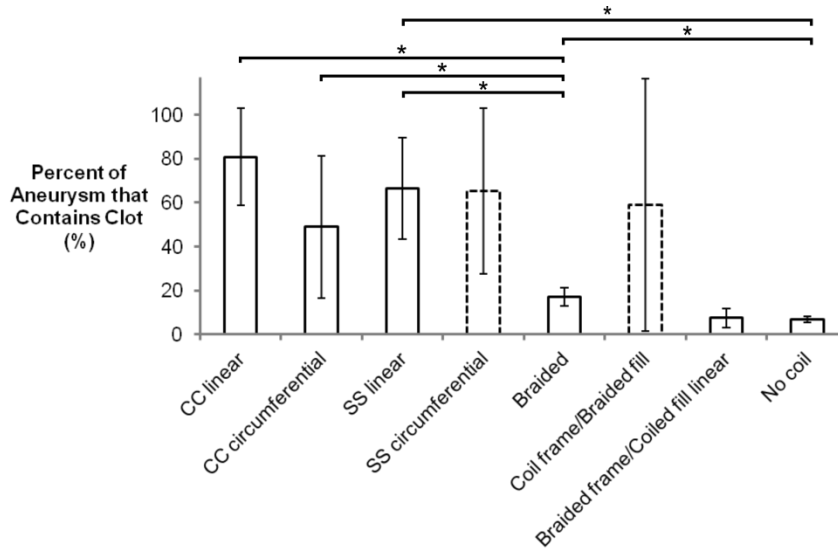


Figure 30: Quantitative analysis of clot sizes after 17 minutes of recirculating flow. Clinical coil arrangements are included for comparison. Dotted outline represents a condition where two or fewer replicates were examined. Significant differences shown in Figure 14 are not displayed. (* $p<0.05$)

Clot accumulation after 4 minutes was similar for all coiled conditions tested ($p=0.27$, Figure 31). There was a significant difference between clot accumulation in a sac with coils and that in a sac without coils ($p<0.05$).

4.4.8 Framing coil type impacted clot structure in hybrid coil arrangements in sac model

SEM imaging of clots after 17 minutes of recirculating flow revealed different clot structures between the two hybrid designs. The clot structures observed on each coil type in each hybrid design were outlined separately (Figure 32). In sacs filled with braided framing and CC filling coils, clots resembled those formed around braided coils and consisted of dense regions of platelets and fibrin as well as adhered and spread platelets on both the coiled coil (Figure 32A-B) and braided coil (Figure 32C) surfaces. Dense regions of platelets and fibrin were seen wrapped around rectangular wires. In sacs filled with CC framing and braided filling coils, similar dense platelet and fibrin clot structures were observed on both coiled coils (Figure 32D) and braided coils (Figure 32F). Again, the dense aggregates were wrapped around rectangular wires.

Additionally, similar to sacs filled with coiled coil framing and filling coils, large fibrin meshes formed on both coiled coil (Figure 32E) and braided coil (Figure 32G) surfaces, which were interspersed with platelet aggregates.

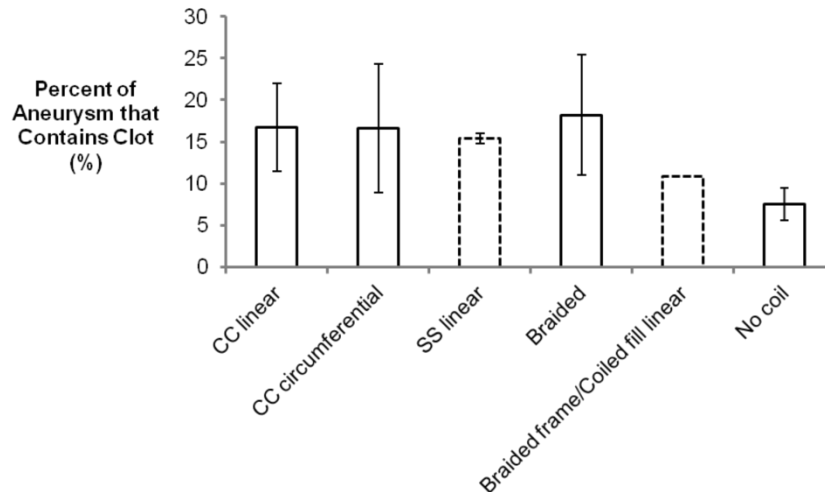


Figure 31: Quantitative analysis of clot sizes after 4 minutes of single-pass flow. Clinical coil arrangements are included for comparison. Dotted outline represents a condition where two or fewer replicates were examined. Significant differences shown in Figure 14 are not displayed.

4.5 DISCUSSION

The results from this study show that coil design modulated hemodynamics in a way that determined clotting. Braided coils in the neck model did not promote more clotting than clinical coils, despite changes in flow pattern and clot structure. However, in the sac model, braided coils promoted less clotting and denser clot structures than clinical coils. Hybrid coil arrangements, where the sac contained filling and framing coils of different types, revealed that framing coil type was likely important to intra-aneurysmal flow velocity and was likely more important to clot structure than filling coil type. This is surprising since filling coils made up a much larger volume than the framing coil in each sac. The results obtained from these two models provided information about hemodynamics and clotting at the neck of an occluded IA and throughout a coiled dome, respectively.

4.5.1 Neck model insights

The neck of an occluded IA is the site of tissue and cell monolayer formation that prevents blood flow into the aneurysm and subsequent recurrence, and is therefore a region of importance in IA modeling. Velocity profiles of flow around braided and clinical coils demonstrate that flow speed was similar between the coil types. The flow patterns show some differences, however. More regions of eddies were observed around braided coils than clinical coils at the neck, which may have been promoted by the irregular secondary shape of the braided coils. Pockets created by wire braiding in these coils may have also contributed to eddies. These hemodynamics observed

in the braided coils may have contributed to large platelet and fibrin-rich clumped clots (Figure 19). Large boundary layer areas of slow flow were observed leading up to both clinical and braided coils (Figure 18 and Figure 19), suggesting that the effect of coils on the flow field may not be limited to the coil surface but also impacts flow in the parent vessel. In samples where large areas of clot accumulated, fibrous mesh was observed in both coil types (Figure 24 and Figure 25,*). Flow pattern also appeared to be dependent on coil orientation and distance from the wall.

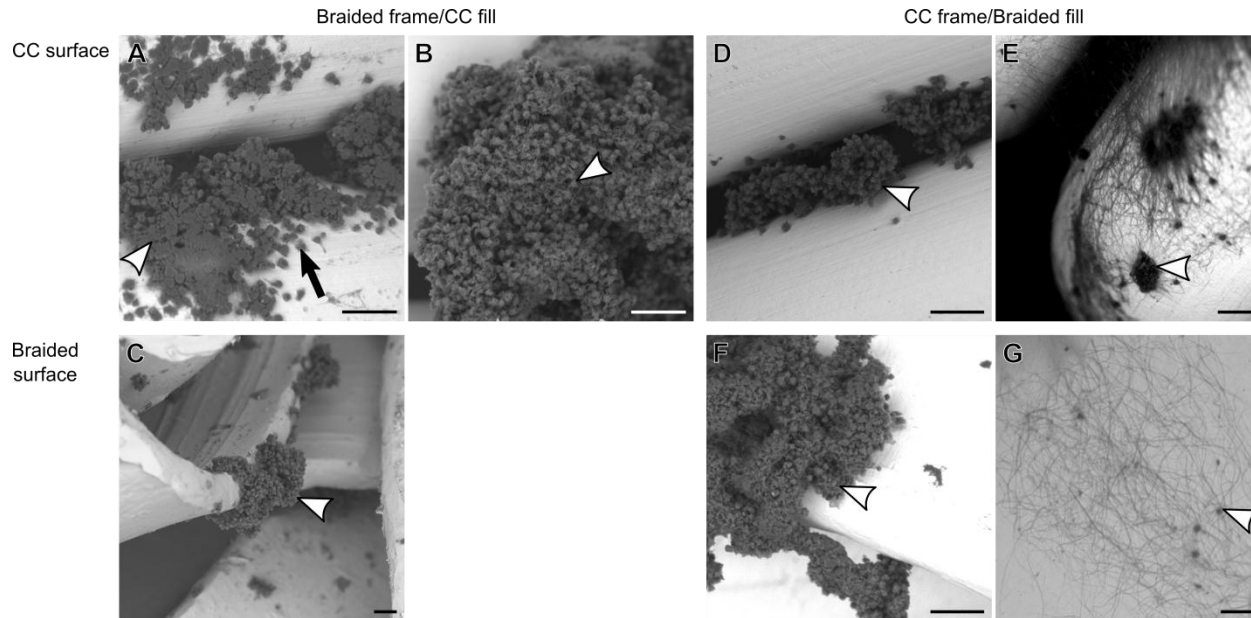


Figure 32: Representative SEM images of clots on hybrid coil designs. Since these designs consist of two different coil types, clot structure trends on the coiled coil (CC) surfaces (above) and braided coil surfaces (below) were outlined separately. In images of sacs filled with braided framing coil and CC filling coils (A-C), adhered platelets (black arrow) and dense clots of platelets and fibrin (white arrowheads) were observed on both CC (A-B) and braided coil (C) surfaces. In images of sacs filled with CC framing coil and braided filling coils (D-G), adhered platelets and dense clots of platelets and fibrin (white arrowheads) were observed on both CC (D) and braided coil (F) surfaces. Additionally, large areas of fibrin mesh were observed on both CC (E) and braided coil (G) surfaces, which were interspersed with small platelet and fibrin aggregates (white arrowheads). Scale bar, 10 μm .

Despite these differences in flow pattern and clot structure, clot accumulation on clinical and braided coils were not significantly different ($p=0.26$). The spatial distribution of clot on clinical and braided coils also appeared to be variable. Average distance between the coil and the wall did not correlate with clot accumulation for either clinical ($R^2=0.001$) or braided ($R^2=0.0167$) coils (Figure 22). Figure 20 shows that clot accumulation correlated with regions of clinical coil closest to the wall in some replicates, although this trend was inconsistent. These results indicate that local or average wall-to-coil distance did not affect clot accumulation. The two braided coil replicates that were recirculated at 20 s^{-1} higher shear rate than the other replicates comprised two of the three samples where clot accumulation was less than 2 mm^2 . Nevertheless, a larger sample size is required to assess whether clot accumulation on braided coils is significantly decreased by a 10% increase in shear rate.

4.5.2 Sac model insights

Results from the sac flow model show that coiled coils slow flow and promote nondivergent flow streamlines compared to braided coils at both the framing and filling coil positions. In sacs filled with coiled coils, wires that made up coils were closer together than in sacs filled with braided coils, which may have contributed to a lower effective permeability that was demonstrated by slower mixing time and slower flow velocities around coiled coils regardless of arrangement. SS coils in a linear arrangement produced similar clot structures, clot sizes, flow patterns and flow velocities as clinical coils in a linear arrangement, indicating that hemodynamics and subsequent clotting are not different between stainless steel and platinum coiled coils of comparable size.

Flow velocities were faster, flow patterns were more erratic and faster mixing occurred in a sac filled with braided coils compared to coiled coils, which may have produced smaller clot sizes and denser fibrin-platelet clot structures than coiled coils. Spatial distributions of fast velocities and diverging flow patterns correlated with that of braided coils in the braided coil, braided frame/CC fill and CC frame/braided fill conditions. Specifically, flow entering the sac was unimpeded by braided coils at the frame in the braided and braided frame/CC fill designs, and flow through the middle of the sac from neck to back was unimpeded by braided filling coils in the braided and CC frame/braided fill designs. In contrast, slow flow with nondivergent streamlines was observed in locations where coiled coils were present. Coiled coils were effective in slowing flow entering the sac when in the framing coil position and between the neck and back of the dome when in the filling coil position. Change in flow velocity across the coil was determined by coil design, although the average velocities in the back of the dome for the hybrid designs were comparable (Table 3).

Clot structure was dependent on coil design and was generally uniform throughout each sample. Dense regions of platelets and fibrin were observed on all coils present in a sac that contained braided coils. However, sacs with a framing coiled coil (SS linear, clinical coils, and CC frame/braided fill conditions) contained fibrin mesh, indicating that slow flow velocity coming into the sac is more important for fibrous mesh clot formation than slow velocity through the middle of the sac. Lower flow velocity entering the sac model likely increased the residence time of PRP in the sac, which may have promoted fibrous mesh clot formation in conditions with a framing coiled coil. These results are consistent with computational modeling results that indicate that high blood flow residence time within a fusiform IA promotes thrombosis.¹⁰⁶

Clot accumulation in the braided frame/CC fill design was similar to that in a sac filled with braided coils, but no conclusions could be made regarding clot accumulation in the CC frame/braided fill design. Similar to clinical coils in a circumferential arrangement, the differences between the two replicates of SS coils in a circumferential arrangement and between

the two CC frame/braided fill replicates were very large, suggesting that clot size in these conditions might be variable. The results from this study indicate that slow flow with nondivergent streamlines through a sac filled with coiled coils was necessary to produce a large space-filling clot after 17 minutes of flow. A summary of the trends observed in flow velocity, flow pattern, clot accumulation and clot structure is outlined in Table 3.

Table 3: Trends in hemodynamics and clotting observed in sac flow model

Sample type	Average velocity in		Clot structure
	back of dome (type, $\mu\text{m}/\text{sec}$)	Clot accumulation (type, avg %)	
Clinical linear	Slow, 16.8	High, 80.8	fibrin mesh
Clinical circumferential	Slow, 21.6	High, 48.9	fibrin mesh
SS linear	Slow, 18.8	High, 66.5	fibrin mesh
CC frame/braided fill	Medium, 281	Inconclusive, 59.1	clumped clots and fibrin mesh
Braided frame/CC fill	Medium, 207	Low, 20.6	clumped clots
Braided	Fast, 439	Low, 17.1	clumped clots

4.5.3 Overall insights

Differences in clot accumulation and hemodynamics between the neck and sac models revealed information about coil design and packing at the IA neck. Clot accumulation in the neck model was variable and independent of coil design, although flow pattern and clot structure were affected by coil design. This suggests that clot accumulation, unlike clot structure, is not dependent on flow pattern in this model. However, it is not clear why the accumulation was variable between experiments, indicating that the relationships between hemodynamics and clot accumulation and structure at the neck require additional investigation. After 17 minutes of flow, clot infrequently occurred at the neck in the sac model (Figure 15A and Figure 25, “Clot accumulation”), suggesting that this area is the last to fill with thrombosis. *In vivo*, the neck is also the location of endothelial cell monolayer formation, which is a marker of a healed IA that is protected from recurrence. The lack of clot but importance of tissue formation at the neck reinforces the necessity to understand coil impingement on the flow field at the neck and its effect on thrombosis in order to develop treatments that promote more clotting and subsequent cellularization at the neck.

Results from the sac model demonstrated that spatial distributions of clot accumulation and flow velocities and patterns are strongly dependent on the type and location of coils. Coiled coils slowed flow entering the sac whether they were placed as the framing coil or the filling coils, and braided coils were permeable in that they did not slow flow entering the sac. Filling coiled coils slowed flow velocities throughout the middle of the dome but only framing coiled coils promoted fibrin formation in the sac, indicating that coil type at the neck has a greater impact on clot structure and possibly also blood residence time in the sac than filling coil type. Occasional “fluffy” clot structures occurred on braided coils in the neck model and SS coils in the sac model after 4 minutes of single-pass flow. These small aggregates on the stainless steel surfaces appeared to be composed of very short fibers and are not observed on any coils at the late time point, indicating that they are comprised of polymerizing fibrin.⁷⁹ Flow speeds around braided coils in the neck and saccular models were comparable in most of the neck model replicates. Both models demonstrated slow flow with diverging streamlines immediately around the coil surface, but eddies were observed in the neck model that were not observed at the neck of the sac model. The island wall was more rigid and less permeable to flow than filling braided coils, which may have initiated these vortexes in the neck model. Eddy flow patterns therefore may occur at the neck of an IA that is fully occluded with a braided coil at the neck but may not occur if the sac is not fully occluded. In both the neck model and the sac model, slow flow occurred in the areas leading up to coils, indicating that a large area around the coil in a parent vessel is affected by the coil’s presence. The neck and sac models provided different information but both demonstrated that coil design affects hemodynamics and clot structure.

The limitations of the neck and saccular models are detailed in Section 5.2, but there are additional limitations specific to this study. Firstly, in designs that included braided coils, there were occasional coil protrusions into the island around the sac. An instance of this protrusion can be observed in the back dome velocity profile of the braided frame/CC fill design (Figure 28). However, flow velocity did not appear to be affected by this protrusion. Flow streamlines followed the edge of the wire, but this had a marginal effect on the overall flow profile. Protrusion regions were removed from clot size during image analysis and did not skew the reported clot sizes. Consequently, protrusions likely did not significantly affect comparisons in flow velocity, flow pattern or clot size between conditions. Secondly, coil orientation and shape in the neck model were variable. Flow velocity was affected by coil-wall distance, and eddies occurred in regions where the braided coil was bent, but these trends did not correlate to trends in clot accumulation. Further studies will be required to elucidate the factors that modulate clot accumulation in this model around both coil types in order to shed light on the variability in clot size that was observed in this study.

This study showed that local trends in hemodynamics and subsequent clot accumulation and structure are modulated by coil designs with different wire shapes and secondary shapes in a novel saccular bifurcation IA model. Studies have explored modifications to coil design at the

tertiary shape level, where coils were designed to fold into helical or complex ball shapes,^{18,19} yet the influence of coil wire shape or secondary coil shape on hemodynamics or this influence on thrombosis rate or structure have not been explored in the literature. The initial hypothesis that braided coils cause flow disturbances that promote clotting in a model IA was only partially supported. Braided coils in the neck and saccular models promoted disturbed flow profiles around the coils, but these disturbances did not promote as much clot accumulation as coiled coils. These results show for the first time that coil design impacts clot progression and structure, which is a phenomenon not largely understood.

4.6 CONCLUSIONS

The results from this study suggest, for the first time, that coil wire and secondary shapes and the placement of different coil designs in the IA modulate intra-aneurysmal hemodynamics and subsequent clot accumulation and structure. In the neck model, braided coils promoted more eddies and denser clot structures than clinical coils, but there was no trend in clot accumulation across the variable replicates. In a sac, braided coils did not slow flow as effectively as coiled coils or a sac without coils, promoted divergent streamlines with rapid mixing and correlated with the formation of dense platelet and fibrin-rich clots instead of fibrous mesh observed in a sac containing only coiled coils. Some fibrous mesh was observed in sacs with a coiled coil frame and braided filling coils, suggesting that framing coil design may impact clot structure more than filling coil design. This study provides new information about coil design and placement that can help drive the development of coil designs and coil techniques that reduce the rate of IA recurrence. Conflicting results in the neck and sac models suggest that the factors that drive hemodynamics and clotting at the neck are important to thrombosis in the IA sac and require further investigation.

CHAPTER 5: LIMITATIONS AND ACHIEVEMENTS

The ebb and flow

5.1 OVERALL CONCLUSIONS

These studies provide new information about the importance of flow velocity and pattern in clotting in a saccular bifurcation IA and how they are modulated by coil design and placement. Each study addresses a different hypothesis using one of the three models that were developed in this work in order to test several coil conditions (Figure 33). The results of these studies are summarized in Table 3 and Figure 34. These studies together support the hypothesis that shear flow is necessary to elucidate physiologically relevant trends in coil thrombogenicity *in vitro* (Chapter 2, Figure 9B). Specifically, coil presence and high local packing density significantly increased clot accumulation under flow but had no effect on accumulation in the absence of flow (Chapter 2, Figure 6 and Figure 7; Chapter 3, Figure 14). Braided coil design promoted less clot accumulation and denser clot structure than coiled coils under flow but also had no effect on clot accumulation or structure in the absence of flow (Chapter 2, Figure 6 and Figure 8; Chapter 4, Figure 30 and Figure 32).

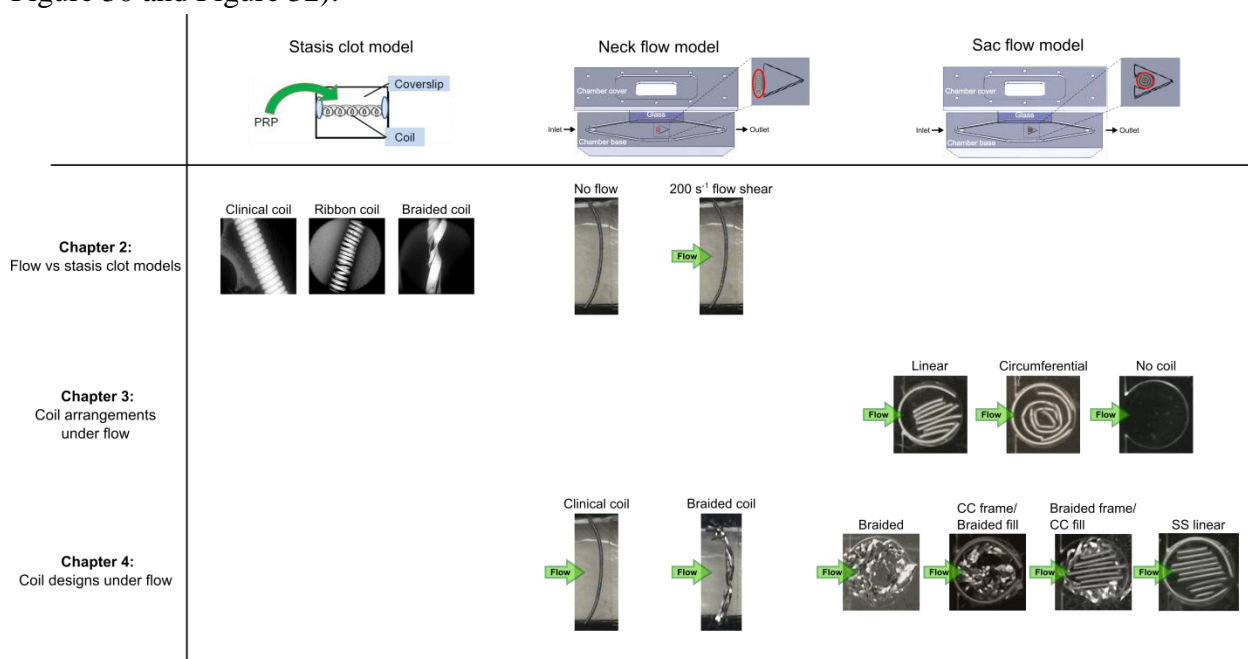


Figure 33: Summary table of conditions tested and the models used to test them in each chapter. Chapter 2 utilized the stasis clot model and neck flow model to test the hypotheses that clot structure is insensitive to coil design and packing in the absence of flow (on clinical, ribbon and braided coils), and that flow is necessary to recapitulate clot structure seen in *ex vivo* human IAs (comparing clots formed in the absence of flow to clots formed under 200s^{-1} shear flow). Chapter 3 used the sac flow model to test the hypothesis that coil arrangements with high local packing densities promote space-filling clot formation under flow (comparing the linear arrangement, the circumferential arrangement and a sac without coils). Chapter 4 used the neck flow model and sac flow model to test the hypothesis that coil designs that create disturbed flow patterns promote space-filling clot formation under flow (comparing clinical coils and braided coils in the neck flow model, and comparing braided coils, stainless steel (SS) coils in a linear arrangement and hybrid designs in the sac model).

Moreover, these studies demonstrate that coil placement in the IA modulated hemodynamics, spatiotemporal trends in clot accumulation and clot structure. Specifically, high local packing density correlated with nondivergent flow streamlines, slower flow velocity, higher clot accumulation at a late time point and more uniform initial clot distribution at an early time point compared to a more uniform packing density (Figure 34). Changes in clot distribution between early and late time points indicated that initial clot formation might not be indicative of final clot size or distribution, since initial clot is likely subject to washout of developing fibrin gel with persistent flow into the IA. This phenomenon may also occur *in vivo* where IAs recurred that were initially observed to be occluded during coiling.^{5,6} The placement of coil designs within the sac also affected hemodynamics and subsequent clotting. Braided coils within the sac and at the neck promoted divergent streamlines and small areas of dense platelet and fibrin-rich clots. Coiled coils (SS and clinical coils) at the neck slowed flow velocity coming into the sac and promoted fibrin mesh clot formation, while coiled coils in the middle of the sac slowed flow velocity from the neck to the back of the dome but did not necessarily promote fibrin mesh formation (Figure 34A and B).

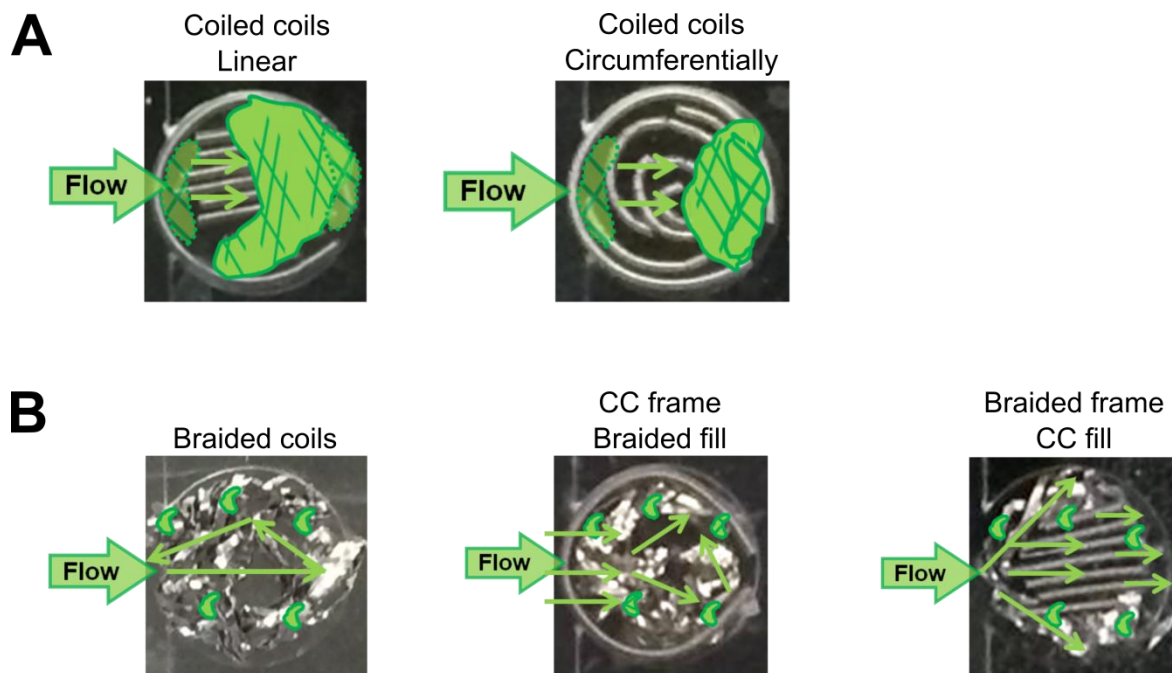


Figure 34: A: Coiled coil arrangement modulated flow velocity (green arrows), initial distribution (dotted outline) and accumulation of fibrin mesh (dark green hatch) clot. B: Coil design modulated flow velocity and pattern (green arrows). The presence of braided coils correlated with small areas of dense platelet-fibrin clot accumulation (light green), and a coiled coil in the framing coil position correlated with small areas of fibrin mesh accumulation (dark green hatch).

Coil design facilitated hemodynamic pattern, flow velocity, and clot accumulation and structure in the sac, although in a way that did not support the original hypothesis that braided coils promote space-filling clot formation. As previously mentioned, flow velocity slowed with

nondivergent streamlines across coiled coils, yet flow velocity did not slow and divergent streamlines were observed across braided coils. Sacs containing braided coils promoted less clot accumulation and small dense aggregates of platelets and fibrin compared to those containing only coiled coils. Clot accumulation and structure in the neck model were variable and appeared to be independent of coil design, contrary to results from the sac model (Chapter 4, Figure 21 and Figure 30). Trends of clot accumulation at the neck therefore require additional investigation in order to better understand the factors that drive clotting in this important region.

These results suggest that slow flow velocity (approximately 15-50 $\mu\text{m}/\text{sec}$) with nondivergent streamlines was optimal for the formation of large clots composed of fibrin mesh in the sac model (Table 3). Coiled coils at the neck that reduced flow into the sac correlated with fibrin mesh polymerization, indicating that the hemodynamics at the neck more strongly impacted clot structure than hemodynamics through the middle of the sac (Chapter 4, Figure 32). This may be due to longer blood residence times in sacs where a coiled coil at the neck slowed flow entering the sac. Preliminary studies of the CC frame/braided fill condition indicate that this design may initiate clot accumulation that is variable but higher than the braided frame/CC fill condition. Additional studies are necessary to indicate correlations between coiled framing coil, blood residence time, and clot accumulation in the sac.

Trends in clot structures formed on different coil designs suggest that hemodynamics facilitated the formation of fibrin mesh and dense aggregates of fibrin and platelets. However, with the absence of macrophages, fibroblasts, endothelial cells and other cell types that remodel the thrombus into tissue, it is not clear which clot structure is ideal to prevent IA recurrence. Studies of cell proliferation, migration and adhesion to fibrous structures indicate that spaces between fibers larger than 5 μm are more optimal for fibroblast infiltration into the matrix than spaces smaller than 5 μm ,¹⁰⁷ suggesting that fibrous mesh would be better suited for fibroblast-mediated clot remodeling than dense clot aggregates. Yet, increased fiber density¹⁰⁸ and the presence of platelets⁷⁴ both correlate with resistance to fibrinolysis, indicating that dense platelet and fibrin aggregates would be stable, fill space in the sac and maintain a scaffold for cells over a longer period of time compared to fibrous mesh clots. Endothelial cells (ECs) also reduce the rate of clot lysis,¹⁰⁹ suggesting that increased EC coverage would further extend the clot lifetime; however, EC adherence was not sensitive to matrix pore sizes less than approximately 5 μm ,⁷⁷ suggesting that EC coverage would be approximately the same between dense and mesh clots. This information together indicates that denser clots are likely to degrade slower and may prevent flow in the sac after initial occlusion, but they are less likely to promote cell infiltration and clot reorganization into tissue, which would inhibit the progression of IA healing. Analyses of cell adhesion, proliferation and migration on these structures are necessary to elucidate which structures, and consequently which flow patterns and coil designs, are ideal to promote IA healing and protection from recurrence.

5.2 LIMITATIONS OF MODELS

Three models were utilized in these studies: the stasis clot model, the neck flow chamber model and the sac flow chamber model. As in all *in vitro* models, these models have limitations. In each of these models, clotting occurred on glass and plastic surfaces instead of on tissue, creating different blood surface activation than that *in vivo*. Also, RBCs were omitted from these models, although they affect clot structure and rate.¹¹⁰ The addition of RBCs and tissue surface activation to the models would affect clotting in each condition equally, so the trends in relative rate of clotting would remain the same. Additional studies in this model can be performed with whole blood, although SEM would be used exclusively to analyze clot size and structure. This would require coil removal from flow chambers, which would potentially disrupt the macroscopic structure of the clot before imaging.

In the neck model, the coil curvature in most replicates was concave against the wall, while coils at the neck of an IA *in vivo* are likely convex against the packed IA. One clinical coil replicate was placed in a convex orientation (Chapter 4, Figure 20), which was associated with faster flow velocities between the coil and wall (Chapter 4, Figure 18B) but promoted similar clot accumulation to the other orientations, indicating that the convex/concave orientation of the coil likely does not affect clotting. However, the variables that did affect clot accumulation in the neck model study could not be clearly elucidated from the variable results, so additional studies are necessary to better understand the coil orientations, flow patterns and other factors that may promote clotting at the neck of coiled IAs.

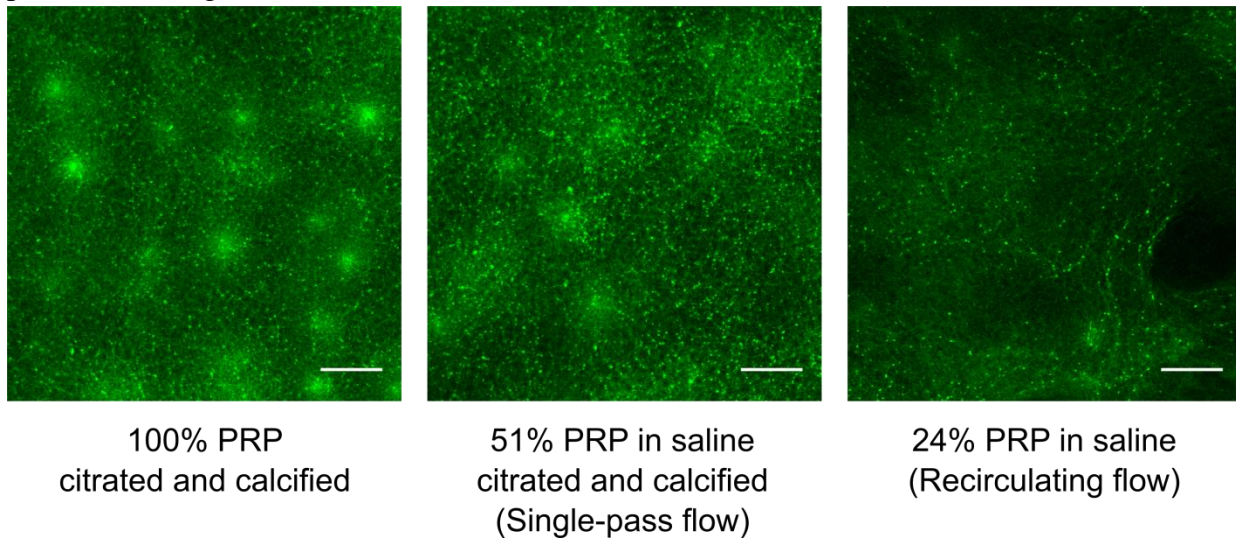


Figure 35: Clots were formed on coverslips using PRP treatments discussed in the methods. Left: PRP was anticoagulated with buffered sodium citrate to 3.2% and activated with 20 mM CaCl_2 . Middle: PRP was diluted to 51% in saline and anticoagulated with buffered sodium citrate, then activated with CaCl_2 . PRP used in the single-pass model was treated using the same protocol. Right: PRP was diluted to 24% in saline. This increases coagulation time so that coagulation around coils could be observed in the recirculating model. Fiber density is independent of dilution. High intensity locations show platelet-mediated fiber bundling. Scale bar, 100 μm .

Many limitations of the sac model also apply to the neck model. First, the PRP used in the studies was diluted, which slowed clotting rate. A control study showed that while regions of platelet-mediated fiber bundling were smaller in diluted PRP than pure PRP, fiber density was retained (Figure 35), indicating that clot structure and accumulation are comparable across the three models. Moreover, the saccular and neck models are not spherical, so they demonstrated different hemodynamic profiles in some areas from a spherical sac, especially at the top and bottom of the flow chamber. Yet, the hemodynamic profile of the sac model was similar to that observed in particle image velocimetry of *in vitro* spherical IA models,¹⁰ so the flow models in this study captured a “slice” of the flow profile in the spherical IA. As *in vivo*, coils in these models were bounded at all sides by surfaces, although *in vivo* coils are bounded by curved, compliant surfaces, rather than the rigid planar glass and polycarbonate surfaces. While this surface geometry and mechanics in the model were not the same as in an IA *in vivo*, the trends in clotting observed in the model are expected to remain the same *in vivo*. Finally, the sac and neck models observed acute thrombosis, but long-term clot development is important to coil thrombogenicity. Acute thrombosis is important in that it creates the essential scaffold for cell infiltration and subsequent tissue formation. Our models measured the spatiotemporal distribution of clotting and its dependency on hemodynamics, which could not be obtained in existing models.

5.3 ACHIEVEMENTS AND CONTRIBUTIONS TO THE FIELD

The flow chamber models developed in this study are the first *in vitro* models to analyze clot progression, accumulation and structure in a coiled saccular bifurcation aneurysm. Clot structure and accumulation are important for cellularization during IA healing, since cell behavior is responsive to properties of its underlying matrix.^{77,89} Therefore, it is important to understand the factors that affect clot accumulation and structure in order to better understand the factors that affect IA healing. These models are also the first to analyze local hemodynamics of flow around coils with high resolution and the first capable of observing live clotting on and around coils under flow. In addition, these studies showed that shear flow was necessary to determine the thrombogenicity of coils with different arrangements and shapes, in contrast to most coil thrombogenicity studies that have been conducted in the absence of flow.^{48,49} These studies also present the first measurements of the spatial distribution of intra-aneurysmal hemodynamics and the spatiotemporal distribution of clot formation as functions of coil arrangement. Specifically, the results indicate that regions of high local packing density promoted slower flow with nondivergent streamlines, more uniform clot distribution at early time points and more fibrous clot accumulation at late time points compared to uniform packing density. This new information agrees with computational models that predict that coil placement modulates intra-aneurysmal hemodynamics.^{11,43} The influence of coil wire shape or secondary coil shape on hemodynamics, or this influence on thrombosis rate or structure, has not been explored in the literature. These studies are the first to examine braided coil wires and to provide evidence suggesting that coil secondary shape impacts flow pattern, flow velocity, clot accumulation and clot structure. They

indicate that slow flow velocities with nondivergent streamlines around coils may be optimal for the formation of large fibrous mesh clots and that hemodynamics at the neck may be more important to clot structure in the IA dome than hemodynamics within the dome. These models can be further used to examine how coiled IA acute thrombosis is affected by factors that cannot be controlled *in vivo*, such as aneurysm geometry and inlet flow velocity. They can also be used to screen coils for thrombogenicity before performing studies in animal trials, saving time and resources. An understanding of the dynamic relationship between IA hemodynamics and thrombosis and how this relationship is sensitive to coil packing, coil shape and other clinically relevant variables would help explain why some IAs recur after treatment. *In vitro* models help reveal the temporal and spatial dynamics of IA healing processes and perturb them in ways that are unavailable *in vivo* and relatively fast and inexpensive. Together with computational and animal models, they help shed light on IA recurrence.

CHAPTER 6: FUTURE WORK

Uncharted waters

6.1 ALTERNATIVES IN COIL PACKING AND COIL DESIGN

The results of this work indicate that the spatiotemporal dynamics of clotting are dependent on coil-mediated hemodynamics. Additional studies using the stasis, neck flow chamber and sac flow chamber models can interrogate how clotting is affected by other coil packing trends and coil designs. First, changes in total coil packing density in the IA are likely to affect clot accumulation and flow velocity. Computational studies show that higher packing density correlates with slow flow velocity,¹⁰ and animal⁸⁶ and clinical⁸⁵ studies indicate that increased packing density correlates with reduced recurrence rate. Sacs with variable packing densities could be analyzed in terms of hemodynamics, clot accumulation, clot distribution and clot structure to evaluate if this trend between packing density and flow velocity is similar in the sac flow model and if packing density affects clotting. This trend could provide a direct relationship between packing density and thrombosis and may also provide a correlation between clotting and recurrence rate.

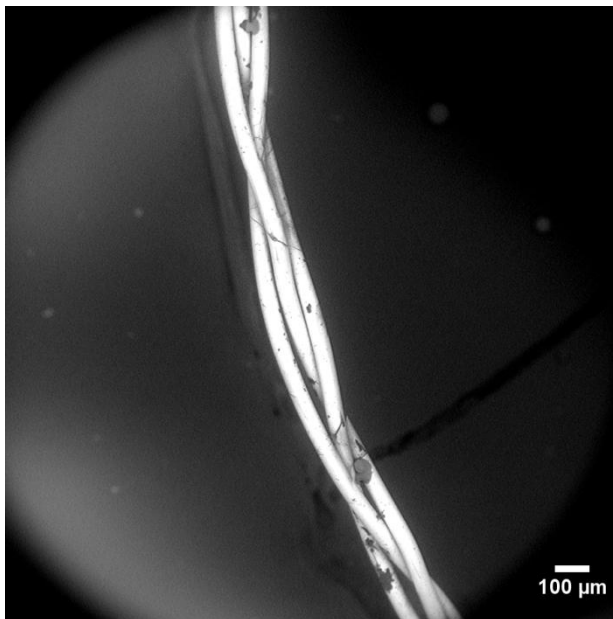


Figure 36: SEM image of three round wires braided together. Scale bar, 100 μm .

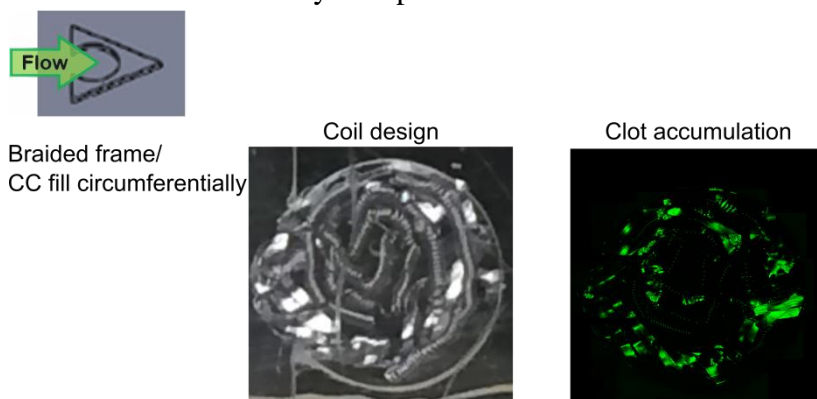


Figure 37: Representative images of a sac filled with braided framing coil and coiled coil (CC) filling coils in a circumferential arrangement before clotting (“Coil design”) and after 17 minutes of clot accumulation. In all images, neck opening is to the left and back dome is to the right (see inset diagram). Flow moved left to right. Aneurysm diameter, 5 mm.

Additional coil designs could also be tested in the models. Ribbon coils that were studied in Chapter 2 (Figure 5) or round wires braided together (Figure 36) could be placed into the sac and neck flow models to ascertain if hemodynamics and clotting are sensitive to wire shape at a constant coil secondary shape. Furthermore, the braided frame/CC fill hybrid design was only tested where CC coils were arranged linearly but could also be tested where the CC coils are arranged circumferentially. This study would provide information about the impact of coiled coil arrangement with a braided framing coil on hemodynamics and clotting. A preliminary experiment measuring clot accumulation in a sac with a braided frame and CC coils arranged circumferentially indicates that clot size at 17 minutes is not different than the hybrid design with CC coils arranged linearly (Figure 37). However, hemodynamics, clot structure and clot progression have not yet been evaluated. In addition, further studies are necessary to elucidate the factors that drive hemodynamics and subsequent clot accumulation at the neck in both the neck and sac models. These studies may focus on variables including coil orientation, coil length, distribution of coil-wall distance and small changes in inlet flow velocity. It is important to better understand these factors since matrix formation at the neck is important to late IA

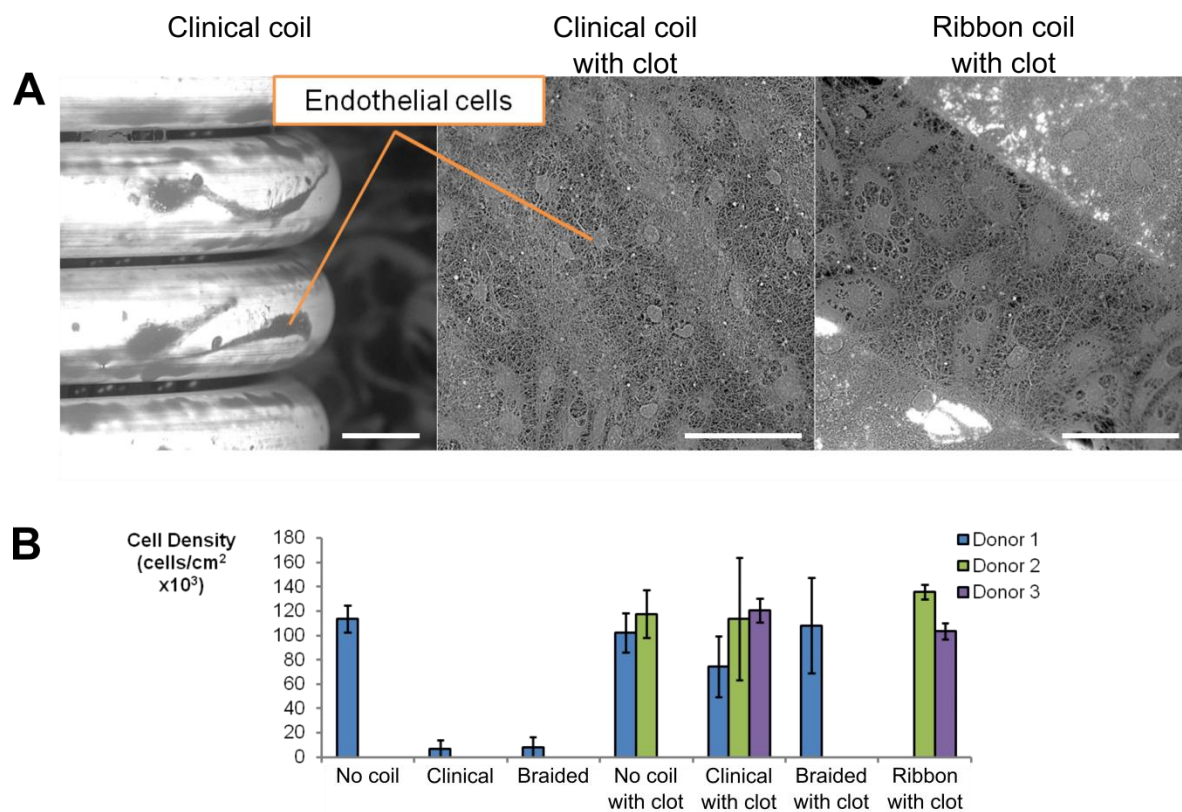


Figure 38: EC attachment is higher on clotted coils than bare coils but is not dependent on coil design. A: Representative SEM images of ECs cultured on a bare clinical coil (left), a clotted clinical coil (middle) and a clotted ribbon coil (right). Scale bar, 50 μm . B: Quantitative analysis of SEM images shows that the number of ECs per field of view is higher on bare tissue culture polystyrene dishes and clotted coils than bare metal coils. EC attachment was not dependent on coil design across three different experiments ($p=0.35$, $p=0.97$, $p=0.83$).

healing.³ These additional studies would help clarify the relationships between coil wire and secondary shapes, flow velocity and pattern, and clot structure and accumulation.

Within the coil packing and design experiments, some changes to the methods may allow the evaluation of processes more specific to clinical practice. Namely, anticoagulants administered to patients during the coiling procedure are likely to affect clot accumulation and structure. Their effects on the relationships between coil-mediated hemodynamics and clotting may prove useful in guiding anticoagulant therapies during coil treatment for specific coil arrangements and designs. In addition, the methods detailed in these studies observe initial thrombosis, but clots in IAs degrade over time. Clot degradation over a longer period of time may be analyzed by incorporating mechanical breakdown in response to persistent flow over time or tissue plasminogen activator-induced fibrinolysis.¹¹¹ These studies would provide new information about the spatiotemporal dynamics of clot degradation and how it is affected by coil shape, coil packing, clot structure and clot size. Since these clots provide the scaffold for IA cellularization in later stages of healing but must also promote cell infiltration, information about how coil packing and design modulate clot degradation in coiled IAs would contribute to a better understanding of IA healing and recurrence.

6.2 MODEL OF CLOTTING AND CELLULARIZATION UNDER FLOW

IA *in vitro* models in the literature have effectively identified some of the factors and mechanisms that drive hemodynamics, thrombosis and cellularization *in vivo*, but do not yet provide complete information on the relationships between these three components. Many available *in vitro* models are insufficient to predict patient outcome,^{53,112} suggesting that models that capture all three healing components are needed. Vascular cells are responsive to surface geometry^{113,114} and edge angle,⁸³ indicating that cell behavior is dependent on coil presence and shape. Well-established *in vitro* models interrogate processes relevant to aneurysm healing, such as endothelial cell (EC),^{65,115,116} vascular smooth muscle cell⁶² and fibroblast^{62,63} phenotypes in response to flow dynamics, interactions between these cell types^{66,117} and platelet-EC interactions.¹¹⁸ Studies of EC behavior on coils in the absence of flow (Chapter 1, Figure 3, “Cellularization” and “Cell-Matrix Model”) indicate that relationships between cellularization and clotting are important to IA healing. Specifically, EC coverage on clotted coils was significantly higher than that on bare metal coils ($p < 0.05$), indicating that clot coverage may be important to cellularization *in vivo*. In this study, cell coverage was independent of coil presence or design across three different experiments ($p = 0.35$, $p = 0.97$, $p = 0.83$, Figure 38), which was expected since clot structure was independent of coil presence or design in the absence of flow (Figure 6). Additionally, ECs cultured on clotted ribbon coils formed monolayers along clot structures (Figure 39, “Coil surface”), indicating that EC monolayers can be manipulated by underlying clot structure. Consistent with known matrix remodeling capabilities,¹¹⁹ ECs cultured on clots formed on glass surfaces reorganized underlying clot structure (Figure 39, “Glass surface”), pointing to feedback between EC monolayer behavior and clot structure. These models

indicate that *in vitro* models of cellularization on clotted coiled saccular aneurysms under flow are achievable and valuable.

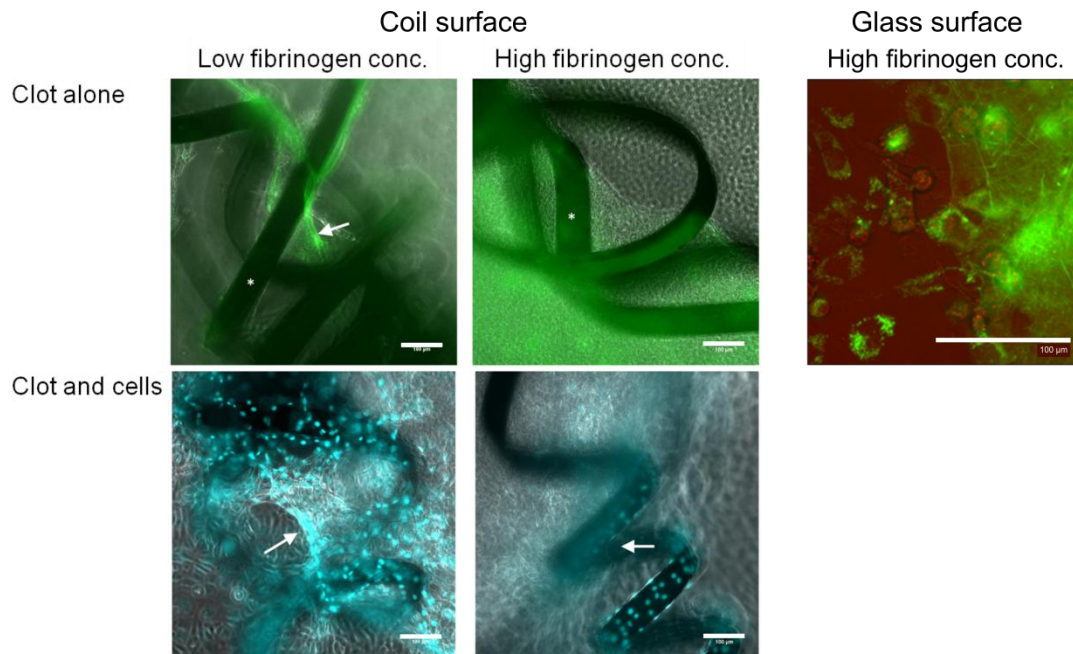


Figure 39: Feedback exists between cell behavior and clot structure. Left: Clots (green) on edged coils (*) formed net structures (above, arrow) that produced EC (cyan) monolayer nets (below, arrow) at low fibrinogen concentration. Scale bar, 100 μm . Right: On glass surfaces, ECs also reorganized clot structure (green) around them. Scale bar, 20 μm .

Models that investigate the relationship between EC behavior and clotting under flow (Chapter 1, Figure 3, “Cellularized Blood Flow Model”) exist and can provide important new information about cellularization in IAs. In a model of microvascular thrombosis,¹¹⁵ whole blood clotting under various shear stress magnitudes was observed in channels lined with ECs. With the introduction of IA geometry and complex flow patterns and by increasing the size of the system to accommodate coils, this model would provide insight into the relationships between IA hemodynamics, EC behaviors, thrombosis and coil design. In a preliminary study, the sac flow chamber model was lined with ECs (Figure 40A and B) and coiled, and a clot was allowed to form on the coils in the absence of flow. ECs from the sac wall adhered to clots that bridged between the coil and the neck wall (Figure 40C), indicating endothelialization of clotted coils. This study demonstrated that a model of endothelialization of clotted coils under flow in a saccular aneurysm is possible, which would produce information about the coil-mediated hemodynamics, coil shapes, clot structures and clot sizes that are likely to promote endothelialization in IAs. Fibroblasts could also be seeded into the model to observe cell-mediated remodeling of the clot, an important step in IA healing and protection of the IA from recurrence. This information would drive coil design and coiling technique. These models would also more effectively screen coil designs and arrangements for optimal cellularization before studies in animal models. In addition to isolated intra-aneurysmal hemodynamics, thrombosis and cellularization models, these three phenomena must be combined in *in vitro* models in order to understand how they affect one another and how these relationships predict IA outcome.

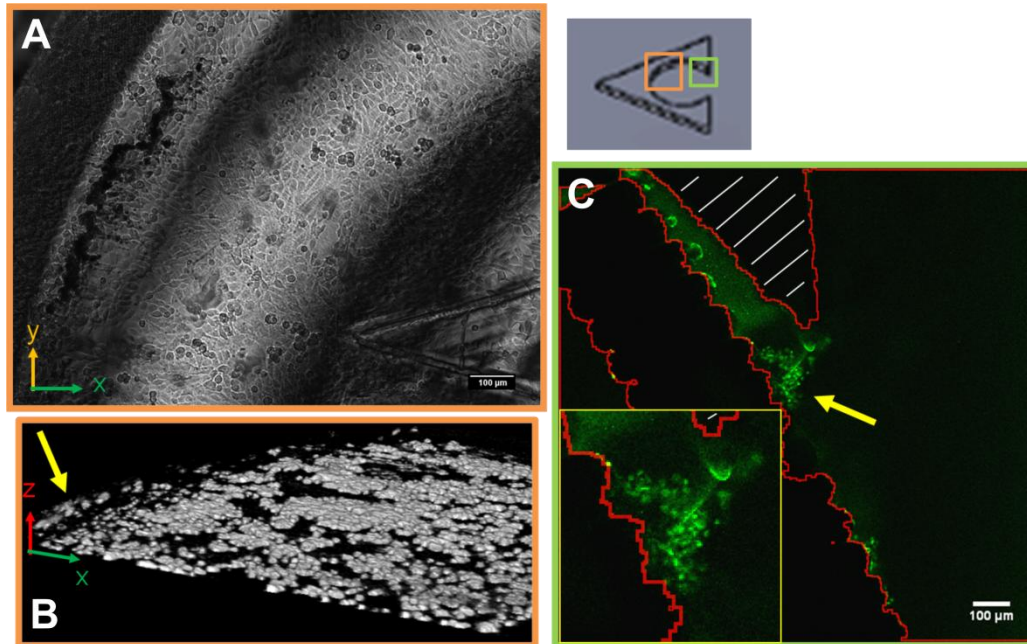


Figure 40: Preliminary studies show that the sac model can be lined with ECs. A: Phase contrast image of an EC monolayer on the bottom surface of the sac flow chamber. Scale bar, 100 μm . B: Nucleus staining shows that the EC monolayer extends up the dome wall (arrow). C: Endothelialized sac was coiled and clotted. ECs (green dots) were observed on clot (green line) that formed between the coils and the wall (red outlines). Inset shows magnified view. Scale bar, 100 μm . Schematic indicates the field of view for A and B (orange) and C (green) within the sac.

WORKS CITED

1. Brain Aneurysm Statistics and Facts – Brain Aneurysm Foundation. Available at: <http://www.bafound.org/about-brain-aneurysms/brain-aneurysm-basics/brain-aneurysm-statistics-and-facts/>. (Accessed: 4th January 2017)
2. Walcott, B. P., Koch, M. J., Stapleton, C. J. & Patel, A. B. Blood Flow Diversion as a Primary Treatment Method for Ruptured Brain Aneurysms—Concerns, Controversy, and Future Directions. *Neurocrit. Care* 1–9 (2016). doi:10.1007/s12028-016-0318-y
3. Brinjikji, W., Kallmes, D. F. & Kadirvel, R. Mechanisms of Healing in Coiled Intracranial Aneurysms: A Review of the Literature. *Am. J. Neuroradiol.* **36**, 1216–1222 (2015).
4. Dai, D. *et al.* Histopathologic and Immunohistochemical Comparison of Human, Rabbit, and Swine Aneurysms Embolized with Platinum Coils. *Am. J. Neuroradiol.* **26**, 2560–2568 (2005).
5. Bavinzski, G. *et al.* Gross and microscopic histopathological findings in aneurysms of the human brain treated with Guglielmi detachable coils. *J. Neurosurg.* **91**, 284–293 (1999).
6. Yuichi Murayama *et al.* Guglielmi Detachable Coil embolization of cerebral aneurysms: 11 years' experience. <http://dx.doi.org/10.3171/jns.2003.98.5.0959> (2003). Available at: <http://thejns.org/doi/abs/10.3171/jns.2003.98.5.0959>. (Accessed: 10th January 2014)
7. Brisman, J. L., Song, J. K. & Newell, D. W. Cerebral Aneurysms. *N. Engl. J. Med.* **355**, 928–939 (2006).
8. Ujiie, H. *et al.* Effects of Size and Shape (Aspect Ratio) on the Hemodynamics of Saccular Aneurysms: A Possible Index for Surgical Treatment of Intracranial Aneurysms. [Miscellaneous Article]. *Neurosurg. July 1999* **45**, (1999).
9. Schneiders, J. J. *et al.* Additional Value of Intra-Aneurysmal Hemodynamics in Discriminating Ruptured versus Unruptured Intracranial Aneurysms. *AJNR Am. J. Neuroradiol.* (2015). doi:10.3174/ajnr.A4397
10. Babiker, M. H. *et al.* Quantitative Effects of Coil Packing Density on Cerebral Aneurysm Fluid Dynamics: An *In vitro* Steady Flow Study. *Ann. Biomed. Eng.* **38**, 2293–2301 (2010).
11. Morales, H. G. *et al.* How Do Coil Configuration and Packing Density Influence Intra-Aneurysmal Hemodynamics? *Am. J. Neuroradiol.* **32**, 1935–1941 (2011).
12. Meng, H., Tutino, V. M., Xiang, J. & Siddiqui, A. High WSS or Low WSS? Complex Interactions of Hemodynamics with Intracranial Aneurysm Initiation, Growth, and Rupture: Toward a Unifying Hypothesis. *Am. J. Neuroradiol.* **35**, 1254–1262 (2014).
13. Kolega, J. *et al.* Cellular and Molecular Responses of the Basilar Terminus to Hemodynamics during Intracranial Aneurysm Initiation in a Rabbit Model. *J. Vasc. Res.* **48**, 429–442 (2011).

14. Tjahjadi, M. *et al.* Factors Determining Surgical Approaches to Basilar Bifurcation Aneurysms and Its Surgical Outcomes. *Neurosurgery* (2015). doi:10.1227/NEU.0000000000001021
15. Sides Media, www.sidesmedia.com. Endovascular Today - Buyer's Guide 2014. Available at: http://www.evtoday.com/buyers-guide/2014/chart.asp?id=embolization_coils. (Accessed: 18th September 2014)
16. Guglielmi, G., Viñuela, F., Sepetka, I. & Macellari, V. Electrothrombosis of saccular aneurysms via endovascular approach. *J. Neurosurg.* **75**, 1–7 (1991).
17. Mangiafico, S., Guarnieri, G., Consoli, A., Ambrosanio, G. & Muto, M. Endovascular strategy for unruptured cerebral aneurysms. *Eur. J. Radiol.* **82**, 1638–1645 (2013).
18. Babiker, M. H., Chong, B., Gonzalez, L. F., Cheema, S. & Frakes, D. H. Finite element modeling of embolic coil deployment: Multifactor characterization of treatment effects on cerebral aneurysm hemodynamics. *J. Biomech.* **46**, 2809–2816 (2013).
19. Piotin, M., Iijima, A., Wada, H. & Moret, J. Increasing the Packing of Small Aneurysms with Complex-Shaped Coils: An *In vitro* Study. *Am. J. Neuroradiol.* **24**, 1446–1448 (2003).
20. White, P. M. *et al.* Hydrogel-coated coils versus bare platinum coils for the endovascular treatment of intracranial aneurysms (HELPS): a randomised controlled trial. *The Lancet* **377**, 1655–1662 (2011).
21. Brinjikji, W. *et al.* HydroCoils Are Associated with Lower Angiographic Recurrence Rates Than Are Bare Platinum Coils in Treatment of 'Difficult-to-Treat' Aneurysms: A Post Hoc Subgroup Analysis of the HELPS Trial. *AJNR Am. J. Neuroradiol.* **36**, 1689–1694 (2015).
22. Broeders, J. A. *et al.* Bioactive versus bare platinum coils for the endovascular treatment of intracranial aneurysms: systematic review and meta-analysis of randomized clinical trials. *J. NeuroInterventional Surg.* neurintsurg-2015-011881 (2015). doi:10.1136/neurintsurg-2015-011881
23. Ren, H., Wei, M., Yin, L., Ma, L. & Peng, L. Endovascular coiling of small intracranial aneurysms using a very soft bare platinum coil: A comparison of the packing performance of new and old HyperSoft® helical coils. *Interv. Neuroradiol. J. Peritherapeutic Neuroradiol. Surg. Proced. Relat. Neurosci.* (2015). doi:10.1177/1591019915617319
24. Piotin, M. & Blanc, R. Balloons and Stents in the Endovascular Treatment of Cerebral Aneurysms: Vascular Anatomy Remodeled. *Front. Neurol.* **5**, (2014).
25. Starke, R. M. *et al.* Technology developments in endovascular treatment of intracranial aneurysms. *J. NeuroInterventional Surg.* neurintsurg-2014-011475 (2014). doi:10.1136/neurintsurg-2014-011475
26. Cognard, C. & Januel, A. C. Remnants and Recurrences After the Use of the WEB Intrasaccular Device in Large-Neck Bifurcation Aneurysms: *Neurosurgery* **76**, 522–530 (2015).

27. Pierot, L. *et al.* Safety and efficacy of aneurysm treatment with WEB: results of the WEBCAST study. *J. Neurosurg.* 1–7 (2015). doi:10.3171/2015.2.JNS142634
28. Pérez, M. A. *et al.* Intra-aneurysmal hemodynamics: evaluation of pCONus and pCANvas bifurcation aneurysm devices using DSA optical flow imaging. *J. Neurointerventional Surg.* (2015). doi:10.1136/neurintsurg-2015-011927
29. Shimizu, S. *et al.* Tissue Response of a Small Saccular Aneurysm after Incomplete Occlusion with a Guglielmi Detachable Coil. *Am. J. Neuroradiol.* **20**, 546–548 (1999).
30. Szikora, I. *et al.* Histopathologic Evaluation of Aneurysms Treated with Guglielmi Detachable Coils or Matrix Detachable Microcoils. *Am. J. Neuroradiol.* **27**, 283–288 (2006).
31. Stiver, S. I., Porter, P. J., Willinsky, R. A. & Wallace, M. C. Acute Human Histopathology of an Intracranial Aneurysm Treated Using Guglielmi Detachable Coils: Case Report and Review of the Literature. *Neurosurgery* **43**, 1203–1207 (1998).
32. Castro, E. *et al.* Long-term Histopathologic Findings in Two Cerebral Aneurysms Embolized with Guglielmi Detachable Coils. *Am. J. Neuroradiol.* **20**, 549–552 (1999).
33. Mizoi, K., Yoshimoto, T., Takahashi, A. & Nagamine, Y. A Pitfall in the Surgery of a Recurrent Aneurysm after Coil Embolization and Its Histological Observation: Technical Case Report. *Neurosurgery* **39**, 165–169 (1996).
34. Frösen, J. *et al.* Saccular intracranial aneurysm: pathology and mechanisms. *Acta Neuropathol. (Berl.)* **123**, 773–786 (2012).
35. Sforza, D. M., Putman, C. M. & Cebal, J. R. Hemodynamics of Cerebral Aneurysms. *Annu. Rev. Fluid Mech.* **41**, 91–107 (2009).
36. Shojima, M. *et al.* Magnitude and Role of Wall Shear Stress on Cerebral Aneurysm Computational Fluid Dynamic Study of 20 Middle Cerebral Artery Aneurysms. *Stroke* **35**, 2500–2505 (2004).
37. Frösen, J. *et al.* Remodeling of Saccular Cerebral Artery Aneurysm Wall Is Associated With Rupture Histological Analysis of 24 Unruptured and 42 Ruptured Cases. *Stroke* **35**, 2287–2293 (2004).
38. Castro, M. A. Understanding the Role of Hemodynamics in the Initiation, Progression, Rupture, and Treatment Outcome of Cerebral Aneurysm from Medical Image-Based Computational Studies. *ISRN Radiol.* **2013**, 1–17 (2013).
39. de Oliveira, I. A. Main Models of Experimental Saccular Aneurysm in Animals. in *Aneurysm* (ed. Murai, Y.) (InTech, 2012).
40. Brinjikji, W., Ding, Y. H., Kallmes, D. F. & Kadirvel, R. From bench to bedside: utility of the rabbit elastase aneurysm model in preclinical studies of intracranial aneurysm treatment. *J. NeuroInterventional Surg.* **8**, 521–525 (2016).
41. Cebal, J. R. *et al.* Characterization of Cerebral Aneurysms for Assessing Risk of Rupture By Using Patient-Specific Computational Hemodynamics Models. *Am. J. Neuroradiol.* **26**, 2550–2559 (2005).

42. Burleson, A. C., Strother, C. M. & Turitto, V. T. Computer Modeling of Intracranial Saccular and Lateral Aneurysms for the Study of Their Hemodynamics. *Neurosurgery* **37**, 774–784 (1995).
43. Schirmer, C. M. & Malek, A. M. Critical Influence of Framing Coil Orientation on Intra-Aneurysmal and Neck Region Hemodynamics in a Sidewall Aneurysm Model: *Neurosurgery* **67**, 1692–1702 (2010).
44. Goubergrits, L. *et al.* *In vitro* Study of Near-Wall Flow in a Cerebral Aneurysm Model with and without Coils. *Am. J. Neuroradiol.* **31**, 1521–1528 (2010).
45. Ngoepe, M. N. & Ventikos, Y. Computational modelling of clot development in patient-specific cerebral aneurysm cases. *J. Thromb. Haemost. JTH* (2015). doi:10.1111/jth.13220
46. Mountrakis, L., Lorenz, E. & Hoekstra, A. G. Where do the platelets go? A simulation study of fully resolved blood flow through aneurysmal vessels. *Interface Focus* **3**, 20120089 (2013).
47. Ou, C., Huang, W., Yuen, M. M.-F. & Qian, Y. Hemodynamic modeling of leukocyte and erythrocyte transport and interactions in intracranial aneurysms by a multiphase approach. *J. Biomech.* **49**, 3476–3484 (2016).
48. Girdhar, G., Read, M., Sohn, J., Shah, C. & Shrivastava, S. In-vitro thrombogenicity assessment of polymer filament modified and native platinum embolic coils. *J. Neurol. Sci.* **339**, 97–101 (2014).
49. Henkes, H. *et al.* *In vitro* and *in vivo* Studies of the Extent of Electrothrombotic Deposition of Blood Elements on the Surface of Electrolytically Detachable Coils. *Interv. Neuroradiol. J. Peritherapeutic Neuroradiol. Surg. Proced. Relat. Neurosci.* **10**, 189–201 (2004).
50. Liebig, T. *et al.* Fibered Electrolytically Detachable Platinum Coils Used for the Endovascular Treatment of Intracranial Aneurysms. *Interv. Neuroradiol.* **10**, 5–26 (2004).
51. Matsumoto, H., Terada, T., Tsuura, M., Itakura, T. & Ogawa, A. Basic Fibroblast Growth Factor Released from a Platinum Coil with a Polyvinyl Alcohol Core Enhances Cellular Proliferation and Vascular Wall Thickness: An *in vitro* and *in vivo* Study: *Neurosurgery* **53**, 402–408 (2003).
52. Kallmes, D. F. *et al.* *In vitro* proliferation and adhesion of basic fibroblast growth factor-producing fibroblasts on platinum coils. *Radiology* **206**, 237–243 (1998).
53. Pandey, A. S. *et al.* Mechanisms of Endothelial Cell Attachment, Proliferation, and Differentiation on 4 Types of Platinum-Based Endovascular Coils. *World Neurosurg.* **82**, 684–695 (2014).
54. Bendszus, M. & Solymosi, L. Cerebral Coils in the Treatment of Intracranial Aneurysms: A Preliminary Clinical Study. *Am. J. Neuroradiol.* **27**, 2053–2057 (2006).
55. Tamatani, S. *et al.* Histological interaction of cultured endothelial cells and endovascular embolic materials coated with extracellular matrix. *J. Neurosurg.* **86**, 109–112 (1997).

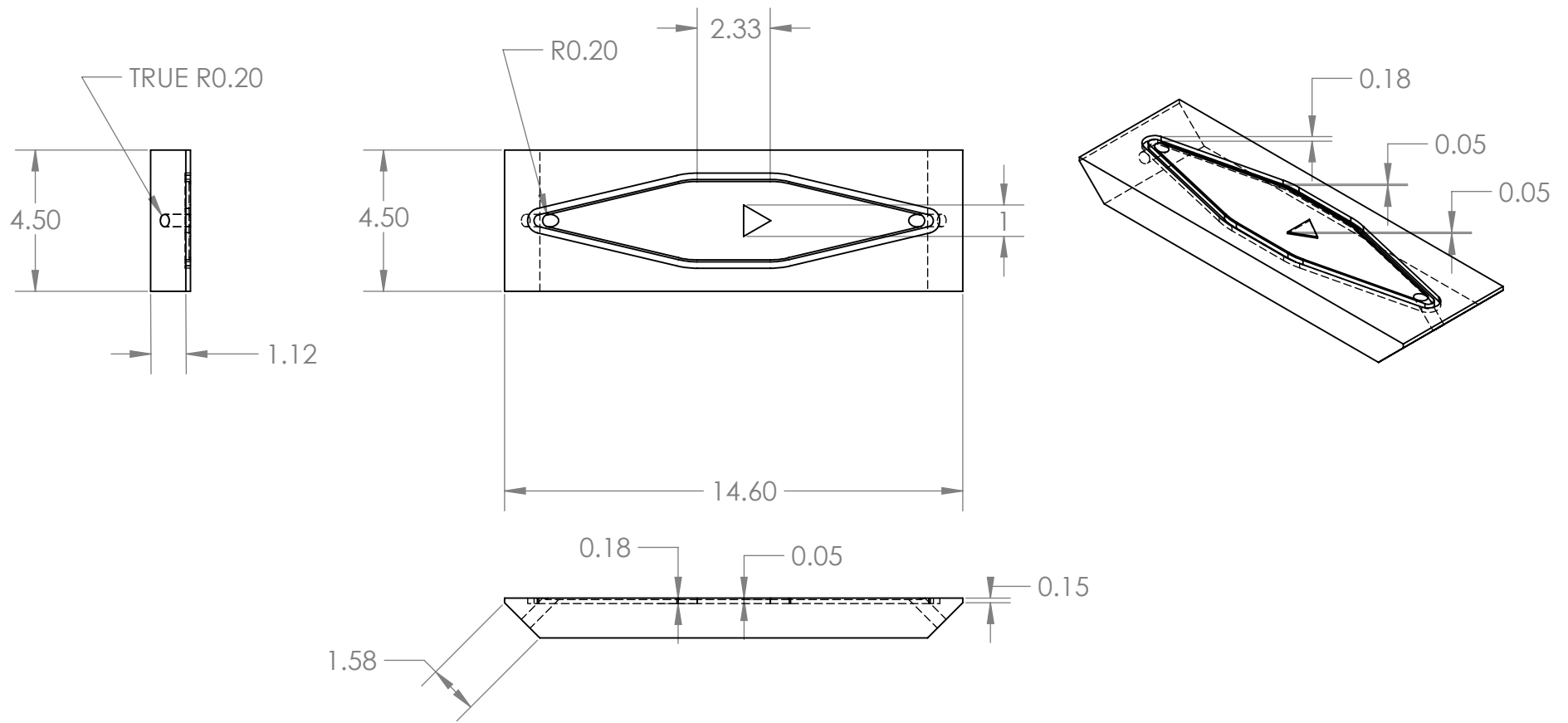
56. Abruzzo, T. *et al.* Interaction of Vascular Smooth Muscle Cells with Collagen-Impregnated Embolization Coils Studied with a Novel Quantitative *in vitro* Model. *Am. J. Neuroradiol.* **23**, 674–681 (2002).
57. Murayama, Y. *et al.* Development of a Biologically Active Guglielmi Detachable Coil for the Treatment of Cerebral Aneurysms. Part I: *In vitro* Study. *Am. J. Neuroradiol.* **20**, 1986–1991 (1999).
58. Hoh, B. L. *et al.* Monocyte Chemoattractant Protein-1 Promotes Inflammatory Vascular Repair of Murine Carotid Aneurysms via a Macrophage Inflammatory Protein-1 α and Macrophage Inflammatory Protein-2–Dependent Pathway. *Circulation* **124**, 2243–2252 (2011).
59. Lerouge, S. *et al.* Nitrogen-rich coatings for promoting healing around stent-grafts after endovascular aneurysm repair. *Biomaterials* **28**, 1209–1217 (2007).
60. Gersh, K. C., Edmondson, K. E. & Weisel, J. W. Flow rate and fibrin fiber alignment. *J. Thromb. Haemost.* **8**, 2826–2828 (2010).
61. Hosokawa, K. *et al.* A novel automated microchip flow-chamber system to quantitatively evaluate thrombus formation and antithrombotic agents under blood flow conditions. *J. Thromb. Haemost.* **9**, 2029–2037 (2011).
62. Shi, Z.-D. & Tarbell, J. M. Fluid Flow Mechanotransduction in Vascular Smooth Muscle Cells and Fibroblasts. *Ann. Biomed. Eng.* **39**, 1608–1619 (2011).
63. Ng, C. P. & Swartz, M. A. Fibroblast alignment under interstitial fluid flow using a novel 3-D tissue culture model. *Am. J. Physiol. - Heart Circ. Physiol.* **284**, H1771–H1777 (2003).
64. Malek AM, Alper SL & Izumo S. Hemodynamic shear stress and its role in atherosclerosis. *JAMA* **282**, 2035–2042 (1999).
65. Helmke, B. P. Molecular Control of Cytoskeletal Mechanics by Hemodynamic Forces. *Physiology* **20**, 43–53 (2005).
66. Rose, S. L. & Babensee, J. E. Smooth muscle cell phenotype alters cocultured endothelial cell response to biomaterial-pretreated leukocytes. *J. Biomed. Mater. Res. A* **84A**, 661–671 (2008).
67. Beamish, J. A., He, P., Kottke-Marchant, K. & Marchant, R. E. Molecular Regulation of Contractile Smooth Muscle Cell Phenotype: Implications for Vascular Tissue Engineering. *Tissue Eng. Part B Rev.* **16**, 467–491 (2010).
68. Siegel-Axel, D. & Gawaz, M. Platelets and Endothelial Cells. *Semin. Thromb. Hemost.* **33**, 128–135 (2007).
69. Baharoglu, M. I., Schirmer, C. M., Hoit, D. A., Gao, B.-L. & Malek, A. M. Aneurysm Inflow-Angle as a Discriminant for Rupture in Sidewall Cerebral Aneurysms Morphometric and Computational Fluid Dynamic Analysis. *Stroke* **41**, 1423–1430 (2010).
70. Can, A. & Du, R. Association of Hemodynamic Factors With Intracranial Aneurysm Formation and Rupture: Systematic Review and Meta-analysis. *Neurosurgery* (2015). doi:10.1227/NEU.0000000000001083

71. Jou, L., Desai, V. R. & Britz, G. W. *In vitro* investigation of contrast flow jet timing in patient-specific intracranial aneurysms. *Quant. Imaging Med. Surg.* **6**, 134–143 (2016).
72. Ohshima, T., Miyachi, S., Takahashi, I. & Ishii, K. Assessment of endovascular coil configuration for embolization of intracranial aneurysms using computational fluid dynamics. *Nagoya J. Med. Sci.* **77**, 383–388 (2015).
73. Qian, Z., Kang, H., Li, C., Wu, Z. & Liu, A. Effect of hemodynamics on the recurrence of posterior communicating artery aneurysm: a computational fluid dynamics simulation study. *Int. Angiol. J. Int. Union Angiol.* (2015).
74. Braaten, J. V., Jerome, W. G. & Hantgan, R. R. Uncoupling fibrin from integrin receptors hastens fibrinolysis at the platelet-fibrin interface. *Blood* **83**, 982–993 (1994).
75. Gester, K. *et al.* *In vitro* Evaluation of Intra-Aneurysmal, Flow-Diverter-Induced Thrombus Formation: A Feasibility Study. *Am. J. Neuroradiol.* (2015). doi:10.3174/ajnr.A4555
76. Kaneko, N. *et al.* A patient-specific intracranial aneurysm model with endothelial lining: a novel *in vitro* approach to bridge the gap between biology and flow dynamics. *J. NeuroInterventional Surg.* neurintsurg-2017-013087 (2017). doi:10.1136/neurintsurg-2017-013087
77. Keun Kwon, I., Kidoaki, S. & Matsuda, T. Electrospun nano- to microfiber fabrics made of biodegradable copolyesters: structural characteristics, mechanical properties and cell adhesion potential. *Biomaterials* **26**, 3929–3939 (2005).
78. Cox, S., Cole, M. & Tawil, B. Behavior of Human Dermal Fibroblasts in Three-Dimensional Fibrin Clots: Dependence on Fibrinogen and Thrombin Concentration. *Tissue Eng.* **10**, 942–954 (2004).
79. Neeves, K. B., Illing, D. A. R. & Diamond, S. L. Thrombin Flux and Wall Shear Rate Regulate Fibrin Fiber Deposition State during Polymerization under Flow. *Biophys. J.* **98**, 1344–1352 (2010).
80. Bluestein, D., Niu, L., Schoepfoerster, R. T. & Dewanjee, M. K. Steady Flow in an Aneurysm Model: Correlation Between Fluid Dynamics and Blood Platelet Deposition. *J. Biomech. Eng.* **118**, 280–286 (1996).
81. Palmaz, J. C., Benson, A. & Sprague, E. A. Influence of Surface Topography on Endothelialization of Intravascular Metallic Material. *J. Vasc. Interv. Radiol.* **10**, 439–444 (1999).
82. SCHEERDER, I. *et al.* Metallic surface treatment using electrochemical polishing decreases thrombogenicity and neointimal hyperplasia of coronary stents. *J. Intervent. Cardiol.* **13**, 179–185 (2000).
83. Hamuro, M., Palmaz, J. C., Sprague, E. A., Fuss, C. & Luo, J. Influence of stent edge angle on endothelialization in an *in vitro* model. *J. Vasc. Interv. Radiol.* **12**, 607–611 (2001).

84. Wang, C. W., Perez, M. J., Helmke, B. P., Viola, F. & Lawrence, M. B. Integration of Acoustic Radiation Force and Optical Imaging for Blood Plasma Clot Stiffness Measurement. *PLOS ONE* **10**, e0128799 (2015).
85. Kaesmacher, J. *et al.* Volume versus standard coils in the treatment of intracranial aneurysms. *J. Neurointerventional Surg.* (2016). doi:10.1136/neurintsurg-2015-012014
86. Ding, Y. H. *et al.* Relationship Between Aneurysm Volume and Histologic Healing after Coil Embolization in Elastase-Induced Aneurysms: A Retrospective Study. *Am. J. Neuroradiol.* **29**, 98–101 (2008).
87. Jou, L.-D., Lee, D. H., Morsi, H. & Mawad, M. E. Wall Shear Stress on Ruptured and Unruptured Intracranial Aneurysms at the Internal Carotid Artery. *Am. J. Neuroradiol.* **29**, 1761–1767 (2008).
88. Sato, K., Imai, Y., Ishikawa, T., Matsuki, N. & Yamaguchi, T. The importance of parent artery geometry in intra-aneurysmal hemodynamics. *Med. Eng. Phys.* **30**, 774–782 (2008).
89. Ho, W., Tawil, B., Dunn, J. C. Y. & Wu, B. M. The Behavior of Human Mesenchymal Stem Cells in 3D Fibrin Clots: Dependence on Fibrinogen Concentration and Clot Structure. *Tissue Eng.* **12**, 1587–1595 (2006).
90. Nehls, V. & Herrmann, R. The Configuration of Fibrin Clots Determines Capillary Morphogenesis and Endothelial Cell Migration. *Microvasc. Res.* **51**, 347–364 (1996).
91. Bashur, C. A., Dahlgren, L. A. & Goldstein, A. S. Effect of fiber diameter and orientation on fibroblast morphology and proliferation on electrospun poly(d,l-lactic-co-glycolic acid) meshes. *Biomaterials* **27**, 5681–5688 (2006).
92. Van Kruchten, R., Cosemans, J. M. E. M. & Heemskerk, J. W. M. Measurement of whole blood thrombus formation using parallel-plate flow chambers – a practical guide. *Platelets* **23**, 229–242 (2012).
93. Kawasaki, J., Katori, N., Kodaka, M., Miyao, H. & Tanaka, K. A. Electron Microscopic Evaluations of Clot Morphology During Thrombelastography??: *Anesth. Analg.* 1440–1444 (2004). doi:10.1213/01.ANE.0000134805.30532.59
94. Schneider, C. A., Rasband, W. S. & Eliceiri, K. W. NIH Image to ImageJ: 25 years of image analysis. *Nature Methods* (2012). doi:10.1038/nmeth.2089
95. BIG > OrientationJ. Available at: <http://bigwww.epfl.ch/demo/orientation/>. (Accessed: 30th January 2018)
96. Ozawa, T. *et al.* Histological Evaluation of Endothelial Reactions after Endovascular Coil Embolization for Intracranial Aneurysm. *Interv. Neuroradiol.* **9**, 69–82 (2003).
97. Zhang, Y., Xing, X., Shen, X. & Zhu, X. The Volume Embolization Ratio of Intraaneurysmal Embolization Using Guglielmi Detachable Coils. *Turk. Neurosurg.* **25**, 866–872 (2015).

98. Jirouskova, M., Smyth, S. S., Kudryk, B. & Coller, B. S. A hamster antibody to the mouse fibrinogen γ chain inhibits platelet-fibrinogen interactions and FXIIIa-mediated fibrin cross-linking, and facilitates thrombolysis. *Thromb. Haemost.* **86**, 1047–1056 (2001).
99. Badiei, N. *et al.* Effects of unidirectional flow shear stresses on the formation, fractal microstructure and rigidity of incipient whole blood clots and fibrin gels. *Clin. Hemorheol. Microcirc.* **60**, 451–464 (2015).
100. Manual Tracking. Available at: <https://imagej.nih.gov/ij/plugins/track/track.html>. (Accessed: 20th December 2016)
101. Quiverc - File Exchange - MATLAB Central. Available at: <http://www.mathworks.com/matlabcentral/fileexchange/3225-quiverc>. (Accessed: 15th December 2017)
102. Mills, J. D., Ariëns, R. A. S., Mansfield, M. W. & Grant, P. J. Altered Fibrin Clot Structure in the Healthy Relatives of Patients With Premature Coronary Artery Disease. *Circulation* **106**, 1938–1942 (2002).
103. Kawanabe, Y., Sadato, A., Taki, W. & Hashimoto, N. Endovascular Occlusion of Intracranial Aneurysms with Guglielmi Detachable Coils: Correlation Between Coil Packing Density and Coil Compaction. *Acta Neurochir. (Wien)* **143**, 451–455 (2001).
104. Stemberman, M. B. Thrombogenesis of the Rabbit Arterial Plaque. *Am. J. Pathol.* **73**, 7–26 (1973).
105. ImageJ - Distance Between Lines, a plugin for ImageJ. Available at: <http://imagej.1557.x6.nabble.com/Distance-Between-Lines-a-plugin-for-ImageJ-td3701802.html>. (Accessed: 31st January 2018)
106. Rayz, V. L. *et al.* Flow Residence Time and Regions of Intraluminal Thrombus Deposition in Intracranial Aneurysms. *Ann. Biomed. Eng.* **38**, 3058–3069 (2010).
107. Powell, H. M. & Boyce, S. T. Fiber density of electrospun gelatin scaffolds regulates morphogenesis of dermal–epidermal skin substitutes. *J. Biomed. Mater. Res. A* **84A**, 1078–1086 (2008).
108. Collet, J. P. *et al.* Influence of Fibrin Network Conformation and Fibrin Fiber Diameter on Fibrinolysis Speed Dynamic and Structural Approaches by Confocal Microscopy. *Arterioscler. Thromb. Vasc. Biol.* **20**, 1354–1361 (2000).
109. Hantgan, R. R., Jerome, W. G. & Handt, S. Platelets and endothelial cells act in concert to delay thrombolysis--evidence from an *in vitro* model of the human occlusive thrombus. *Thromb. Haemost.* **79**, 602–608 (1998).
110. Gersh, K. C., Nagaswami, C. & Weisel, J. W. Fibrin network structure and clot mechanical properties are altered by incorporation of erythrocytes. *Thromb. Haemost.* **102**, 1169–1175 (2009).
111. Carr, J. M. & Alving, B. M. Effect of fibrin structure on plasmin-mediated dissolution of plasma clots. *Blood Coagul. Fibrinolysis Int. J. Haemost. Thromb.* **6**, 567–573 (1995).

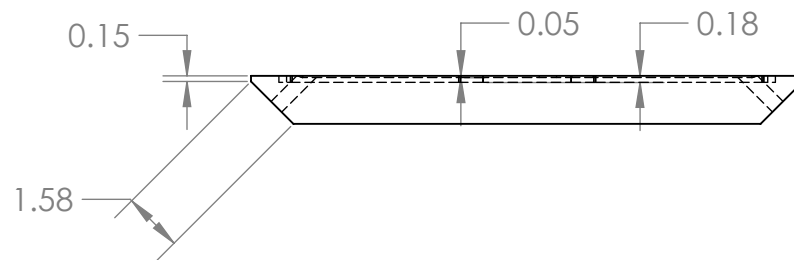
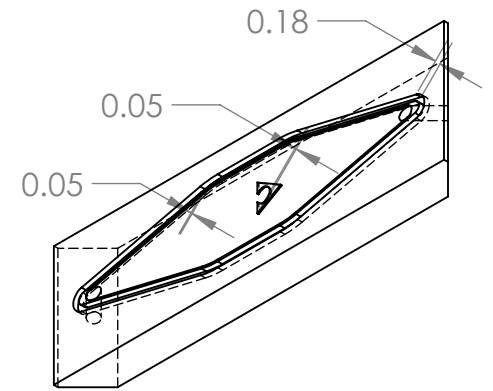
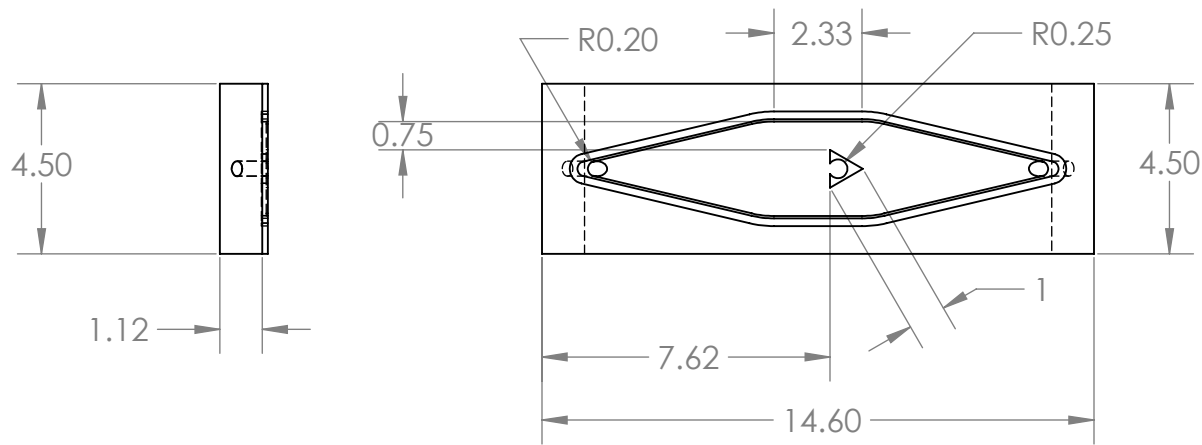
112. Molyneux, A. J. *et al.* Cerecyte Coil Trial Angiographic Outcomes of a Prospective Randomized Trial Comparing Endovascular Coiling of Cerebral Aneurysms With Either Cerecyte or Bare Platinum Coils. *Stroke* **43**, 2544–2550 (2012).
113. Chen, C. S., Alonso, J. L., Ostuni, E., Whitesides, G. M. & Ingber, D. E. Cell shape provides global control of focal adhesion assembly. *Biochem. Biophys. Res. Commun.* **307**, 355–361 (2003).
114. Alves, N. M., Pashkuleva, I., Reis, R. L. & Mano, J. F. Controlling Cell Behavior Through the Design of Polymer Surfaces. *Small* **6**, 2208–2220 (2010).
115. Tsai, M. *et al.* *In vitro* modeling of the microvascular occlusion and thrombosis that occur in hematologic diseases using microfluidic technology. *J. Clin. Invest.* **122**, (2011).
116. Thoumine, O., Nerem, R. M. & Girard, F. R. Oscillatory shear stress and hydrostatic pressure modulate cell-matrix attachment proteins in cultured endothelial cells. *Vitro Cell. Dev. Biol. - Anim.* **31**, 45–54 (1995).
117. Kunz-Schughart, L. A. *et al.* Potential of fibroblasts to regulate the formation of three-dimensional vessel-like structures from endothelial cells *in vitro*. *Am. J. Physiol. - Cell Physiol.* **290**, C1385–C1398 (2006).
118. Rose, S. L. & Babensee, J. E. Procoagulant phenotype of endothelial cells after coculture with biomaterial-treated blood cells. *J. Biomed. Mater. Res. A* **72A**, 269–278 (2005).
119. Jerome, W. G., Handt, S. & Hantgan, R. R. Endothelial Cells Organize Fibrin Clots into Structures That Are More Resistant to Lysis. *Microsc. Microanal.* **11**, 268–277 (2005).



PROPRIETARY AND CONFIDENTIAL
 THE INFORMATION CONTAINED IN THIS DRAWING IS THE SOLE PROPERTY OF <INSERT COMPANY NAME HERE>. ANY REPRODUCTION IN PART OR AS A WHOLE WITHOUT THE WRITTEN PERMISSION OF <INSERT COMPANY NAME HERE> IS PROHIBITED.

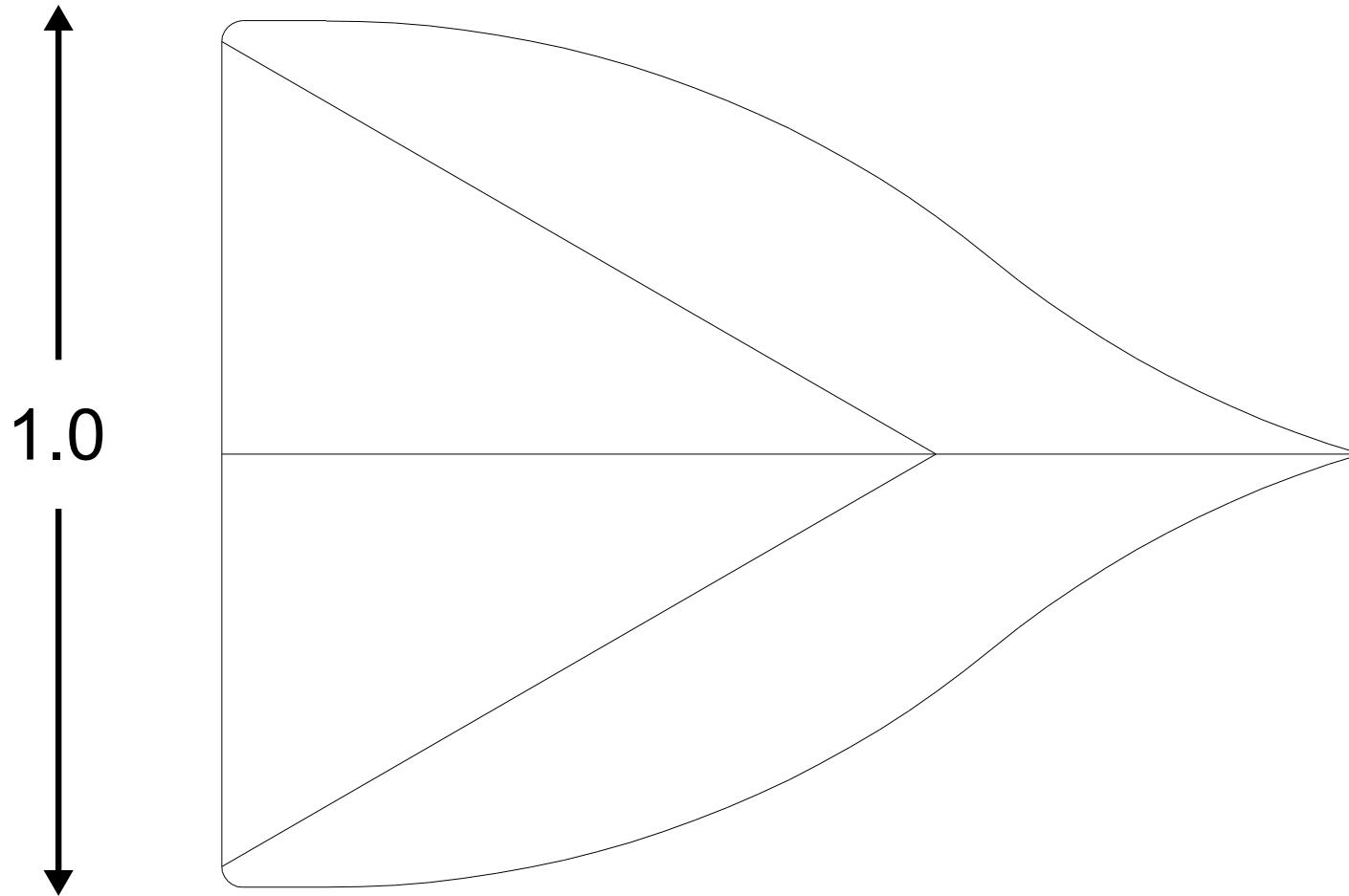
		UNLESS OTHERWISE SPECIFIED:		NAME	DATE
		DIMENSIONS ARE IN CM	DRAWN	BJE	
			CHECKED		
			ENG APPR.		
			MFG APPR.		
		INTERPRET GEOMETRIC TOLERANCING PER:	Q.A.		
		MATERIAL	COMMENTS:		
		Polycarbonate			
		FINISH			
NEXT ASSY	USED ON				
APPLICATION		DO NOT SCALE DRAWING			

TITLE:		
Neck model		
Chamber base		
SIZE	DWG. NO.	REV
A	DESIGN #9	
SCALE: 1:2	WEIGHT:	SHEET 1 OF 1



PROPRIETARY AND CONFIDENTIAL
 THE INFORMATION CONTAINED IN THIS DRAWING IS THE SOLE PROPERTY OF <INSERT COMPANY NAME HERE>. ANY REPRODUCTION IN PART OR AS A WHOLE WITHOUT THE WRITTEN PERMISSION OF <INSERT COMPANY NAME HERE> IS PROHIBITED.

		UNLESS OTHERWISE SPECIFIED:		NAME	DATE	Sac model		
		DIMENSIONS ARE IN CM	DRAWN	BJE				TITLE:
			CHECKED			Chamber base		
			ENG APPR.					
		INTERPRET GEOMETRIC TOLERANCING PER:	MFG APPR.			SIZE	DWG. NO.	REV
		MATERIAL	Q.A.			A	DESIGN 9	
		Polycarbonate	COMMENTS:			SCALE: 1:2	WEIGHT:	SHEET 1 OF 1
		FINISH						
NEXT ASSY	USED ON							
APPLICATION		DO NOT SCALE DRAWING						



PROPRIETARY AND CONFIDENTIAL
 THE INFORMATION CONTAINED IN THIS DRAWING IS THE SOLE PROPERTY OF <INSERT COMPANY NAME HERE>. ANY REPRODUCTION IN PART OR AS A WHOLE WITHOUT THE WRITTEN PERMISSION OF <INSERT COMPANY NAME HERE> IS PROHIBITED.

		UNLESS OTHERWISE SPECIFIED:		NAME	DATE
		DIMENSIONS ARE IN CM	DRAWN	BJE	
			CHECKED		
			ENG APPR.		
			MFG APPR.		
		INTERPRET GEOMETRIC TOLERANCING PER:	Q.A.		
		MATERIAL Polycarbonate	COMMENTS:		
NEXT ASSY	USED ON	FINISH			
APPLICATION		DO NOT SCALE DRAWING			

TITLE:		
Neck model		
Island contouring		
SIZE	DWG. NO.	REV
A	DESIGN #9	
SCALE: 1:2	WEIGHT:	SHEET 1 OF 1

5

4

3

2

1